Use Of Optical Techniques In Studies Of Wear Rates Of Anodized Aluminum And Polymer Coatings On Aluminum (lithography, Wettability, Sealing).

Chou, Shem-Mong

USE OF OPTICAL TECHNIQUES IN STUDIES OF WEAR RATES OF ANODIZED ALUMINUM AND POLYMER COATINGS ON ALUMINUM

Lehigh University PH.D. 1984

PLEASE NOTE:

In all cases this material has been filmed in the best possible way from the available copy. Problems encountered with this document have been identified here with a check mark _✓_.

1. Glossy photographs or pages _✓_
2. Colored illustrations, paper or print _✓_
3. Photographs with dark background _____
4. Illustrations are poor copy _____
5. Pages with black marks, not original copy _____
6. Print shows through as there is text on both sides of page _____
7. Indistinct, broken or small print on several pages _____
8. Print exceeds margin requirements _____
9. Tightly bound copy with print lost in spine _____
10. Computer printout pages with indistinct print _____
11. Page(s) _____ lacking when material received, and not available from school or author.
12. Page(s) _____ seem to be missing in numbering only as text follows.
13. Two pages numbered _____. Text follows.
14. Curling and wrinkled pages _____
15. Other _____

USE OF OPTICAL TECHNIQUES IN STUDIES OF WEAR RATES OF ANODIZED ALUMINUM AND POLYMER COATINGS ON ALUMINUM

by

Shem-Mong Chou

A Dissertation

Presented to the Graduate Committee

of Lehigh University

in Candidacy for the Degree of

Doctor of Philosophy

in

Chemistry

Lehigh University

1984

CERTIFICATE OF APPROVAL

Approved and recommended for acceptance as a dissertation in partial fulfillment of the requirements for the degree of Doctor of Philosophy.

9/14/84
(date)

Henry Leidheiser, Jr.
(Professor in Charge)

Accepted 9/14/84
(date)

Special Committee directing the doctoral work of Mr. Shem-Mong Chou

Henry Leidheiser, Jr.
Dr. H. Leidheiser, Jr., Chairman

F. J. Micale
Dr. F. J. Micale

James E. Sturm
Dr. J. E. Sturm

A. C. Zettlemoyer
Dr. A. C. Zettlemoyer

M. C. Hughes
Dr. M. C. Hughes

TO MY PARENTS AND FAMILY

ACKNOWLEDGMENT

The author wishes to express his sincere appreciation and gratitude to:

Dr. Henry Leidheiser, Jr. and Dr. Michael C. Hughes for their guidance, encouragement and support throughout this study.

Dr. Albert C. Zettlemoyer, Dr. James E. Sturm and Dr. Fortunato J. Micale for their interest and service on the dissertation committee and for their valuable comments.

Mr. Wayne Bilder for his contribution to the absorbance method for thickness determination.

Mr. Yung-Haw Hu for his assistance in preparing electron micrographs.

Dr. Chi-Ming Tseng and Mrs. Olga Shaffer for their help in photographic work.

Mr. Jeffrey Parks and Miss Michelle DeCrosta for their assistance in editing the first draft.

Mr. William Anderson, Jr. for technical assistance with instrumentation.

The Photo Products Division of the du Pont Company for the financial support.

Finally, his parents and family, for their love, patience, support and encouragement that enabled the author to complete his graduate study.

TABLE OF CONTENTS

LIST OF FIGURES

LIST OF TABLES

ABSTRACT

The rates of wear of anodized aluminum and polymer coatings on aluminum were determined under conditions that simulate wear of lithographic printing plates by abrasive inks. The rates of wear were determined using optical techniques which employ the interference fringes and absorption bands formed during specular reflection. Wear rates of unsealed anodic coatings, prepared under a wide range of anodizing conditions, vary widely with the rate being proportional to the contact pressure and inversely proportional to the apparent density of the anodic coatings. Surface material is removed by cutting and plowing mechanisms for both anodic oxide and polymer coatings. A wear theory was developed for anodized aluminum under three-body abrasion conditions. Sealing of the anodized surface and superficial oxidation of the polymer surface occurs concurrently with the abrasion process.

Wear rates were also determined on anodic coatings that were sealed in different aqueous media. The highest wear rate was obtained with coatings sealed in sodium silicate solution. The rate of wear of coatings sealed in boiling distilled water, nickel acetate solution, or potassium dichromate solution was initially high before falling to a rate typical of the unsealed coating. Superior wettability of the anodic coating by distilled water during short sealing times was exhibited by panels sealed in sodium silicate solution. The differences in the wear and wettability behavior of anodic coatings

sealed in sodium silicate solution and other sealants are ascribed to different mechanisms of sealing. Sealing proceeds via a surface conversion mechanism in the former case and a pore-plugging mechanism in the latter.

The rates of wear of polystyrene and poly-n-butylmethacrylate on aluminum anodized under different conditions were also determined. The nature of the polymer and the preparation method for the anodized aluminum substrate affect appreciably the resistance of the polymer to abrasive wear. Applications to the lithographic plate-making were proposed.

CHAPTER 1

INTRODUCTION

The oxide coating anodically produced on aluminum and its alloys is hard, dense and thick. It renders the metal more resistant to corrosion and wear. The characteristics of this oxide coating may be changed by variation in the anodizing conditions. In general, the denser the oxide coating, the higher is its resistance to wear. Anodized aluminum has found wide applications in the building industry and in the automotive industry. Much harder, denser and thicker oxide coatings may be produced at low electrolyte temperatures, high anodizing voltages, or dilute acid solutions. This process has been referred to as hard anodization. The hard anodized aluminum in its unsealed state has in many cases replaced heavier metals for such things as gears, slides, pistons, and many aircraft applications [1], where the environment is not strongly corrosive.

Organic finishes on anodized aluminum are desirable in some aircraft and marine applications when both corrosion and wear are the main reasons causing the failure of the system [2]. The unsealed anodized aluminum is an excellent base for paints, lacquers, resins, etc., due to the porous structure of the oxide film which promotes the anchoring of organic coatings to the substrate [3, 4, 5]. Such finishes produce the best possible corrosion and wear resistance for aluminum and its alloys. As a consequence, anodized aluminum has also been applied to the process of lithographic printing [6]. A

photosensitive polymer is applied as a thin coating on the anodized aluminum. After exposure and development, the anodized aluminum functions as the non-image area whereas the photopolymer coating functions as the image area.

Many techniques have been developed for evaluating the wear resistance of anodized aluminum and polymer coatings. These techniques include the abrasive jet method, essentially a measure for erosive wear, and Taber and Erichsen abrasers for two-body abrasive wear. The abrasive jet results may be affected by a number of factors that cause the agreement between laboratories to be very poor. Wear resistance or wear rate as evaluated by the Taber abraser is usually measured by the weight loss of the sample. The results have been questioned since the weight measurements may be influenced by the air humidity because of the hygroscopic property of anodic oxide coatings. Seasonal fluctuations of abrasion resistance results for hard anodized aluminum were obtained using Taber abraser at Duralectra, Inc., during a period of several years [7]. The main cause of such fluctuations was ascribed to the change of humidity conditions during abrasion testing. Thomas [8] also showed that the weight loss in 2000 revolutions of Taber testing could be almost completely balanced by the subsequent gain in weight by taking up water vapor. He suggested the measurement of thickness reduction instead of the weight loss measurement, because the thickness measurement would be unaffected by water adsorption. The measurement of weight loss is further complicated by the pick-up of abrasives by the wearing surface. A short preliminary run, which is disregarded, is generally made in the

Taber testing to eliminate this effect. Study of the topmost surface layer is sacrificed. Moreover, the dimensions of the coated parts are more critical in many applications than the weight.

Non-destructive methods for measuring the thickness of a coating are called for if the wear rate, i.e., the changes in coating thickness as a function of wear, is to be determined. Magnetic, beta back-scatter, X-ray spectrometric, eddy current, and optical techniques are suitable for this purpose [9]. Instruments based on the eddy current principle were proved to be excellent for measuring anodic coatings which were 25 μm or more thick. The limit of their sensitivity, however, is about 1 μm. They are not applicable to relatively thin coatings or sensitive enough to differentiate a slight change in thickness by wear process, though they are currently used in conjunction with the Erichsen abraser to determine the wear rate of anodized aluminum.

Optical techniques have been proven to be simple and accurate for this purpose [10]. Coating thickness greater than about 4 μm can be calculated from the interference fringes in the infrared region; below this value thickness can be obtained from the interference fringes in the ultraviolet and visible regions. The thickness of polymer coatings may also be determined by measurement of the transmittance of the coating at an absorbing wavelength vs. the transmittance of the bare substrate. An accurate calibration curve is required for this technique. The theories of optical methods for thickness measurement are reviewed in Section 2.1.

Wear is an extremely complicated phenomenon. It can not be

determined by the measurement of any single property. The wear rate depends not only on the material itself, but also on the entire interacting system. Any change in the loading or the ambient conditions may cause a catastrophic change in the wear rate or even a change in the type of wear. The surface material of brittle solids may be removed under abrasive wear conditions by either brittle fracture or plastic deformation mechanisms [11], depending on the material and wear environments. The wear rate by fracture mechanisms is about an order of magnitude higher than that by plastic deformation mechanisms. Fracture mechanisms predominate when the depth of indentation of the abrasive is high, i.e. when the applied load is high and the abrasive particle size is large. Sharp abrasive particles and the low ratio of fracture toughness to hardness of the material also favor fracture mechanisms. A comprehensive survey on the nature of wear and wear mechanisms of engineering materials is presented in Section 2.2.

The wear properties of anodized aluminum have been investigated for more than three decades. Though the effects of anodizing and sealing conditions and the basis metal composition on the abrasion resistance of anodized aluminum have been thoroughly studied, much less attention has yet been paid to the quantitative correlation of wear resistance to the physical and/or mechanical properties of anodic oxide coatings. Mechanisms of material removal and the dependence of wear rate on the applied test conditions are still lacking. It is the purpose of this study to remove this deficiency and to optimize the optical techniques useful in the evaluation of wear rate. The wear

theory for anodized aluminum under three-body abrasion conditions developed in this study correlates the wear rate of the anodic coating to its apparent density and the wear environments. Hopefully, some applications to lithographic plate-making could be obtained from this study.

Section 2.3 reviews the principles of anodic oxidation of aluminum and the structural features of oxide coatings. Literature results of the abrasion resistance of anodized aluminum are summarized in Section 2.4. Chapter 3 details the experimental techniques utilized in this study. Experimental results are summarized in Chapter 4 and discussed in Chapter 5. Section 5.6 presents the development of wear theory. Conclusions drawn from the experimental and theoretical work carried out in this study are listed in Chapter 6.

CHAPTER 2

GENERAL BACKGROUND

2.1 Optical Techniques for Thickness Measurement

The thickness of a coating can be calculated directly from the interference fringes obtained in a suitable spectral range, depending on the thickness of the coating. The thickness of a coating can also be determined by the absorbance of the coating at an absorbing wavelength. A calibration curve is generally required for the latter technique. Both techniques are applicable to transparent coatings only. The reflectance spectrum cannot be obtained if the coating is opaque.

2.1.1 Interference Method

The interference method for thickness measurement depends on the reflections of radiation from the air-coating interface and from the coating-substrate interface, and subsequent interference of the two beams. In order to obtain the interference fringe pattern, two conditions must be satisfied. First, there must exist a suitable spectral range in which the coating is transparent. Second, the substrate must have a different dielectric constant from that of the coating. These two requirements ensure fractions of the incident light to propagate through the coating and to reflect from the coating-substrate interface.

Wendlandt and Hecht [12] have discussed the theory of specular

reflectance spectroscopy in detail. Several workers have described the use of infrared specular reflectance to measure the thickness of epitaxial films on silicon [13, 14, 15, 16, 17, 18, 19], germanium [13] , and gallium arsenide [20] substrates, but cautioned against the use of the technique because the phase change at the film-substrate interface is a function of wavelength. This technique is capable of measuring the thicknesses of both n- and p-type layers greater than 2 μm thick, and with reduced precision it may also be applied to both n- and p-type films from 0.5 to 2 μm thick. In fact, the infrared interference method has been adopted by the American Society for Testing and Materials as a standard method of measuring the epitaxial layer thickness on silicon [21]. Saifi and Stolen [22] have shown that a combination of infrared and far-infrared interference spectra may yield not only the thickness of the epitaxial layer but also valuable information regarding the interface carrier concentration profile.

The specular reflectance spectra produced in the ultraviolet, visible, and near-infrared regions have been used to measure the thicknesses from several hundred angstroms to a few micrometers of thin anodic oxide films on aluminum [23, 24], tantalum [25, 26], and zirconium [27, 28] , and of thin thermal oxide films on titanium [29] and zirconium [28]. The dependence of both the refractive index and the phase change at the film-substrate interface on wavelength in this short wavelength range complicates the application of the interference technique to the thickness measurement. Knowing the dependence of the refractive index and phase change upon the wavelength, Hass [23]

claimed an accuracy of $\pm$ 2 nm in the thickness measurement of the anodic films on aluminum.

Harrick [30] has demonstrated that the infrared interference method is equally applicable to the thickness measurement of an absorbing polymer film (Mylar). Himics et al. [31] have determined the thickness of thin electron beam-sensitive polymer films from the specular reflectance spectra produced in the visible region.

2.1.1.1 Theory

The geometry of the interference method is illustrated in Figure 2-1. Here, the light falling on the coating with an incident angle θ_1 is split by reflection and refraction. The reflected ray r_1 undergoes a phase change Φ_1 at the air-coating interface (point A). The refracted ray travels through the coating to the coating-substrate interface and is reflected at point B with a phase change Φ_2. The refracted and reflected ray then passes back through the coating and is again split into a reflected ray and a refracted ray at the air-coating interface (point C). The refracted ray r_2 interferes with the directly reflected ray r_1, whereas the reflected ray executes multiple reflections (r_3, r_4, etc.). This interference is either constructive or destructive depending on the relative phase of the two beams. The additional outgoing rays r_3, r_4, etc., from the multiple reflections interfere with the resultant of rays r_1 and r_2 decreasing the intensity of fringe extrema by a small amount. They are not considered further in the development of the theoretical derivation because they do not affect the locations of the interference fringe

extrema.

For incident radiation normal to a nonabsorbing coating ($k_1=0$), the phase shifts Φ_1 and Φ_2 can be expressed in terms of the indices of refraction and the extinction coefficients of medium o, 1, and 2 [15] as

$$\tan \Phi_1 = 2 n_o k_1 / (n_o^2 - n_1^2 - k_1^2) = 0 \qquad (1)$$

and

$$\tan \Phi_2 = 2 n_1 k_2 / (n_1^2 - n_2^2 - k_2^2) \qquad (2)$$

where n_i is the index of refraction and k_i is the extinction coefficient of medium i. Equation (1) indicates that the reflected ray r_1 undergoes a phase change (Φ_1) of π ; and equation (2) indicates the phase change (Φ_2) of the reflected light from the coating-substrate interface depends on the refractive index of the coating and the complex refractive index of the substrate.

In addition to the phase changes at the air-coating and coating-substrate interfaces, there exists an optical path difference, $\delta = n_1(AB+BC)-AD$, between rays r_1 and r_2. Multiplying the apparent optical path length in the film, (AB+BC), by the refractive index n_1 converts the apparent optical path length to an equivalent air path length. It is evident from Figure 2-1 that the optical path lengths are

$$AD = 2 t \tan \theta_2 \sin \theta_1 \qquad (3)$$

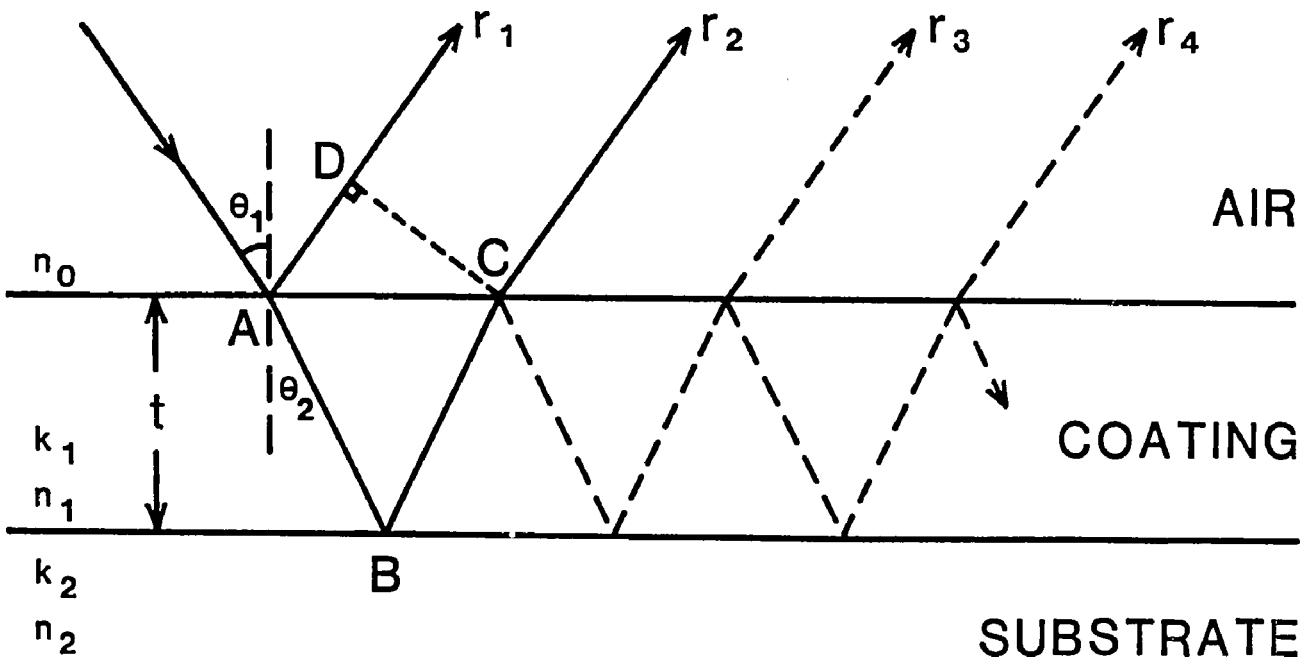

Figure 2-1. Geometry of interference method of measuring coating thickness.

and

$$n_1 (AB + CD) = 2 n_1 t / \cos \theta_2 \tag{4}$$

Using Snell's law ($n_o \sin \theta_1 = n_1 \sin \theta_2$), it can be shown that

$$AD = 2 n_1 t \sin^2 \theta_2 / \cos \theta_2 \tag{5}$$

where θ_1 = angle of incidence

θ_2 = angle of refraction

t = thickness of the coating

For a nonabsorbing coating the phase change of the transmitted ray at point A is zero. Then, the phases of rays r_1 and r_2 at points D and C can be expressed in terms of the optical path length and the phase change as

$$\Phi_D = 4 \pi \nu t n_1 \sin^2 \theta_2 / \cos \theta_2 - \Phi_1 \tag{6}$$

and

$$\Phi_C = 4 \pi \nu t n_1 / \cos \theta_2 - \Phi_2 \tag{7}$$

where ν is the wavenumber of the incident beam. The difference in phase, Φ , of rays r_1 and r_2 is therefore given by

$$\Phi = \Phi_C - \Phi_D = \Phi_1 - \Phi_2 + 4 \pi \nu t n_1 \cos \theta_2 \tag{8}$$

Destructive interference requires that

$$\Phi = (2m - 1)\pi \tag{9}$$

where m is the order of interference fringe (1, 2, 3, ...). The thickness of the coating can be obtained from equations (8) and (9).

$$t = [m - 1/2 - (\Phi_1 - \Phi_2)/2\pi] \; / \; 2 \; \nu_m \, n_1 \cos\theta_2 \tag{10}$$

where ν_m is the wavenumber of the m-th order of interference fringe minimum.

A convenient thickness relationship can be obtained from equation (10) utilizing two wavenumbers corresponding to fringe minima, ν_m and ν_{m+x}.

$$t = x \; / \; [2 \, n_1 \cos\theta_2 (\nu_{m+x} - \nu_m)] \tag{11}$$

where x is an integer representing the number of fringes occurring from ν_m to ν_{m+x}. Equation (11) is independent of the phase change provided that the phase change and the refractive index are constant over the interval ν_m to ν_{m+x}.

For a nearly normal incidence of radiation, $\cos\theta_2 \simeq 1$ and equations (10) and (11) reduce to

$$t = [m - 1/2 - (\Phi_1 - \Phi_2)/2\pi] \; / \; 2 \, n_1 \, \nu_m \tag{12}$$

and

$$t = x \; / \; [2 \, n_1 \, (\nu_{m+x} - \nu_m)] \tag{13}$$

2.1.2 Absorbance Measurement

In studies of the oxidation of iron and copper, Poling [32] has demonstrated that not only is the infrared reflectance method capable of discriminating the various iron or copper oxide species grown on the metal surfaces with a high degree of accuracy, but is also useful for determining the thickness of oxide films. Through the use of a multiple reflectance system, copper and iron oxide films as thin as 3 to 5 angstroms could be detected. By using only one reflection, oxide films up to about 0.5 μm thickness could be studied.

The thickness of a coating as determined by the absorbance measurement is based on the application of Beer's law. The absorbance ΔA of a dilute solution is directly proportional to the molar concentration c of the absorber when the length b of the light path is fixed, and directly proportional to the path length when the concentration is fixed [33], as given by

$$\Delta A = \epsilon b c \tag{14}$$

where the constant ϵ is the molar absorptivity of the absorber. Deviations from the linear relationship between absorbance and concentration arise for solutions at high concentrations. Nonlinearity is partly due to close encountering of absorbers which may affect the charge distribution around each molecule and hence alter the molecule's ability to absorb a given wavelength of radiation. ϵ is also dependent upon the refractive index of the solution which may be altered as the concentration of the solution

changes. Coatings are considered to be highly concentrated solutions and, therefore, accurate calibration curves are generally necessary when Beer's law is applied to the thickness measurements. The absorbance of a coating can be determined by measuring the transmittance of the coating at an absorbing wavelength relative to the transmittance of the bare substrate.

$$\Delta A = \log(T_s/T_c) \tag{15}$$

where T_c and T_s are transmittances observed for the coating and for the coating-free substrate, respectively.

Several workers have used this technique to study the thickness or the amount of oxide films on aluminum [34, 35, 36, 37, 38, 39, 40] and titanium [41]. Hannah [34] found that the plot of absorbance at 960 cm^{-1} versus the thickness of barrier-type anodic films on aluminum is linear and passes through the origin. Similarly, the weights of zinc phosphate coatings as determined by the absorption measurement were reported by Cheever [42]. Using a multiple reflectance technique, Poling [43] was able to determine the thickness of adsorbed polymer films on iron and steel from 2 to 20 nm thick.

2.2 Abrasive Wear of Materials

Wear is generally defined as the removal of material from either one of the two contact surfaces in relative motion as a result of mechanical action. Based on the entire interacting system, there are at least four principal types of wear [44, 45]: adhesive, abrasive,

corrosive, and surface fatigue. Adhesive wear is characterized by the fracture of the adhesive junctions formed under the applied load between asperities on two nominally smooth surfaces, causing material transfer from one surface, usually the softer, to the harder countersurface. These transferred fragments may be transferred back to the original surface or form loose wear debris. Abrasive wear will be discussed in great detail later. Corrosive wear takes place when a corrosive environment produces a corrosive product on one or both of the rubbing surfaces and this corrosive product is subsequently removed by the sliding action. Consequently, the corrosion reaction can continue. Surface fatigue wear is the predominant mode of failure of rolling contact bearings. The repeated loading and unloading of the counterformal contact area may induce the formation of surface or subsurface cracks, which will eventually result in the delamination of a surface film, leaving large pits in the surface.

Eyre [46] has estimated that approximate 50% of the equipment failure caused by wear is due to abrasive wear. A further insight into this major type of wear processes becomes very important. The Research Group on Wear of Engineering Materials of the Organization for Economic Cooperation and Department has defined abrasive wear as the displacement of material from one of the two surfaces in relative motion caused by the presence of hard protuberances on the second contact surface or hard particles either between the surfaces or embedded in one of them, usually the softer surface [47]. The former type is generally known as "two-body abrasive wear" in the literature and the latter as "three-body abrasive wear". Most of the abrasive

wear problems arising in agricultural and industrial equipment are three-body, while two-body abrasive wear is encountered primarily in material removal operations.

It is convenient to subclassify three-body abrasive wear according to the specific combinations of abrasive and wearing material, as closed and open three-body abrasion [48]. Open three-body abrasive wear may be further classified into one of three groups: gouging, high-stress grinding, and low-stress scratching. Closed three-body abrasive wear occurs when the loose abrasive particles, which may be the work-hardened wear debris resulting from adhesive wear processes or the foreign particles accidentally intruding into the system, embed in the softer surface with subsequent abrasive wear of the counter surface. This type of wear usually takes place in the bearing systems and can often be eliminated by filters, seals, or flushing.

Open three-body abrasive wear occurs when the two surfaces are far apart or when only one surface is involved in the wear process. Gouging abrasion is encountered, for example, in shovels digging into a pile of rocks or in impact-type pulverizers when rocks or other coarse abrasive particles cut into the tool surface to remove relatively large amounts of material. High-stress grinding abrasion takes place when the objective of the process is to crush the abrasive particles as in ball mill grinding. If, during the wear process, the abrasive particles do not fracture, the action is termed low-stress scratching abrasion. Low-stress scratching abrasion is observed in printing presses and will be investigated in this study.

2.2.1 Material Removal Mechanisms for Brittle Solids

The anodic oxide films on aluminum are very brittle. Even under the most favorable conditions for producing flexible coatings, the maximum elongation before cracking occurs does not exceed 0.3% [49]. During the abrasive wear of brittle material, the surface material may be removed by plastic deformation or indentation fracture, depending on the material and wear environments [11]. The rate of material removal for anodic oxide films on aluminum is controlled by the plastic deformation processes under the applied conditions employed in this study. Therefore, only the abrasion theories based on the plastic deformation processes will be discussed here.

It is very difficult to write a single description to cover all mechanisms occurring simultaneously because the rate-controlling process depends on the entire interacting system. In many cases, the wear mechanism may be changed as wear proceeds. Quantitative expressions derived from some simple models are, however, very important in understanding the wear processes and very helpful in selecting materials for abrasive wear resistance. Abrasive wear by plastic deformation has generally been treated as a simple cutting process with the assumption that the abrasive particles have a simple shape such as a sphere [45, 50, 51, 52, 53, 54, 55, 56, 57], a cone [45, 50, 51, 53, 54, 55, 57], a pyramid [51, 53, 58, 59, 60, 61], or a cone with a hemispherical tip [62, 63, 64].

Figure 2-2 shows a schematic diagram of a rigid conical abrasive grain carrying a load L, penetrating and abrading a plane surface through a distance dS [45, 50]. The force equilibrium requires that

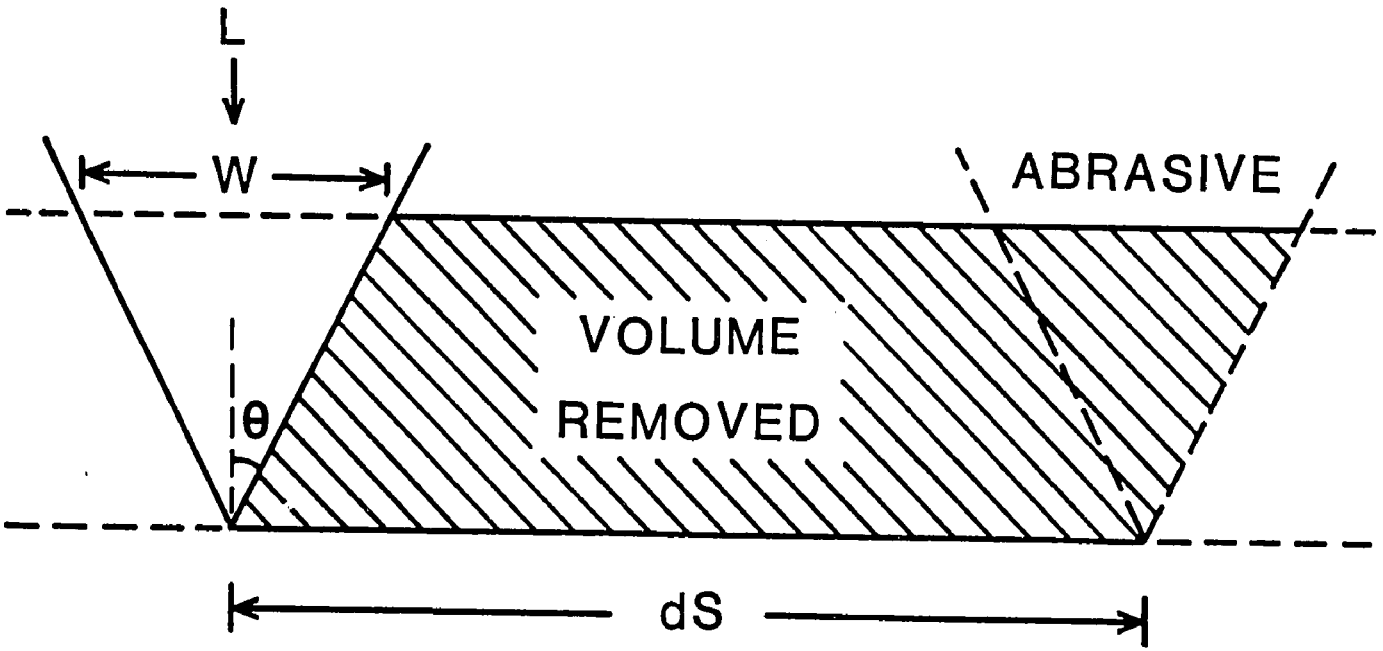

Figure 2-2. Schematic diagram of a conical abrasive grain which removes material from a surface (taken from [50]).

$$L = (\pi/4)\, w^2\, H \tag{16}$$

where H is the hardness of the wearing surface and w the groove width. The groove area A_g, i.e. the projected area of the penetrating cone in the vertical plane, is

$$A_g = (1/4)\, w^2 \cot\theta \tag{17}$$

where θ is the half angle of the scratches formed on the abraded surface. Thus the volume dV swept out by the cone is given by

$$dV = A_g\, dS = L \cot\theta\ \ dS\ /\ \pi\, H \tag{18}$$

When the contributions of all the abrasive grains are taken into account, the overall volume wear rate becomes

$$dV/dS = L\, \overline{\cot\theta}\ /\ \pi\, H \tag{19}$$

where $\overline{\cot\theta}$ is a weight average of $\cot\theta$ of all individual cones, and L is the total load applied to the system.

Sedriks and Mulhearn [60, 65] have shown that equation (19) is a severe oversimplification. They used pyramidal tools to simulate abrasive particles and observed that these tools may either cut or merely rub the wearing surface depending on the attack angle, the angle between the contacting surface of abrasive particle and the material surface. Rubbing is generally referred to as plowing in the literature. When the attack angle is below the critical value, the

contacting abrasive particle plows up material in front of it, resulting in ridges around the abrasive particle and on either side of the groove, whereas above the critical value the abrasive particle cuts a microchip. The geometry of these ridges depends on the material and the shape of the abrasive particle [55, 57], while the critical attack angle is determined primarily by the coefficient of friction between the contacting surfaces [65]. The groove area plowed by the rubbing mechanism is much smaller than that by cutting. Figure 2-3 shows good agreement between experimental results and the theoretical curves derived from the mechanics of cutting [65]. Mulhearn and Samuels [59] applied the critical attack angle approach to derive a wear equation in terms of the fraction α of abrasive particles that cut. The equation can be rewritten in the following form

$$dV/dS = \alpha A_g L / A_c H \tag{20}$$

where A_c is the horizontal projected area of indentation. Because the amount of material removed by the rubbing mechanism is much smaller than that by cutting, it is neglected in this approach.

It is generally true that only a fraction of the groove volume may become loose and the remainder is displaced to ridges [66, 67, 68, 69, 70], even when the attack angle is greater than the critical value [64]. Taking into account these two factors, Buttery and Archard [70] derived a wear equation

$$dV/dS = 0.5 \alpha \beta L \cot \theta / H \tag{21}$$

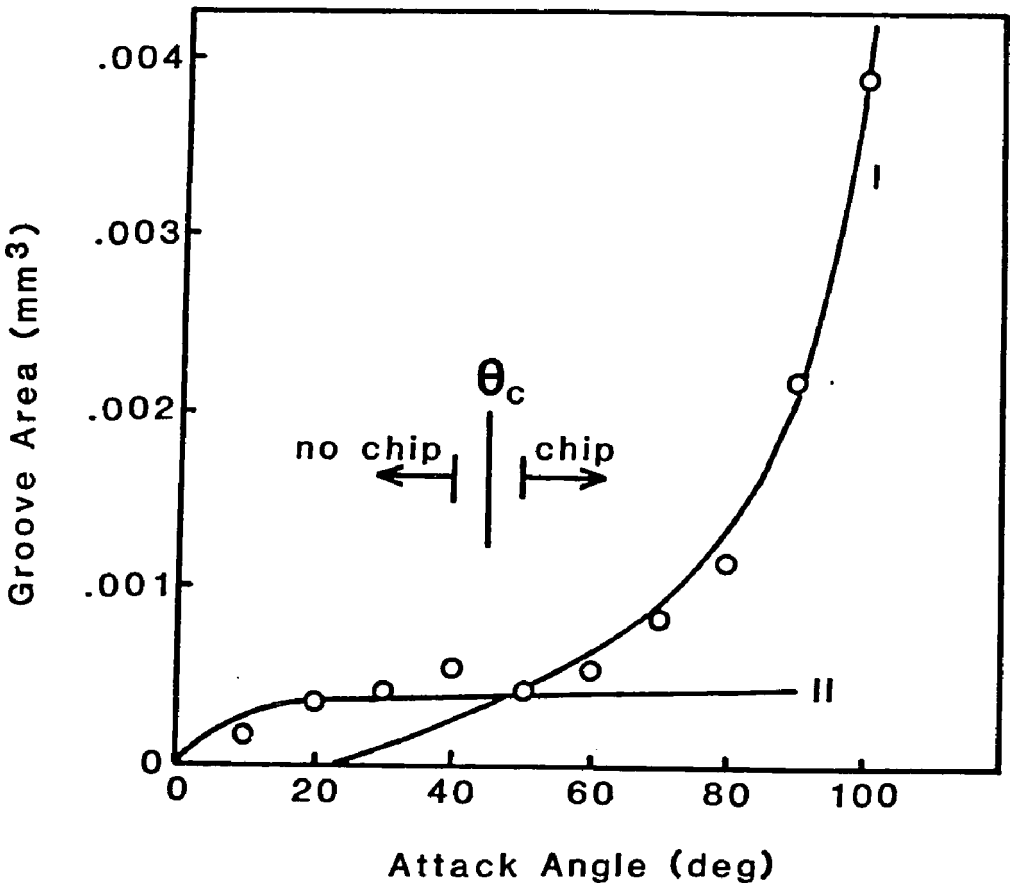

Figure 2-3. Variation of the groove area with attack angle of the abrasive particle. Theoretical curves I for chip cutting and II for pure rubbing with experimental values for copper (taken from [65]).

where β is the proportion of the groove volume removed as wear debris. Moore and King [11] obtained a linear wear equation by assuming $\alpha = 0.6$, $\beta = 0.6$, and $\theta = 60^{\circ}$

$$dt/dS \simeq 0.1\ P\ /\ H \tag{22}$$

where t is the apparent thickness of the specimen in units of mm, P the applied pressure in units of MNm^{-2} and H in units of GNm^{-2}. During the study of abrasion of a number of metals on emery papers, Wilman and coworkers [66, 67] found experimentally that

$$(dV/dS)(H/L) = (A_g/A_c)[1 - (A_r/A_g)] \simeq \text{constant} \tag{23}$$

where A_r is the cross-sectional area of the ridges.

In summary, the amount of material removed from the surface is linearly dependent upon the sliding distance and the applied pressure or load, and is inversely proportional to the surface hardness. The same relationships can be derived from the dimensional analysis of wear systems [71].

Though equations (19) to (23) are derived primarily for two-body abrasive wear, the relationships are equally applicable to three-body abrasive wear. The wear rate under three-body abrasion conditions is about an order of magnitude smaller than that under two-body conditions [45, 50, 72, 73]. Rabinowicz et al. [50] suggested that the abrasive grains in the three-body case spend about 90% of time rolling, producing no abrasive wear debris, and only about 10% of time

sliding and abrading the surface. Misra and Finnie [74] also proposed that the abrasive particles are rolling as well as sliding during three-body abrasion, even at higher loads, because the frictional coefficients for two-body systems are generally greater than for three-body abrasion. The surface material under three-body abrasion conditions is removed mainly by the rubbing mechanism [73, 74], and in some cases the formation of microchips was observed [75].

Equations (19) to (23) could be generalized, in accordance with Archard's adhesive wear equation [76], as

$$dV/dS = (k/3)\ L\ /\ H \tag{24}$$

where k is a wear constant dependent upon the nature of the abrasive and its interaction with the wearing material. Equation (24) is applicable to both two-body and three-body abrasive wear. The wear constant, k, is much greater for two-body abrasive wear, where the cutting mechanism predominates, than for three-body abrasive wear, where the rubbing mechanism is the rate-controlling process of material removal.

2.2.2 Experimental Evidence for Abrasive Wear Equations

The amount of material removed from the surface is generally determined by weight loss measurement. Figure 2-4 presents the weight loss for AISI 1020 steel and aluminum specimens as a function of wear path length under three-body abrasion conditions [74]. In the initial stage of abrasive wear the specimen actually gains weight. After this

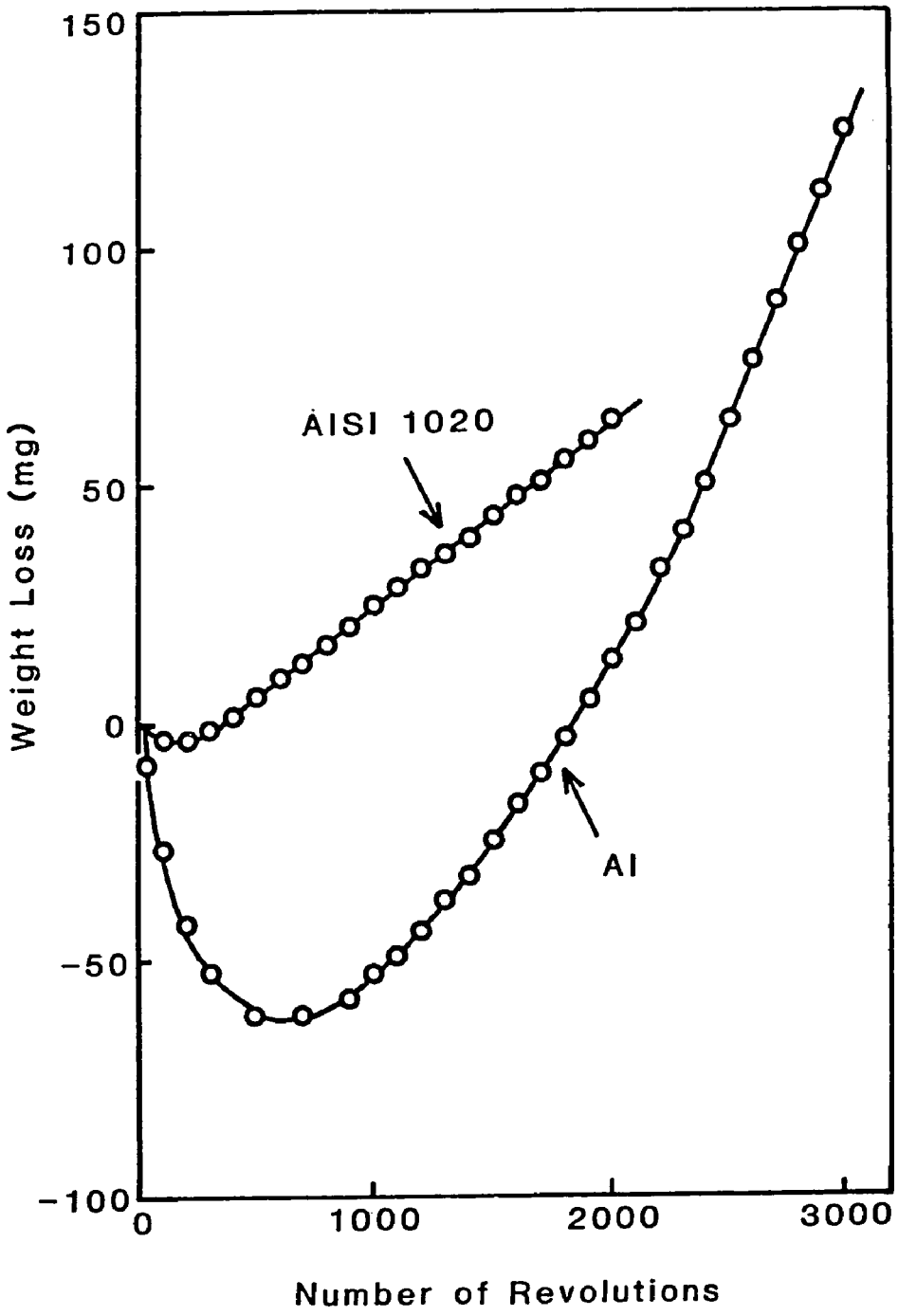

Figure 2-4. Weight loss as a function of sliding distance for aluminum and AISI 1020 steel samples abraded by 250 μm SiC abrasive particles (taken from [74]).

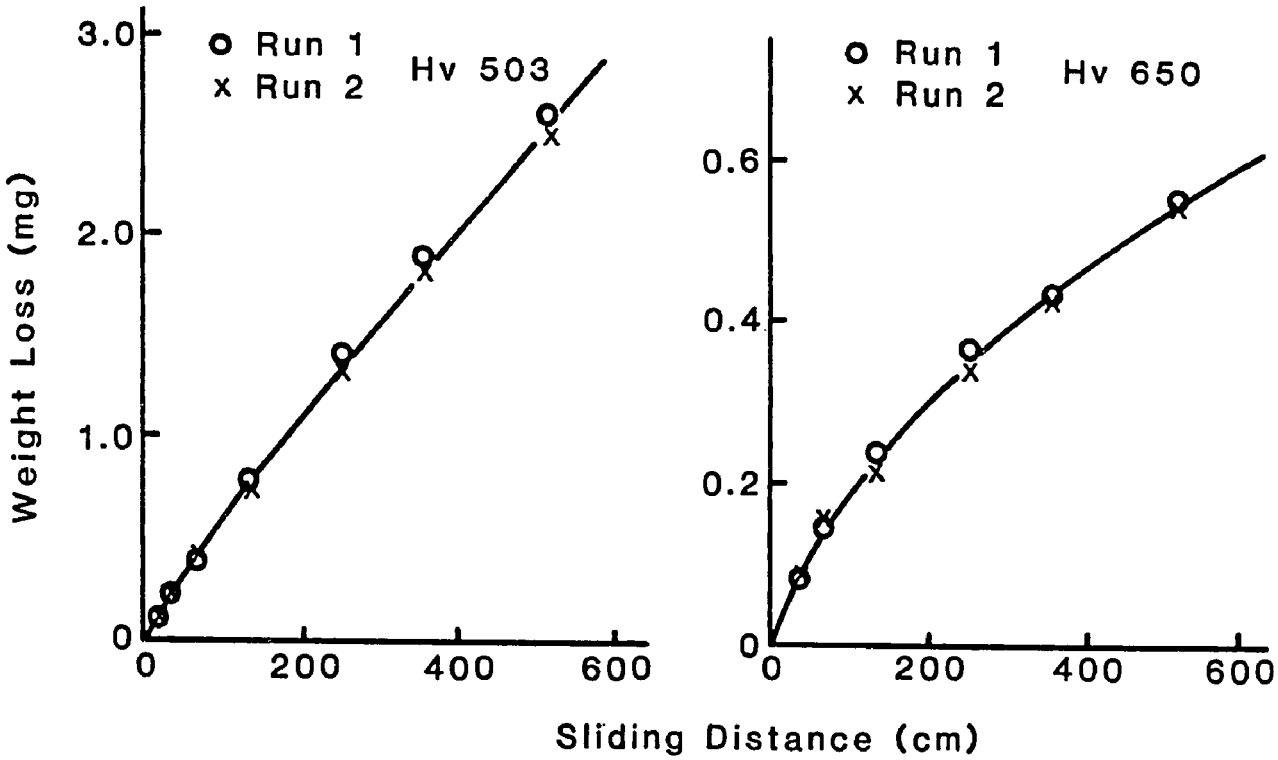

Figure 2-5. Relationship between weight loss and sliding distance for polished 0.74% C Steel abraded by 500 μm glass paper of hardness H_a=590 Kg/mm^2 (taken from [77]).

incubation period, there is a steady increase in the weight loss. The length of the incubation period is determined by abrasive hardness, the softer the material the longer the incubation period. The initial weight gain is ascribed to the pick-up of abrasives by the wearing surface [78]. Figure 2-5 reveals an initially nonlinear region followed by a linear relationship between weight loss and sliding distance under two-body abrasion conditions [77]. The initial nonlinear portion occurs when the surface deforms plastically and strain hardens to an equilibrium hardness [79]. With softer abrasives the wearing material takes much longer to strain harden to an equilibrium condition. These results indicate that the initial stage of abrasive wear processes is complicated either by the pick-up of abrasives or the work-hardening of the surface by abrasive particles under load. A linear increase in weight loss with sliding distance is obtained after these effects reach equilibrium conditions.

Experimental data [80, 81, 82, 83, 84] show that the amount of material removed from the surface is linearly dependent upon the applied load or pressure up to the load at which abrasive grains deteriorate [69]. The deterioration of abrasive grains will result in an increase in the fraction of elastic contact and, therefore, a decrease in the rate of material removal. Figure 2-6 and 2-7 show this relationship for ductile and brittle materials, respectively.

Khrushchov and Babichev [85, 86, 87] found, as shown in Figure 2-8, that the relative wear resistance was directly proportional to the Vickers hardness number for pure metals and some annealed alloys, while different relations apply for hardened and tempered steels.

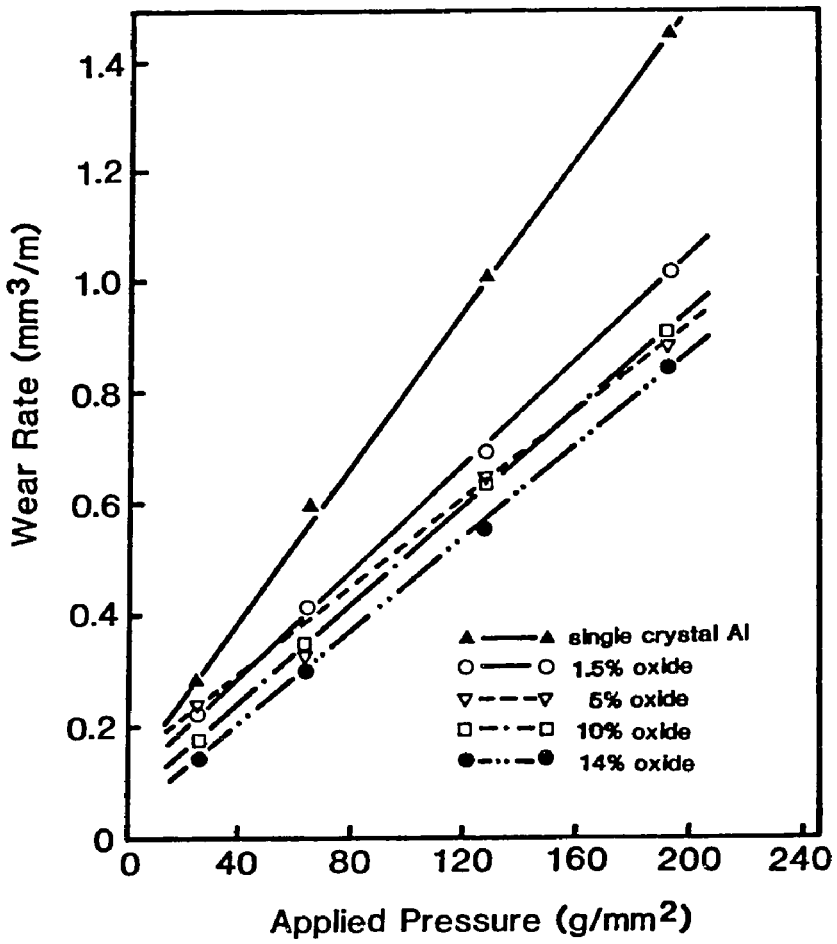

Figure 2-6. Wear rate as a function of applied pressure for some Al-Al_2O_3 alloys on 240 grit SiC paper (taken from [81]).

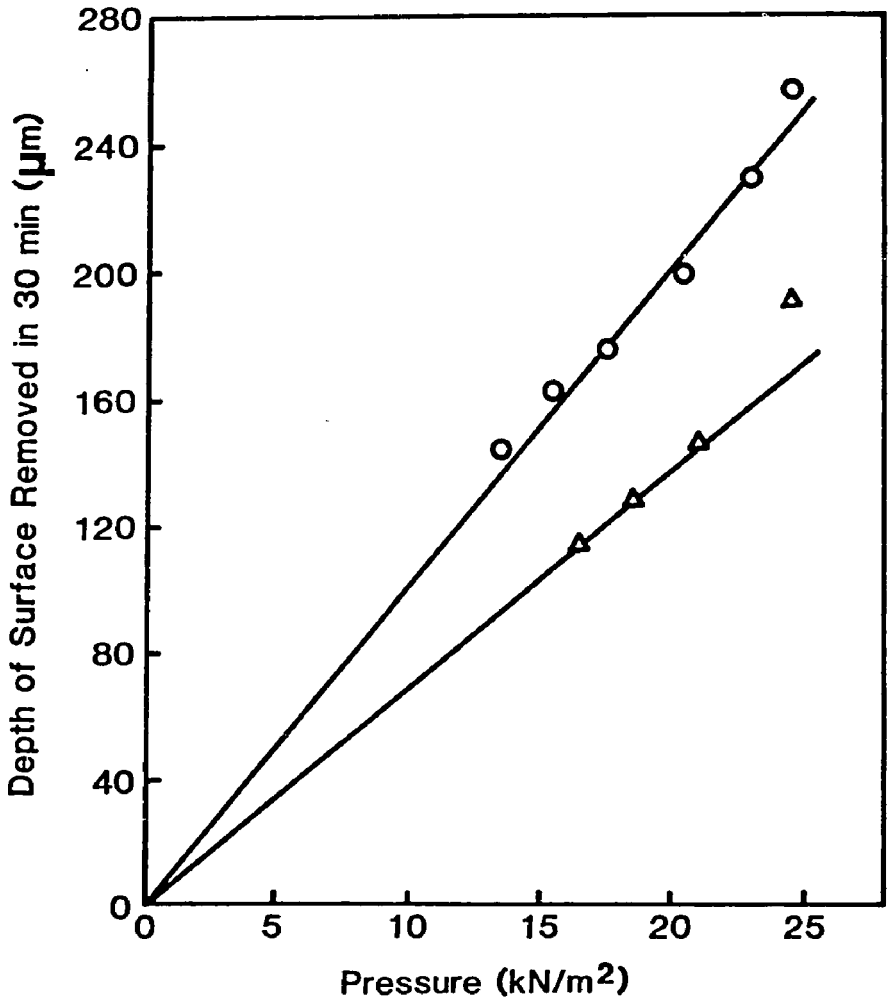

Figure 2-7. Variation of wear rate with applied pressure for soda-lime glass (o) and silica (Δ) on 30 μm SiC water slurry (taken from [82]).

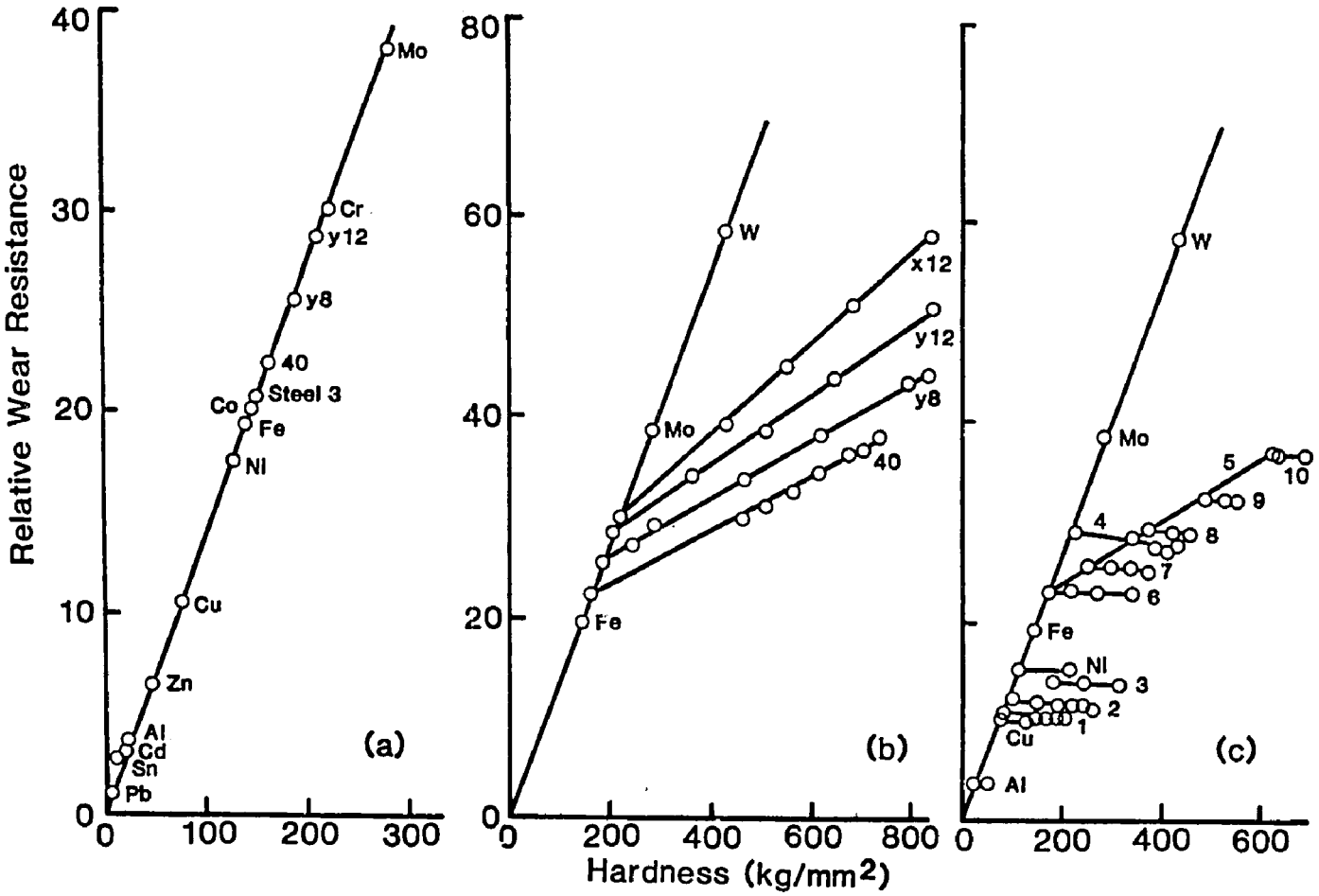

Figure 2-8. Correlation between the hardness prior to wear test and the relative wear resistance under two-body abrasion conditions: (a) technically pure metals and annealed steels; (b) thermally treated structural steels; and (c) cold-hardened materials (taken from [85]).

Work hardening prior to abrasion did not result in any increase in wear resistance. It has been shown by several workers [63, 67, 79] [88, 89, 90] that a surface can undergo severe plastic deformation and strain hardening under wear. The degree of strain hardening by wear is higher than that by any pre-test hardening [85, 91]. Consequently, the wear resistance is independent of the hardness of cold work hardened materials. Though it is generally accepted that the wear resistance is better correlated with the surface hardness after wear, clearly the generalized wear equation does not completely account for the effect of mechanical properties of the surface material on the wear rate.

It was also observed [84] that the relationship between wear resistance and annealed hardness of pure metals is dependent upon the size of abrasive particle, as seen in Figure 2-9. Tungsten was found to have higher wear resistance for smaller abrasive particles and lower wear resistance for larger particles than the values expected by equation (24). Tungsten behaves like a brittle solid when abraded with larger abrasive particles, whereas smaller abrasive particles abrade tungsten in a ductile manner. Thus, the deviation of experimental data from the values calculated using wear equations based on a cutting mechanism is not surprising when fracture or rubbing mechanisms become increasingly important in material removal processes.

It is well known that the rate of material removal in abrasive wear decreases drastically as the hardness H of the material approaches the hardness H_a of the abrasive [74, 92, 93, 94, 95, 96].

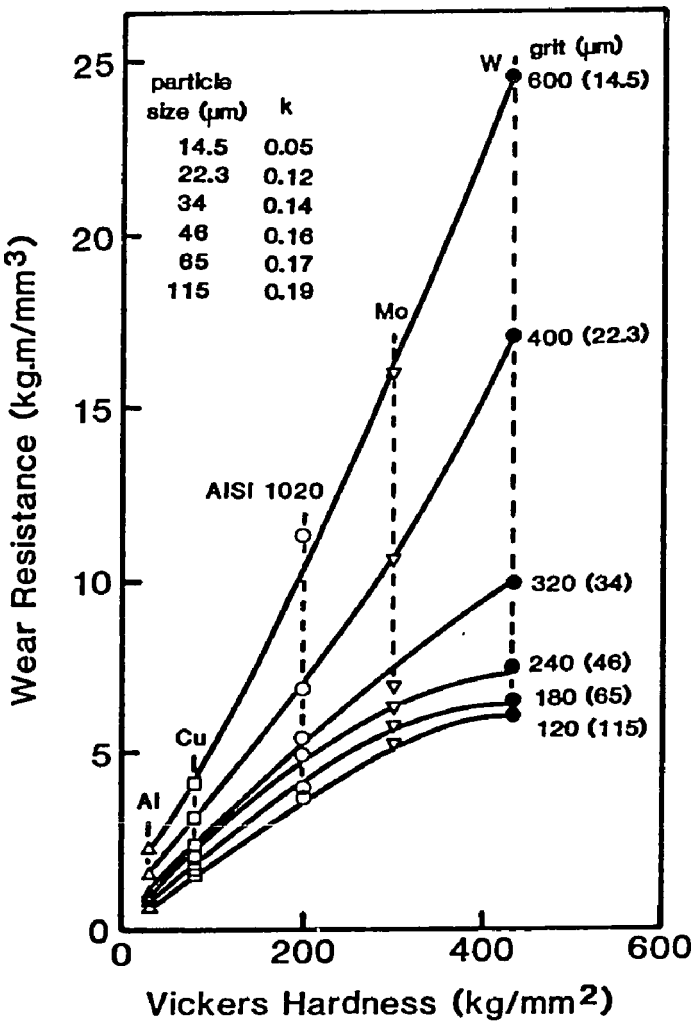

Figure 2-9. Wear resistance as a function of the Vickers hardness for various pure metals when abraded by SiC abrasive paper of different grit sizes at a sliding speed of 75 mm/sec. The value of k was obtained by taking the slope of the curve in the region between 100 and 300 Kg/mm^2 (taken from [84]).

Figure 2-10 shows this behavior for AISI 4340 steel under three-body abrasion conditions [74]. The wear rate is very low when $H/H_a > 1.0$ and it starts to increase and reaches a maximum value when $H/H_a < k$, where k lies between 0.6 and 0.7 [93]. Richardson [95] quoted a value for k of about 0.8 using the hardness of fully strain hardened surface. These k values are probably in basic agreement if the hardness of fully strain hardened surface is used in the former case. The results are generally consistent with Tabor's observations [97] that the ratio between successive hardness values on the Moh's scale of scratch hardness for minerals is 1.2. In order for one material to scratch another, the former should have a Vickers hardness at least 20% greater than the latter. Thus, cutting is the rate-controlling process of material removal when the hardness of abrasive is 1.2 times greater than the hardness of a fully work-hardened surface, while a rubbing mechanism predominates as the ratio of H_a/H falls below 1.2.

2.3 Anodic Oxidation of Aluminum

The physical and mechanical properties of aluminum and its alloys combine to make this metal extremely versatile. The density of the pure metal is low (2.7 g/cm^3), while the naturally formed oxide on the aluminum surface provides high corrosion resistance. The mechanical strength of the pure metal is relatively low, but can be improved by suitable alloying and heat treatments at the sacrifice of corrosion resistance. High resistance to corrosion and abrasion can be achieved by anodic oxidation which converts the surface of aluminum and its alloys to a hard oxide film much thicker than the one formed naturally

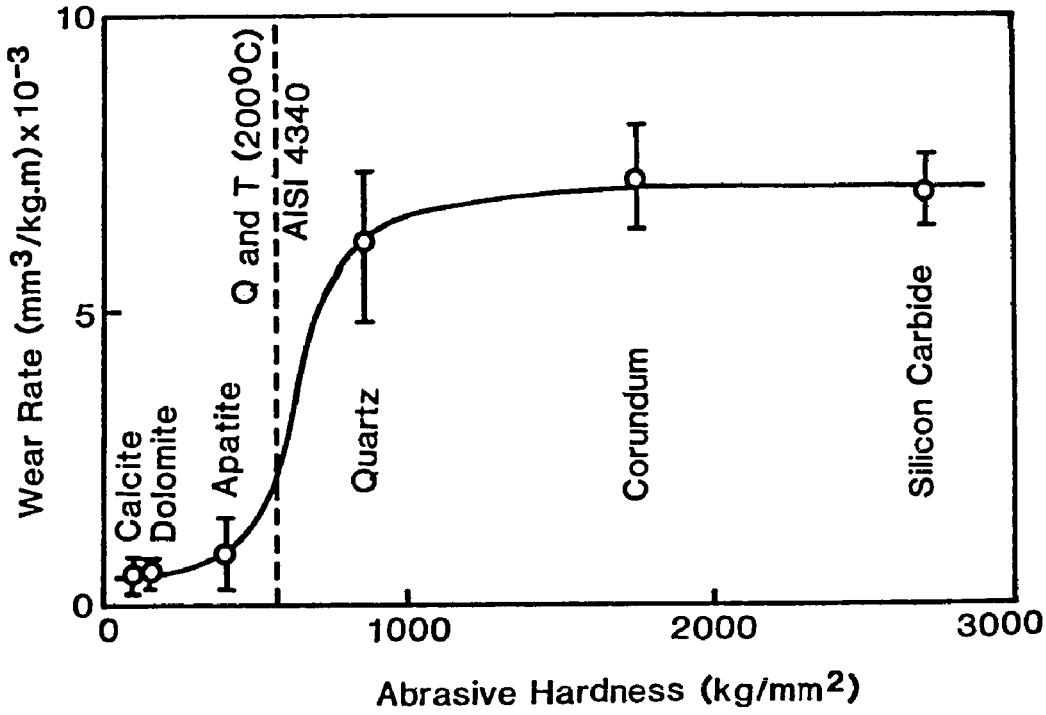

Figure 2-10. Wear rate as a function of abrasive hardness for AISI 4340 sample, quenched and tempered at 200°C and abraded by 250 μm size particles under three-body abrasion conditions (taken from [74]).

without applied potential.

There is a number of review articles [98, 99, 100, 101, 102, 103, 104, 105, 106, 107, 108] and books [2, 49, 109, 110, 111] in this field. Almost all of them deal with the fundamentals of anodic oxidation of aluminum. Less attention has been paid to the mechanical properties of anodized aluminum. This section surveys the classification of anodic coatings, the structure and substructure of oxide films, the formation mechanism, and the sealing of anodized aluminum. Although an extensive literature exists on these topics, definite conclusions have not yet been made on the basis of published results.

2.3.1 Classification of Anodic Coatings

When aluminum is made the anode in a suitable electrolytic cell, with a metal or carbon cathode, and an electric current is passed through the cell, the aluminum surface is converted to aluminum oxide. The thickness and properties of anodic coatings are determined by the nature of electrolyte and anodizing conditions employed.

Three types of anodic coatings are generally recognized according to the solubility of the oxide film in the electrolyte.

1. Barrier-type or nonporous anodic coatings: this type of coating is formed in aqueous or organic electrolytes having very low solvent power for oxide, e.g. neutral borate or tartrate solution and citric and malic acids. In this case film growth continues until the resistance of the film

prevents current flow. The thickness of barrier-type coatings is therefore dependent upon the anodizing voltage, the unit barrier thickness being about 14 Å/V [99]. Such films are extremely thin and dielectrically compact and are used principally on high purity aluminum foil as electrodes in electrical capacitors.

2. Conventional porous-type anodic coatings: this type of coating is produced in aqueous acid electrolytes having moderate oxide solvent power, e.g. sulfuric, phosphoric, oxalic, and chromic acid solutions at almost any concentration. In this case film growth is accompanied by the dissolution of oxide at the surface, resulting in the formation in the coating of pores which are wide enough to allow continuous access of the current to the metal. Film growth continues until the rate of film growth is equal to the dissolution rate of oxide in the electrolyte. Further anodization does not increase the film thickness, and this limiting film thickness varies with the electrolyte and anodizing conditions employed. Such films are generally in the range of 1 to 30 μm thick and are normally used for corrosion protection and decorative finishes.
3. Hard anodic coatings: this type of coating is a special class of porous-type anodic coatings. They are formed in the same electrolytes as the porous-type anodic coatings, but under conditions which minimize the solvent action by the electrolyte on the oxide, e.g. at lower bath

temperatures, higher forming voltages, or dilute acid solutions. Consequently, oxide films so obtained are denser and thicker than conventional porous-type coatings. Such films are generally 50 to 100 μm thick and are used principally for the good wear and scratch resisting properties they confer upon aluminum alloy surfaces.

2.3.2 Structure of Anodic Films on Aluminum

The structure of porous oxide films on aluminum has been investigated for many years, the results of which have produced essentially two main proposals: (a) geometrical model (Figure 2-11) by Keller, Hunter, and Robinson [112] and (b) colloidal gel model (Figure 2-12) by Murphy and Michelson [113].

Keller et al. [112] have hypothesized that the simultaneous formation and dissolution of oxide at selected points results in the formation of porous anodic film consisting of an approximately hexagonal close-packed arrangement of cells. Each cell of aluminum oxide contains a star-shaped pore extending perpendicularly from the surface to a point near the metal. At the bottom of the pore there is a thin-layer of nonporous oxide, called the barrier layer. The end of the cell represents a spherical section less than a hemisphere. The hexagonal cell structure and the scalloped contour of cell base were demonstrated by electron micrographs, but oval and circular pores were observed instead of star-shaped ones. They also found that the cell size, barrier layer thickness, and cell wall thickness are dependent

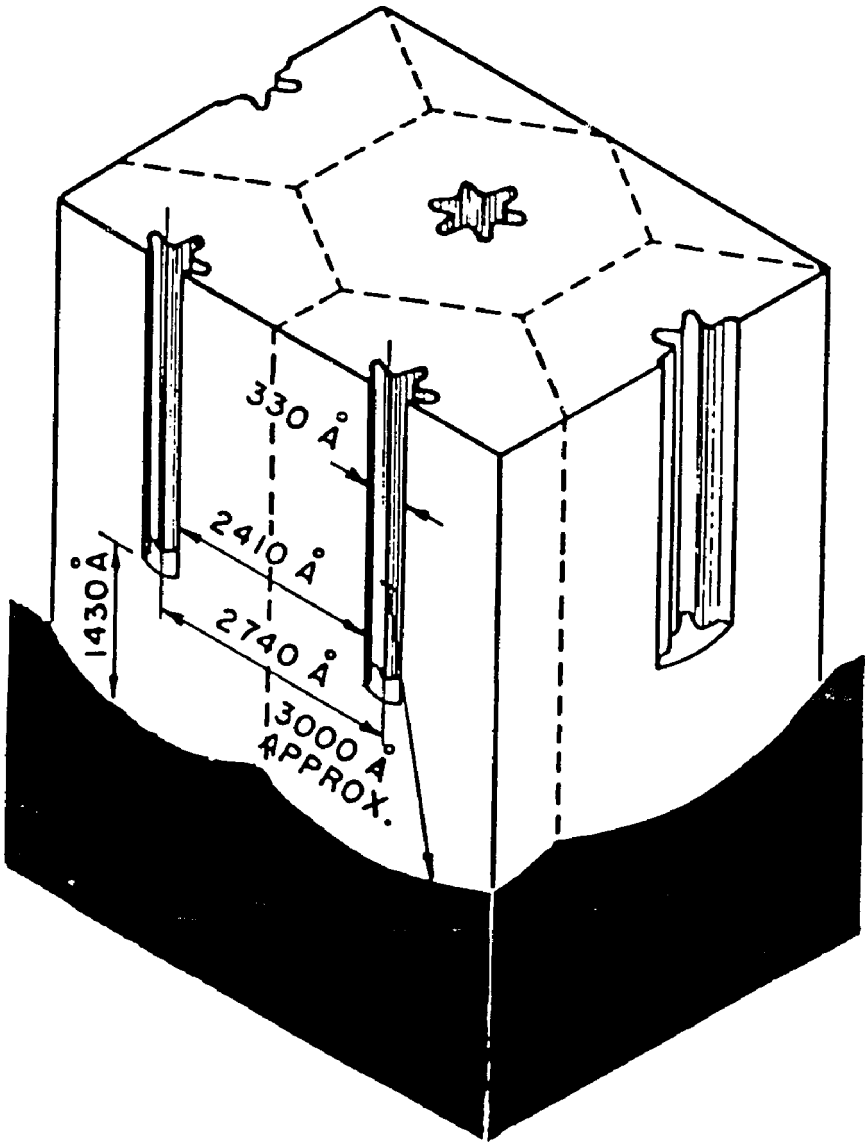

Figure 2-11. Schematic representation of the cell structure of a 120-V phosphoric acid coating. Dimensions of pore, cell, cell wall, barrier, and radius of curvature are shown (taken from [112]).

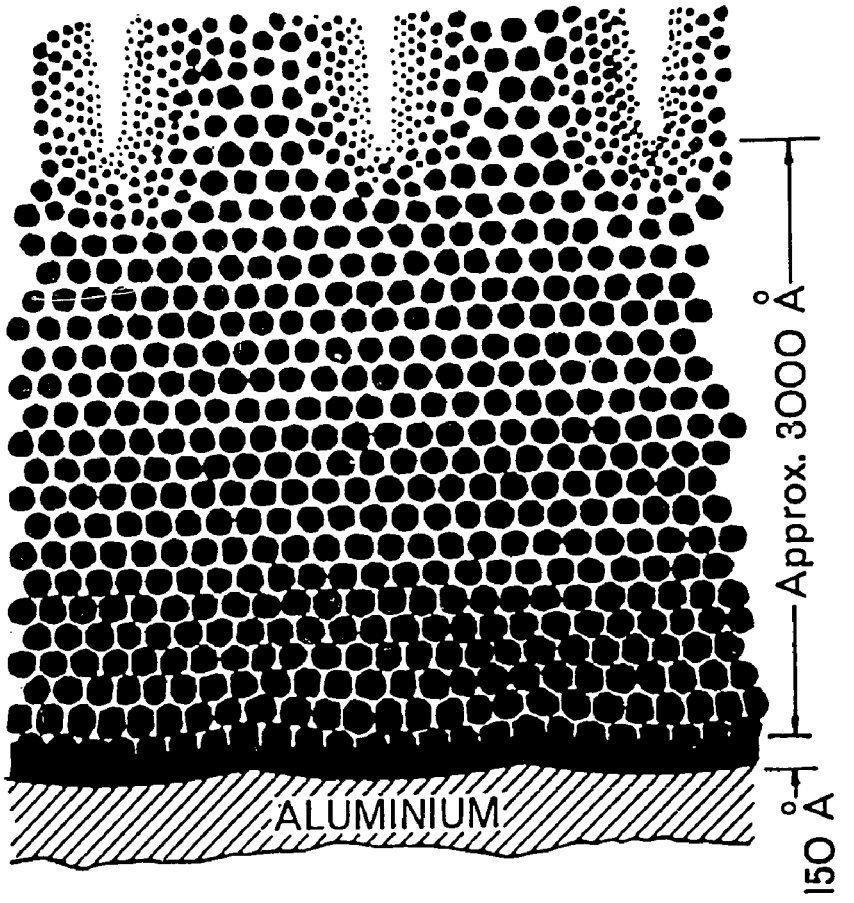

Figure 2-12. Schematic representation of possible structure of a porous anodic coating within about 3000 angstroms of metal surface. Black areas represent essentially anhydrous oxides. White areas represent hydrated and hydrous oxides which provide for electrolytic conduction between the electrolyte and the barrier layer. Bottom of the pore represents a scalloped metal/oxide interface which is required for the singularity in conduction. Not to scale (taken from [113]).

upon the electrolyte and applied voltage, increasing linearly with the applied voltage. The pore diameter is determined solely by the electrolyte and is independent of the applied voltage. Table 2-1 summaries their results [112, 114].

In the colloidal gel model, Murphy and Michelson [113, 115, 116] assumed the oxide film to be an agglomeration of submicrocrystalline particles of anhydrous alumina surrounded by acid anion-containing hydrated alumina. Acid anions are considered to be stabilizers for these colloidal microcrystallites. The innermost layer is a relatively compact, anhydrous form of aluminum oxide, which is identical to the barrier layer. Moving outward from the metal surface there is a region of transition in which the state of hydration of the oxide increases from the anhydrous state of the barrier layer to the hydrous state of the porous outer layer. Above the transition region is found the porous outer layer which is inhomogeneous and contains, in addition to the internal surfaces, physically distinguishable regions which exhibit different hydration states and oxide densities. Regions of low oxide densities are probably the precursors of pores formed upon drying and evacuation in preparation for electron microscopy.

The geometrical model of oxide films was confirmed by studies of carbon replicas of fractured sections [102, 117, 118, 119, 120, 121] and ultramicrotomed sections [122, 123, 124, 125, 126] in the transmission electron microscope. The electron micrographs do not exhibit the transition region hypothesized in the colloidal gel model. However, the colloidal gel model can complement the geometrical model

Table 2-1. Basic Dimensions of Oxide Cells Formed in Major Acid Solutions (taken from [112, 114]).

Electrolyte	Temp. °C	Barrier Å/V	Cell Wall Å/V	Pore Diameter Å
4% H_3PO_4	24	11.9	10.0	330
2% $H_2C_2O_4$	24	11.8	9.7	170
3% H_2CrO_4	38	12.5	10.9	240
15% H_2SO_4	10	10.0	8.0	120

from viewpoints of the incorporation of acid anions, the substructure of the cell material comprising the oxide films, and the film growth mechanism. These viewpoints will be discussed in great detail later.

It was found that the pore diameter is not independent of but proportional to the forming voltage [102, 127, 128, 129]. Because both cell diameter and cell wall thickness are directly proportional to the forming voltage V, the linear relationship between pore diameter and forming voltage becomes quite obvious from the following expression.

$$D_p = D_c - 2\ t_w = a_1 V - 2\ a_2 V = aV \qquad (25)$$

where D_p and D_c are the diameters of pore and cell, respectively. t_w is the thickness of cell wall. a, a_1, and a_2 are proportionality constants.

The chemical dissolution of cell wall by the anodizing electrolyte [121, 123, 129, 130, 131, 132, 133, 134, 135, 136] results in the increase in pore diameter on the surface of the oxide film with anodizing time [121, 128, 129]. The outermost oxide, formed first during the anodization process, undergoes the most severe chemical dissolution, resulting in the formation of conical rather than cylindrical pores. The rate of chemical dissolution increases gradually with anodizing time owing to the increased surface area of oxide film. When the pore mouths merge into each other at the surface of the oxide coating, the dissolution rate becomes equal to the formation rate and the oxide coating reaches its limiting thickness.

The chemical dissolution rate depends on the nature of electrolyte employed and the temperature of the anode during anodizing. The activation energies of this dissolution process are 14.6, 14.3, 19.3, and 15.4 kcal/mole for 10% sulfuric, oxalic, phosphoric, and chromic acid solutions [137], respectively. The temperature of the anode rises during anodization because of the generation of Joule heating and heat of formation of Al_2O_3. The temperature rise on the anode is remarkably influenced by the electrolyte flow rate, i.e. by the agitation conditions. Mason [138] observed that the temperature rise on the anode for 15% H_2SO_4 bath increases with current density and anodizing time even with good agitation. The range of temperature rise is from a few to several tens of degrees Centigrade, depending on the anodizing conditions. The temperature rise without agitation is about 3 to 4 times greater than with agitation. Applewhite et al. [139] also found that the temperature rise on the anode is approximately proportional to the anodizing voltage or to the current density at constant anodizing voltage. They estimated that the Joule heating is about 100 times greater than the formation heat of alumina. About 80% of the heat generated at the pore base is due to the Joule effect, as calculated by Nagayama and Tamura [134]. The importance of electrolyte agitation is quite clear now.

The slant of the cell wall and hence the solid content per unit volume or the apparent density of oxide film, is controlled by the extent of chemical dissolution. The mechanical properties of anodic coatings are, therefore, strongly dependent upon the anodizing

conditions. In order to minimize the amount of oxide dissolved into the solution, the anodic oxidation must be carried out in dilute acid solutions, at lower bath temperatures, or at higher forming voltages. The former two factors reduce primarily the aggressiveness of electrolyte, while the last decreases the anodizing time required to form a film of desired thickness, i.e. decreases the exposure time of oxide to the anodizing electrolyte. Consequently, the oxide films so obtained are dense and thicker, and are generally referred to as hard anodic coatings in the literature.

2.3.3 Acid Anion Incorporation and Substructure of Oxide Films

There is some divergence of view as to the composition of barrier layers based on data obtained from infrared studies. Maeland et al. [140] and Handke et al. [141, 142] suggested that barrier layers are composed of essentially anhydrous alumina. Dorsey [36, 37, 38, 143, 144] presented a completely different view. He proposed that the barrier layer is a trihydrate and consists of two layers; the primary layer next to the metal/oxide interface is a cyclic aluminic acid trihydrate, while the secondary layer close to the oxide/solution interface is a decyclized form of the primary layer. The former layer is more compact than the latter. His results were questioned by Thompson and Wood [108]. Wood and coworkers confirmed the duplex nature of the barrier layer, but disagreement appeared as to the composition of film material [145, 146, 147, 148, 149, 150]. The barrier layer was found to be composed of a compact inner region of virtually pure anhydrous alumina and an outer region of acid anion

contaminated, slightly hydrated alumina, as revealed by secondary ion mass spectrometry [145, 146]. The extent of acid anion incorporation into the barrier layer depends primarily on the nature of the electrolyte and to a much lesser extent on the anodizing conditions. Further evidence was provided from studies of ultramicrotomed sections of oxide films in the transmission electron microscope in conjunction with energy-dispersive analysis of X-rays [147, 148, 149, 150] and with Auger electron and FT-IR spectroscopy [151]. The results suggest that the inner region is relatively pure alumina which may undergo rapid crystallization in the electron microscope by electron heating, while the crystallization of the outer, acid anion contaminated region is inhibited until the crystallization of the inner region is completed. The retarded crystallization of the outer region is ascribed to the stabilization of alumina microcrystallites by acid anions, in accordance with Murphy's and Michelson's hypothesis.

The film material comprising the porous layer is usually regarded as contaminated oxide, largely anhydrous and appears amorphous when studied by conventional diffraction methods. The amorphous behavior is attributed to substantial acid anion incorporation into the coating during film growth. The extent of acid anion contamination is determined primarily by the nature of the electrolyte and to a much lesser extent by the anodizing conditions [137, 138, 152]. The sulfate content, generally expressed as SO_3, of anodic films formed in sulfuric acid solutions is between 10 and 17% [138, 143, 153, 154, 155, 156, 157]. For films prepared in phosphoric acids, the content of PO_4^{2-} ions ranges from 6 to 8% [143, 155, 158]. Anodic coatings

contain 2 to 9% oxalate when formed in oxalic acids [154, 155, 157]. About 0.1% chromate was quoted for oxide films obtained from chromic acid electrolytes [154, 155]. The acid anion content is relatively high in the region adjacent to the pore, higher in the intermediate region, and decreases significantly to a relatively low level in the inner region [159, 160, 161].

Pullen [154] has reported 1 to 15% water content for films formed in sulfuric and oxalic acid solutions, whereas the oxide coatings prepared in chromic acid were essentially anhydrous. Edwards and Keller [162] found 1 to 6% water in films formed in sulfuric acid. IR spectra of anodic coatings also confirm the presence of hydrated alumina [36, 37, 141, 142, 143, 144, 163], though there appears some arguments about the hydration state.

Studying the specific surface area of anodic coatings, Baker and Pearson [164, 165] observed considerable disagreement between values estimated from gas adsorption and wide-line NMR spectroscopy. They concluded that the anodic coating consists of an array of microcrystallites estimated to be about 2.5 nm in radius and that gas adsorption analyzes only the major pore surfaces, but NMR analyzes the microcrystallite surfaces as well. Although the direct observations of ultramicrotomed sections of anodic films do not show the presence of crystalline alumina [166, 167], both porous and barrier layers may undergo crystallization upon further exposure to the electron beam, forming α-Al_2O_3 [168], γ-Al_2O_3 [148, 149, 151], or γ'-Al_2O_3 [147, 150]. It is not yet clear whether this latter structure is genuine or not. Microcrystallites ranging from 2.0 to 3.0 nm have

been reported [148, 167, 168, 169, 170]. The crystallization proceeds more rapidly in the inner region nearest to the cell boundary [160, 169, 170, 171], indicating that the film material is more compact and consists of relatively pure alumina.

The experimental data suggest that the film material of oxide coatings consists of alumina microcrystallites of a few nm in size which are too small to be detected by conventional diffraction methods. Therefore, the film material is generally regarded as amorphous. Two regions in the oxide coatings can be distinguished by the state of acid anion incorporation into the film. The inner region adjacent to the cell boundary of the porous layer and extending to the metal/oxide interface of the barrier layer is composed of relatively pure alumina, while the outer region close to the pore consists of an agglomeration of acid anion contaminated and partially hydrated alumina microcrystallites, as shown schematically in Figure 2-13. The ratio of the inner to outer region depends first on the nature of the electrolyte and second on the anodizing conditions employed. Microcrystallites comprising the outer region are probably held together by a hydrogen-bonded intercrystallite magma, which consists of alumina, acid anion, and molecular water [108].

2.3.4 Formation of Porous-type Coatings

2.3.4.1 Pore Initiation

Porous anodic films are generally formed under constant voltage conditions because dimensions of the oxide cell and hence properties

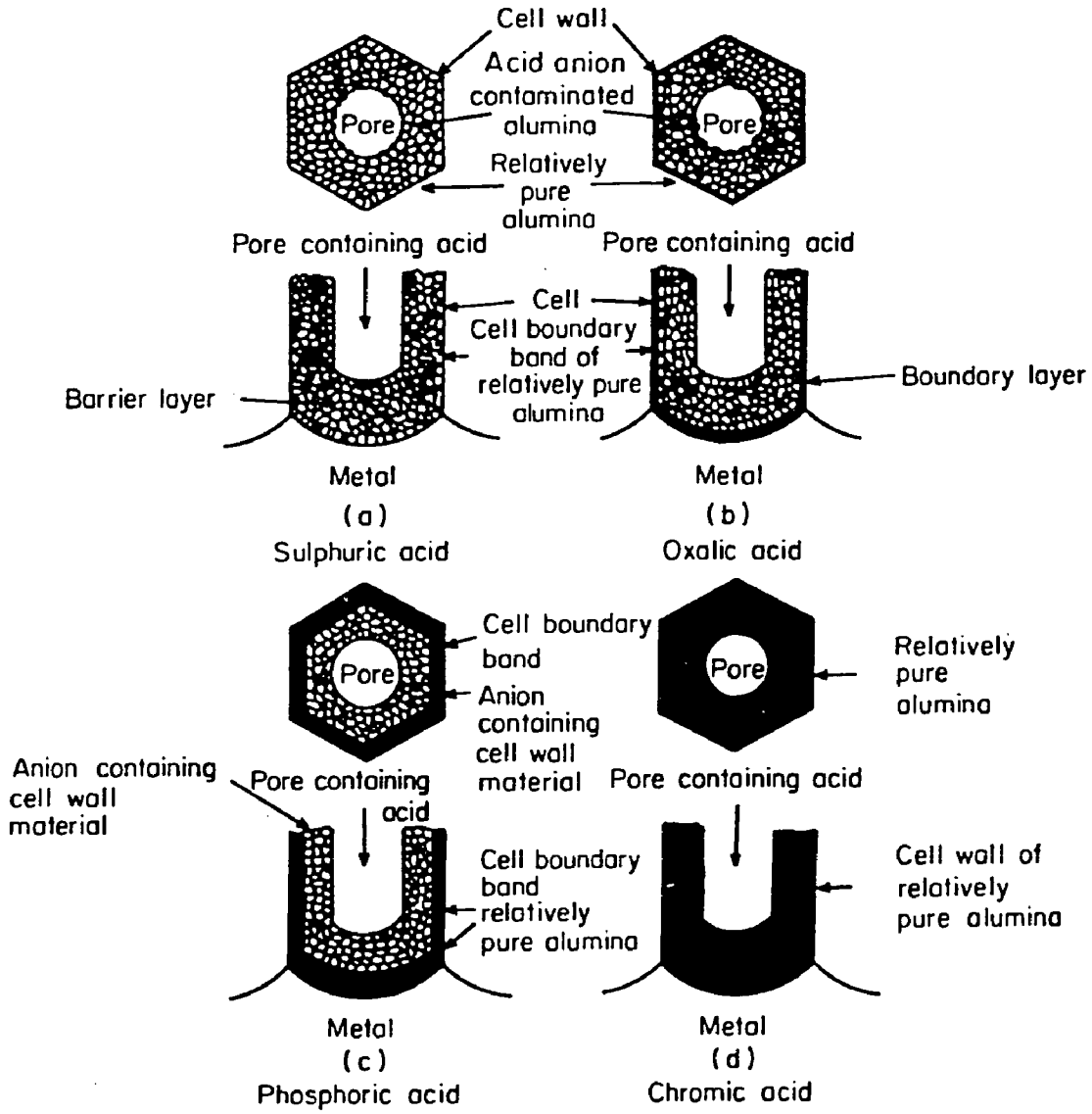

Figure 2-13. The plan and sectional views of cell structure for films formed in each of the major acids: (a) sulfuric; (b) oxalic; (c) phosphoric; and (d) chromic acid. The cell comprises acid anion contaminated film material adjacent to the pore and relatively pure alumina where cells meet (taken from [171]).

of oxide coatings are determined by the applied voltage. Figure 2-14 shows schematically the current density-time transients for the formation of both porous and barrier coatings under constant voltage mode [99]. There is an identical initial current surge, followed by a rapid fall in current density for both coatings. At point A, the two curves begin to diverge. The barrier film current density continues to fall exponentially, while the porous film current density, after a short period of continued decrease, begins to increase to a steady-state value. The final current densities for these two coatings differ widely. The final barrier film current is mainly electronic current, usually known as leakage current, while the final porous film current is almost completely ionic. Pore initiation occurs at some point close to A, and a decrease in the barrier layer thickness at this point is required for the rise in the current density. This behavior has been examined by Hunter and Fowle [114], as shown in Figure 2-15 for a 15-V coating produced in 15% H_2SO_4 at 21°C.

The time scale and the current density changes involved in these current-time transients are dependent upon the voltage applied and the electrolyte [138, 172]. The minimum current density occurs earlier the higher the applied voltage and the more acidic the electrolyte. The value of this minimum current density is larger the greater the applied potential, the lower the pH of the electrolyte, and the higher the bath temperature. This behavior is also reflected by the unit barrier layer thickness, as shown in Table 2-2. The unit barrier layer thickness decreases with an increase in acid strength, bath temperature, applied voltage, and anodizing time [172]. These

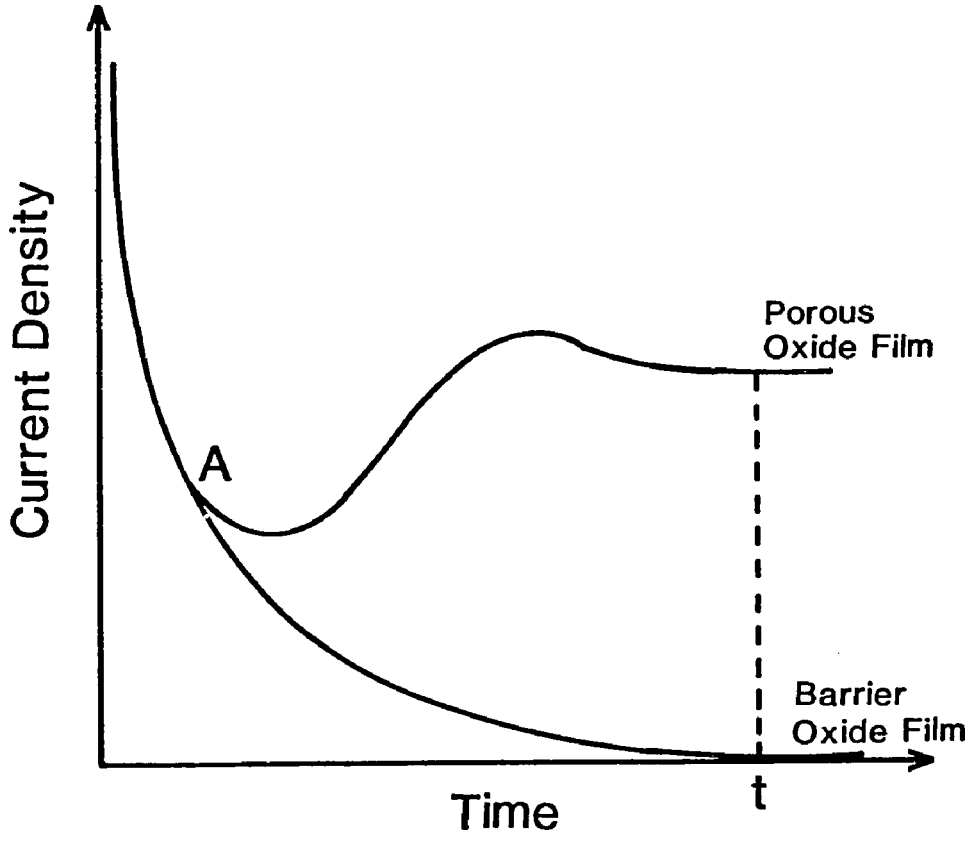

Figure 2-14. Current density-time transients for the formation of a barrier-type and a porous-type anodic film on aluminum. Point A represents the point at which divergence of the two curves occurs, and hence may be related to pore initiation phenomenon. Time t is typically 25 seconds for oxide film produced in 15% sulfuric acid at 15 volts (taken from [99]).

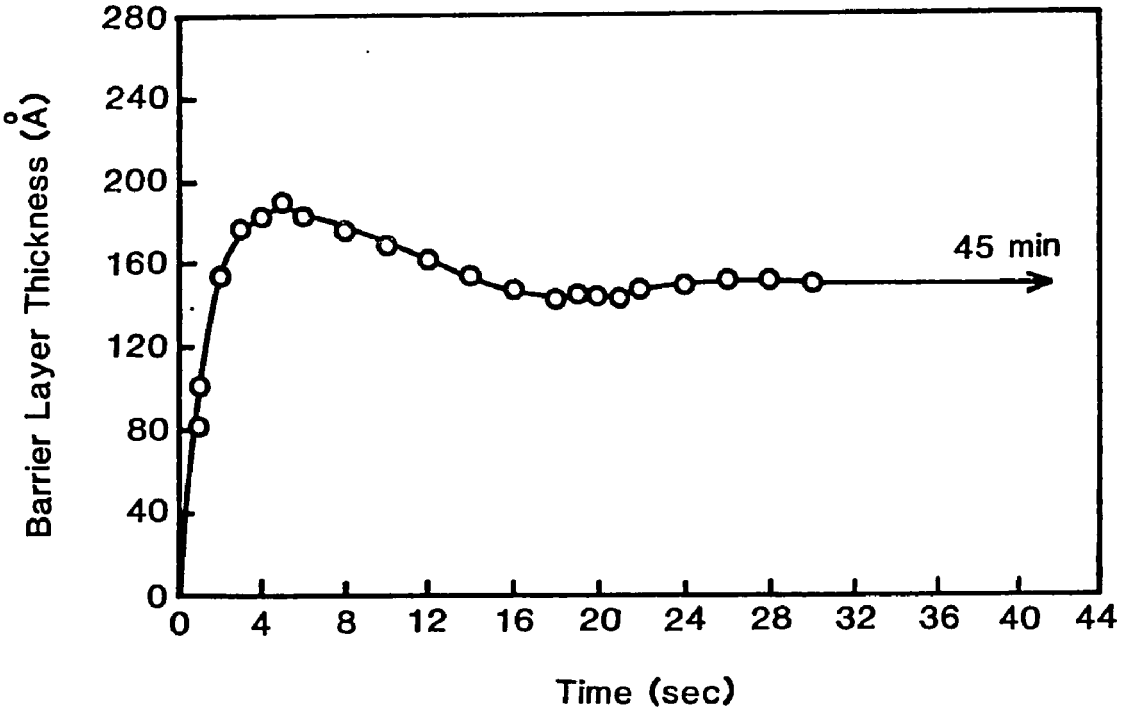

Figure 2-15. Variation of barrier layer thickness of a 15-V coating formed in 15% H_2SO_4 at 21°C with anodizing time. Barrier layer thickness remains constant after about 25 seconds (taken from [114]).

findings are in contradiction with Hunter and Fowle [114, 173] who found the unit barrier layer thickness to be independent of the applied voltage and the anodizing time (Table 2-1). In either case, the unit barrier layer thickness of porous-type coatings is smaller than that of barrier-type coatings (14 Å/V). The smaller unit barrier layer thickness of porous-type coatings indicates that the barrier layer is not thick enough to prevent the current from flowing. Thus, film growth can continue.

How and where the pore initiation starts are ambiguous in the study of the current-time transient. A great contribution to the formation of porous films at the initial stage was made by the research group at the University of Manchester [102, 126, 166, 167, 174, 175]. Due to the current surge in the constant voltage mode, the initial film growth rate is so high that detailed information on the pore initiation processes cannot be obtained. In order to avoid this difficulty, the anodic oxidation was carried out in the constant current density mode so that the initial film growth rate was under control and the sequences in the development of the porous anodic film could be observed more clearly. These sequences are revealed by the examination of stripped anodic films, carbon replicas of fracture sections, and ultramicrotomed sections in the transmission electron microscope. Figure 2-16 schematically shows the sequence of events [174]. The initial film growth is relatively uniform. With further anodization, the film grows preferentially above the pre-existing metal ridges and a flattening of the metal/oxide interface occurs (Figure 2-16b). These ridges may be from the cell boundaries

Table 2-2. Dependence of the Unit Barrier Layer Thickness upon the Anodizing Conditions and Electrolyte (taken from [172]).

Electrolyte	Temp. °C	Forming Voltage V	Total Charge Passed Coul/cm^2	Unit Barrier Thickness Å/V
15% H_2SO_4 (pH=0.02)	17	15.3	2.8	9.3
	17	15.3	20.0	9.0
	17	21.4	19.9	8.3
	25	15.2	19.7	8.9
	25	21.1	19.7	7.8
7.5% H_2SO_4	25	11.3	2.8	9.3
	25	11.3	19.7	9.0
	25	15.3	19.7	9.0
	25	21.2	19.7	6.6
H_2SO_4 + $NaHSO_4$ (pH=0.23)*	25	15.7	5.7	9.2
18.36% $NaHSO_4$ (pH=0.36)*	25	15.8	2.8	9.2
$NaHSO_4$ + Na_2SO_4 (pH=1.19)*	25	15.8	0.9	10.1

* SO_4^{2-} concentration same as in 15% H_2SO_4.

introduced by electropolishing [166, 167] or from the ridges introduced by mechanical polishing [174] and scratching [175]. The greater flaw density present in the thin naturally-produced film above ridges offers less resistance to current flow. As the oxide along the ridges thickens, the current shifts to the thinner low resistance film regions between protuberances. Pores are developed at these areas with the associated scalloped appearance of the metal/oxide interface (Figure 2-16c), as aluminum is consumed during oxidation. The appearance of scalloping is necessary in order to maintain a uniform field strength within these areas. Further pore development occurs at some preferred thin areas (Figure 2-16d), resulting in the spreading of scalloped regions in a radial manner at the metal/oxide interface. Consequently, the pore diameters increase until the scalloped regions merge to create the approximately hexagonal close-packed arrangement of cells. The incipient pores at non-preferred sites cease to grow at this stage. During further anodization the cell film material thickens relatively uniformly with the pore and cell diameters remaining constant (Figure 2-16e). The growth of oxide films at this stage is in a steady-state condition.

2.3.4.2 Growth Mechanism

Siejka and coworkers [176, 177] studied oxygen transport processes during anodization by nuclear microanalysis and ^{18}O tracer techniques. They found that the excitation curves are nearly identical for oxide film formed in an ^{18}O enriched solution and duplex films obtained by reoxidation of the ^{18}O enriched film in ^{16}O solution for

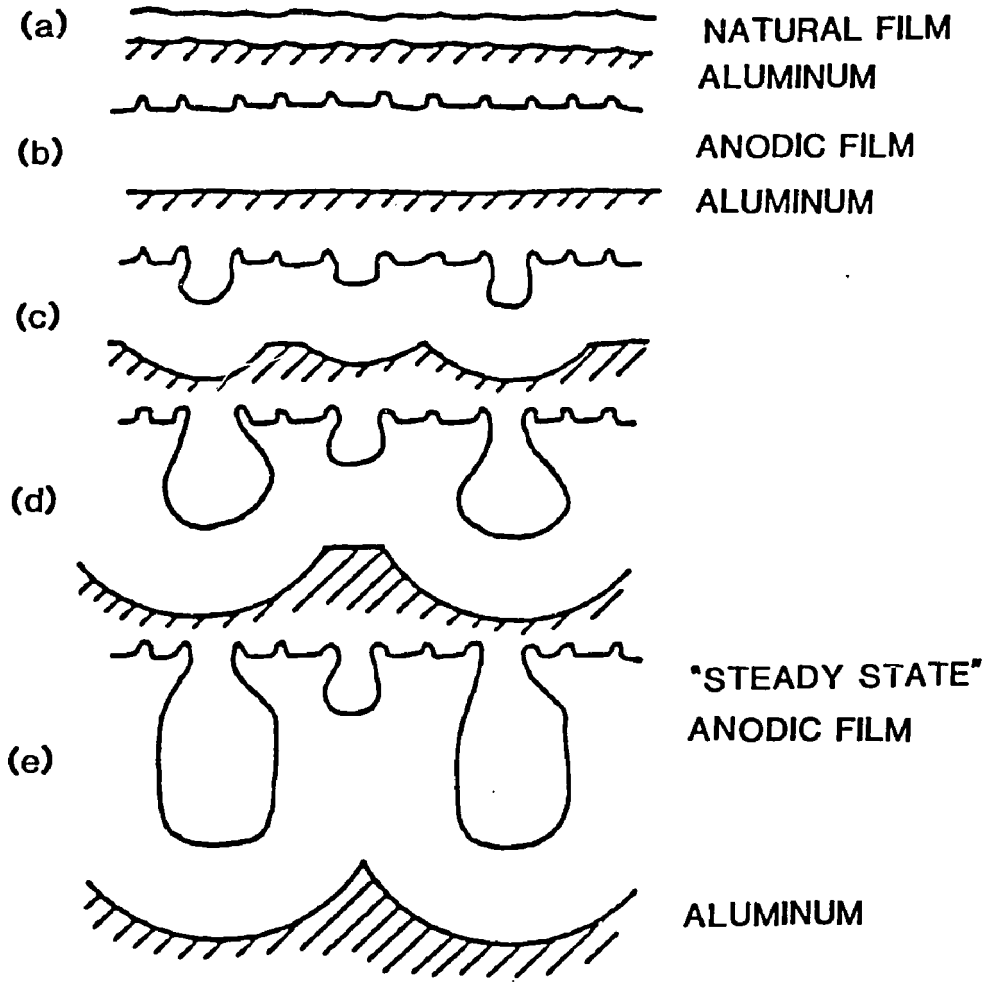

Figure 2-16. Schematic representation of cross-sections of films showing the structural changes during the early stages of growth: (a) the natural air-formed oxide film; (b) the development of protrusions and flattening of the metal/oxide interface; (c) pore initiation; (d) further pore growth and spreading of the scalloping at the metal/oxide interface; and (e) the steady-state film with certain pores propagating, others having terminated (taken from [174]).

53 and 113 seconds. The nearly identical excitation curves imply that most of the ^{18}O atoms exist at the top of the oxide films. Diggle et al. [131] analyzed the $^{35}SO_4$ concentration of stripping solutions used to dissolve duplex films as a function of dissolution time. The films were prepared by varying exposure times to radioactive $H_2{}^{35}SO_4$ and nonradioactive H_2SO_4 electrolytes. They concluded that the electrolyte used last characterized the oxide layer lying nearest the metal. Using pore-filling techniques, Dekker and Middelhoek [178] also found that the first formed oxide was at the top of the oxide coating. These results suggest that the oxidation takes place at the metal/oxide interface via the inward migration of oxygen-carriers to the metal surface.

During the course of steady state anodization the thickness of the barrier layer remains nearly constant, and the dissolution rate of oxide of the pore bases should equal the oxide growth rate. It has been found that the dissolution rate of the oxide at the bottoms of pores is about 10^4 to 10^5 times higher than the purely chemical dissolution rate [121, 134, 176]. In order to account for this high dissolution rate, Hunter and Fowle [173] assumed, for anodization carried out at 21°C in a 15% H_2SO_4 electrolyte using a constant current density of 1.29 amp/dm^2, that the acid at the pore bases should have a concentration of approximately 51% at its boiling point of 124°C. This thermal mechanism can not be entirely acceptable since small changes in the bulk temperature or concentration of anodizing bath significantly affect the current density and hence the dissolution rate in the constant voltage mode.

Several researchers [102, 132, 134, 135, 136, 176, 177, 179, 180] have postulated that the high dissolution rate at the pore bases is a field-assisted process. Hoar and Mott [179] suggested that the lattice OH^- ions at the oxide surface formed in the presence of acid are forced to move through the oxide towards the metal/oxide interface where they react with metal ions and release H^+ ions which move back through the oxide. This process facilitates the successive removal of the surface Al ions into the solution. O'Sullivan and Wood [102] considered that the applied field across the film polarizes the Al-O bonds at the outer surface of the barrier layer by increasing the bond length. This bonding is weakened further by hydrogen bonding of the O^{2-} ions with OH^- ions momentarily trapped in the lattice prior to moving on or decomposing into O^{2-} and H^+ ions, facilitating Al^{3+} dissolution. The dissolution rate of oxide at the pore bases is also enhanced by the local heating effect. Cherki and Siejka [176] and Siejka and Ortega [177] have shown that in addition to the field-assisted decomposition of oxide in the barrier layer, there is a large fraction of Al cations moving interstitially through the barrier layer and discharging directly into the solution.

The growth mechanism based on the geometrical model of oxide films cannot satisfactorily explain how acid anions are incorporated into the film. Murphy and Michelson [113, 115, 116] have hypothesized, in accordance with their colloidal gel model, that aluminum ions migrate under the influence of the anodizing field from the metal through the barrier layer to the transition region where they react with oxygen or hydroxyl ions to form essentially anhydrous

alumina. The oxygen carriers are transported by the anodizing field from the solution through the intercrystallite region to the transition region. This barrier layer is subsequently modified by the hydroxyl ion, water, and acid anion to a structure which consists of an agglomeration of submicroscopic particles with a highly developed internal surface between, among and around the submicrocrystallites of alumina. Thereby, the effective thickness of the barrier layer is kept constant. The acid anions play an important role in stabilizing the surface of microcrystalline alumina converted from the barrier layer by preventing or decreasing drastically the rate of crystallization of alumina gel. Consequently, anodic films are amorphous according to the usual crystallographic tools. Moreover, these anions are capable of forming hydrogen-bonded complex surfaces containing water, protons, and anions through which the ionic conduction occurs at relatively high rates.

In summary, the most probable growth mechanism as drawn from the experimental data and hypotheses discussed so far is the following. The inner layer of the barrier layer grows at the metal/oxide interface via inward migration of O^{2-} or OH^{-} ions. The Al^{3+} ions are transported by the anodizing field from the metal through the inner region to the outer region of the barrier layer, where they may pass directly into the solution or react with oxygen-carriers forming alumina particles which are stabilized by the acid anions. The oxide at the outer layer close to the pore base is decomposed by a field-assisted process; meanwhile, the oxide at the inner layer adjacent to the inner layer/outer layer interface is transformed by the water,

hydroxyl ion, and acid anion to acid contaminated alumina microcrystallites. These processes (formation, dissolution, and transformation) must proceed at the same rate in order to maintain a constant thickness of the barrier layer during the steady-state anodization. The extent to which the acid anion can penetrate into the barrier layer depends on the nature of the electrolyte and, to a much lesser extent, on the anodizing conditions.

2.3.5 Sealing of Anodized Aluminum

When the porous oxide films are heated in media such as water, steam, or certain salt solutions, they undergo a reduction in porosity and a change in crystal structure, and show improved resistance to staining. This process is usually known as "sealing". It is generally agreed that the most satisfactory operating pH range of the sealing solution is between 5.5 and 6.5 [111]. Only after this treatment does the oxide coating have commercial value for it not only improves the corrosion resistance of aluminum but, for dyed samples, seals the dyestuff in the film and reduces external influences (bleaching, light fastness, etc.). Sealing theories and applications have been reviewed by several authors [2, 49, 99, 108, 111, 157] [181, 182, 183, 184].

It is generally accepted that sealing of a porous oxide film in water results in at least a partial plugging of pores by a dissolution/precipitation process [99, 108, 157, 184, 185]. This mechanism of sealing is generally referred to as pore plugging in the literature and is schematically shown in Figure 2-17. The pore

plugging phenomenon was confirmed positively by electron micrographs [157, 185]. The most probable sealing mechanism is laid out below.

1. Hot water is able to penetrate very rapidly into the pores of the film and into cell wall oxide initiating oxide dissolution. This dissolution process is associated with the replacement of incorporated acid anions by hydroxyl ions, lowering the pH near the oxide/liquid interface. Hence, the transport distances for aluminum ions in the pores are increased appreciably.
2. Precipitation of hydrated aluminum ions takes place within the pores, resulting in plugging the pore mouths and partially blocking the intercrystallite region. This process is most extensive in the outer region where a nearly neutral pH is maintained by exchange with the bulk solution. Precipitation is favored within this pH range. The pH gradient across the film results in a decrease in the precipitation rate with penetration depth.
3. Crystallization of precipitated hydrated alumina to pseudoboehmite or more probably boehmite occurs on the exterior film surface, where acid anions which may inhibit crystallization are rapidly dispersed to the bulk solution. The crystalline hydrated alumina on the surface is generally referred to as "sealing smut".
4. An intermediate layer of featureless morphology develops beneath the surface crystallites and grows progressively

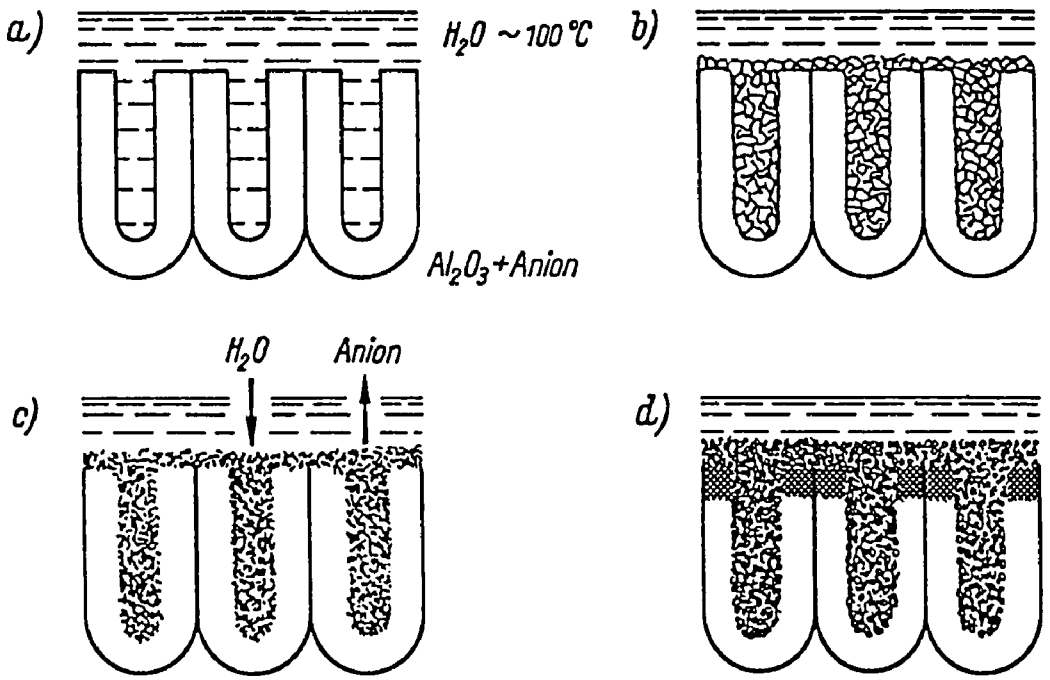

Figure 2-17. Sealing mechanism by pore plugging: (a) unsealed coating; (b) pore closure by a dissolution/precipitation process; (c) reaction rate controlled by diffusion of water into film and anions into bulk solution after pores are closed; and (d) recrystallization of boehmite in precipitate, starting at external surface, intermediate layer formed by diffusion process (taken from [157]).

towards the metal surface.

5. Agglomeration takes place within the cell walls and the precipitated material in the pores during prolonged sealing.

In general, the pore closure rate is higher for oxide films formed in sulfuric acid than in oxalic acid, while oxide coatings obtained in phosphoric acid exhibit the lowest rate. The closure rate differences are partially due to pore sizes of the oxides (Table 2-1) but are more likely related to the adsorption of acid anions which affects the initial precipitation. Pores in sulfuric or oxalic coatings are completely plugged in a few minutes. As soon as the pores are completely closed, the sealing reaction is controlled by the diffusion of both water from bulk solution into pores and acid anions from pores to the bulk solution. Both the thickness of the intermediate layer and quantity of sulfate released into the sealing solution from sulfuric coatings increase nearly exponentially with sealing time [157], confirming the diffusion-controlled process.

The sealing theory proposed by Murphy [115] considers the migration of hydroxyl ions through the intercrystallite region into the cell wall oxide. These hydroxyl ions replace acid anions incorporated there and neutralize the proton space charge. This process produces relatively inert surfaces of gibbsite or bayerite which block the entrance to the interior of cell walls, as shown schematically in Figure 2-18. The adsorption capacity of anodic coatings is, therefore, significantly reduced. The presence of phosphate ions in the sealing solution reduces the sealing quality of

sulfuric coatings due to their strong adsorption onto the surface of oxide. They replace sulfate ions and inhibit the migration of hydroxyl ions into the intercrystallite region so that the formation of inert hydrated alumina is inhibited. The pore plugging mechanism is rejected in his hypothesis.

Diggle et al. [99] suggests that both theories could be regarded as complementary to each other. Murphy's theory is applicable to the initiation period because the dissolution/precipitation process is strongly affected by the anions either released from oxide coatings or present in the sealing solution, while the pore plugging mechanism is applicable for sealing times longer than the initiation period.

Solutions of various metal salts such as nickel acetate and potassium dichromate are widely used for sealing anodic oxide coatings [183]. It is generally agreed that in addition to the formation of hydrated alumina, metal salts when absorbed into the oxide coating are hydrolyzed and precipitated in pores as hydroxides. These hydroxides may participate in plugging pores. Wood and Marron [186] have determined with the electron microprobe the uptake of nickel by 45 μm thick coatings formed in sulfuric acid as a function of sealing time and electrolyte temperature (figure 2-19). The results suggest that sealing solution may reach the pore bases relatively rapidly. There is little change in the nickel profile after about one minute sealing time, indicating that pores are probably completely plugged within this period. The rate of the sealing reaction is highest in the outer region of the film because most of the nickel hydroxide precipitates are located towards the outer surface of the coating. Additional

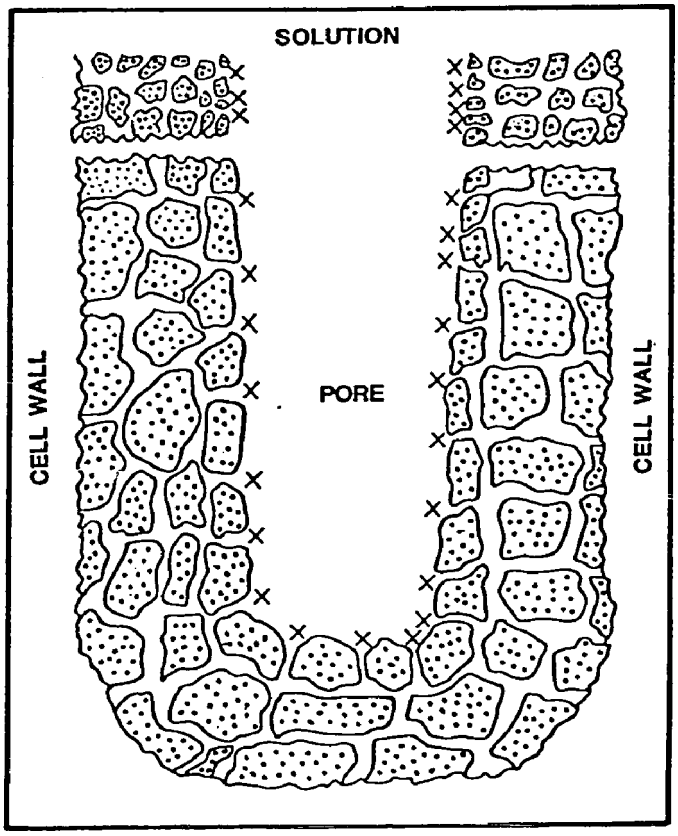

Figure 2-18. Murphy's hypothesis of sealing. Entry and exit of soluble materials can be blocked by modification of surfaces at points marked X (taken from [115]).

sealing reaction is controlled by diffusion. The pore diameter on the coating surface is greater the higher the anodizing temperature due to the increasingly high rate of chemical dissolution. The time required for pore closure is therefore longer for oxide coatings formed at higher bath temperatures. Consequently, both the amount of nickel uptake and the penetration depth of nickel hydroxides are greater. These results also support the pore plugging mechanism.

2.4 Abrasion Resistance of Anodized Aluminum

Anodically produced oxide coatings are much thicker than the natural surface oxide films and, thus, yield a significant increase in the abrasion resistance of aluminum surface. This increased resistance to abrasion is very valuable in many applications where rubbing and frictional contacts must be withstood. George and Powers [187] and Campbell [188] have listed more than 50 applications for hard anodic coatings on aluminum covering aircraft, marine, vehicle, and architectural industries.

The hardness values of good, hard anodic coatings generally range from 400 to 500 Kg/mm^2, which are very low in comparison with high-speed steel and hard chrome plate, their hardness values ranging from 950 to 1100 Kg/mm^2. However, the wear resistance of hard anodic coatings is normally equivalent to or exceeds the wear resistance of high-speed steel or hard chrome plate [188]. It is probably due to the low frictional coefficient of the oxide surface. Figure 2-20 compares the wear resistance of a hard anodic coating with hard chrome plate and cyanide-hardened and heat-treated steels [189].

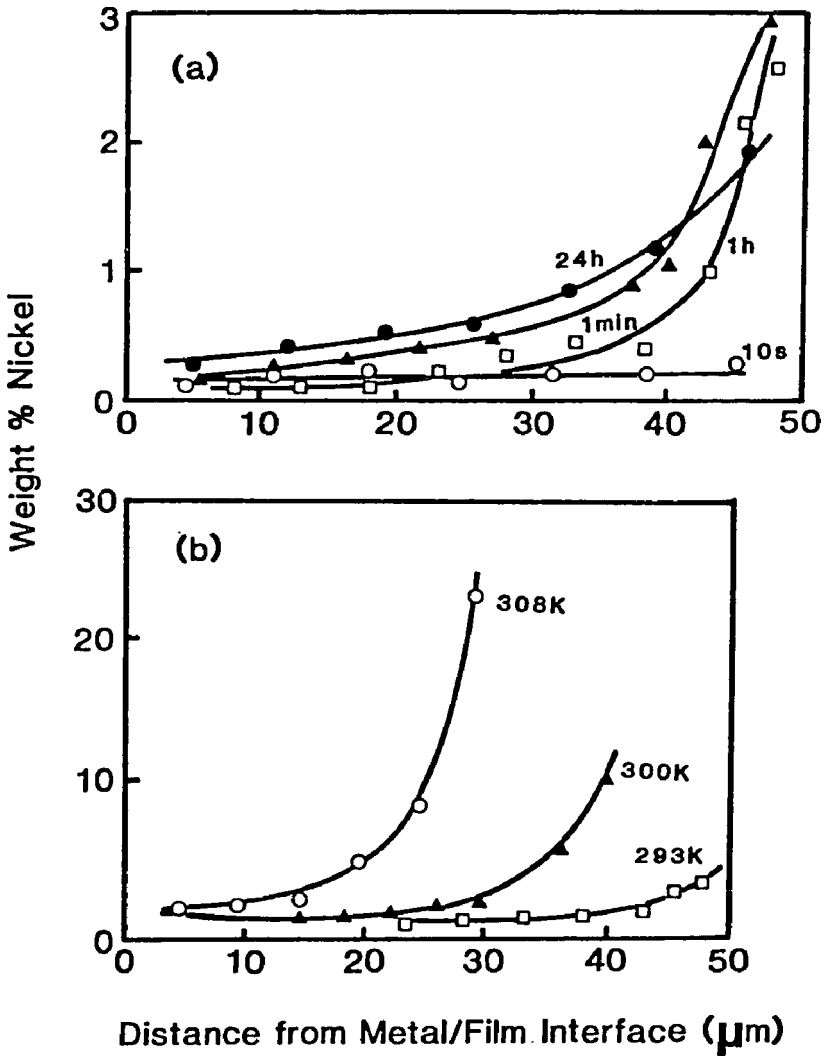

Figure 2-19. Nickel concentration profiles through oxide films formed at 25 amp/dm^2 in 1.5M H_2SO_4 for 56 minutes and then sealed at 373°K in a solution of nickel acetate (60 g/L) and boric acid (80 g/L), buffered to pH=5.9: (a) influence of sealing time on films formed at 293°K; and (b) influence of film formation temperature on subsequent uptake of nickel from sealing solution after one hour (taken from [186]).

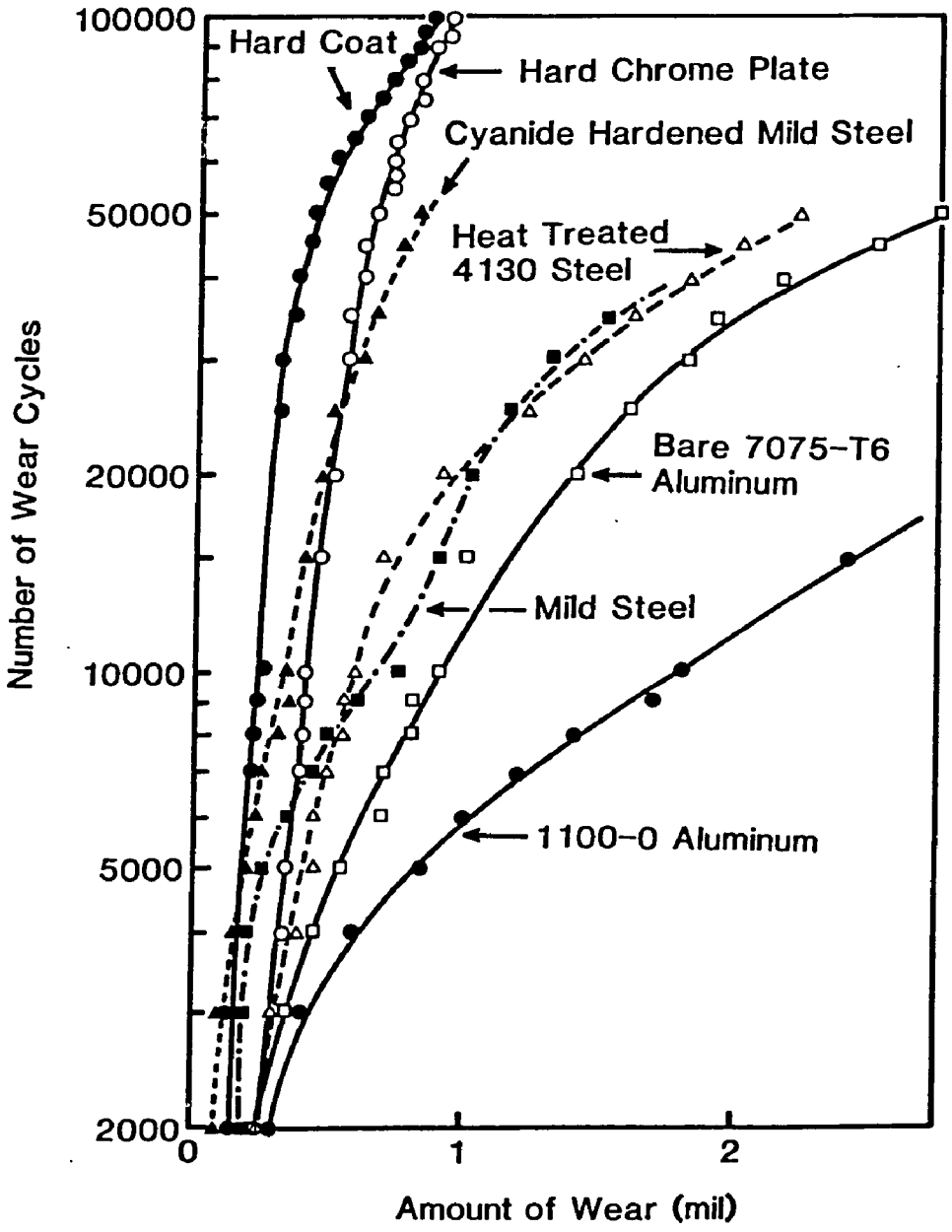

Figure 2-20. Comparison of wear resistance of M.H.C. hard coating with that of other materials and coatings. Data from Taber abrasion tests using CS-17 wheels with 1000 g load (taken from [189]).

Many techniques have been developed so far for evaluating the abrasion resistance of anodized aluminum. These techniques may be divided into three categories: (1) impact-type, such as the abrasive jet method; (2) rubbing-type, such as Taber and Erichsen abrasers; and (3) scratch-type. The impact-type method is essentially a measure of erosion resistance and the rubbing-type methods for two-body abrasion resistance, whereas the scratch-type methods generally serve as modeling techniques for abrasive wear studies in tribology. Misra and Finnie [72] found that the effects of various variables such as the applied load, the distance traveled, the relative hardness of abrasive to material, and the size of abrasive particles are almost the same for two-body abrasion, three-body abrasion, and erosion. Two-body abrasion is similar to small angle erosion and three-body to large angle erosion. It was concluded by them that the relative rankings of materials for one of these wear processes could be used for other processes under certain conditions. A comparison of literature data of abrasion resistance of anodized aluminum as determined by various techniques is, therefore, very interesting and informative.

2.4.1 Impact-type Method

Schuh and Kern [190] developed a method of measuring the abrasion resistance of paints, varnishes, and lacquers in the form of thin films. This method was modified and applied to anodic coatings by Arlt [191] and Edwards [192]. Their work formed the basis for the standard ASTM and British Standard abrasive jet techniques, respectively.

The abrasion test consists essentially of admitting a stream of abrasive particles with controlled flow rate into a rapidly flowing air stream under controlled pressure and allowing the uniform mixture of air and abrasive particles to impinge on the specimen. The end point of the test is indicated by the appearance of a dark spot 2 mm in diameter in the center of the wear pattern. The weight of abrasive or the time required for the abrasive to penetrate the coating is a measure of abrasion resistance. Specific abrasion resistance is expressed in grams or seconds per unit thickness of the coating and, thus, permits direct comparison of the results from films of varying film thickness.

The abrasion resistance measured by this technique may be affected by a number of factors [192, 193]. They include the distance and angle between the nozzle and specimen, the mixing length of the jet, the air pressure, the flow rate of abrasive, the surface roughness of the bore of outer tube and the dimension of the inner tube, and the size and nature of abrasive particles. Therefore, it is not surprising that tests carried out with different jets made to the same design often yield varying results. Although the agreement between different laboratories employing different sets of apparatus is relatively poor, this technique is very useful for comparative measurement of anodic coatings.

It is understandable that the abrasion resistance of anodic films is greater the thicker the film, but the specific abrasion resistance is dependent upon the anodizing conditions. Arlt [191] and Spooner [194] found that the specific abrasion resistance increased with

increasing anodizing time to a maximum value and then decreased with prolonged time (Table 2-3). Laszewska [195] did not obtain any definite trend for this effect, while Deal [196] observed a constant specific abrasion resistance for hard anodic coatings on 1100 alloy, as shown in Figure 2-21. The specific abrasion resistance decreases with an increase in the electrolyte temperature for conventional anodic coatings (Table 2-4), and it appears independent of temperature from -8 to 0°C for hard anodic coatings [195]. Edwards [192] found that the specific abrasion resistance is slightly increased by raising the current density from 0.9 to 1.0 amp/dm^2 and then remains constant up to 1.1 amp/dm^2. Decreasing the strength of the electrolyte increases the specific abrasion resistance of anodic coatings [8, 197]. An example is shown in Figure 2-22. The specific abrasion resistance also depends on the alloy constituents and the nature of the anodizing electrolyte [1, 155, 198]. These effects are illustrated in Tables 2-5 and 2-6, respectively.

Sealing treatments convert the hard anhydrous alumina to the soft boehmite and, hence, reduce the abrasion resistance of oxide films. The reduction in the abrasion resistance depends on the nature of the sealing solution employed as well as the degree of sealing reaction. Figure 2-23 shows the effect of sealing solution on the abrasion resistance of coatings formed in sulfuric acid [191]. The unsealed coatings have better abrasion resistance than either sodium dichromate or water-sealed coatings, whereas the water-sealed coatings have the lowest abrasion resistance at any thickness level. The effect of sealing time on the specific abrasion resistance of water-sealed

Table 2-3. Specific Abrasion Resistance of Anodic Coatings as a function of Anodizing Time.

Material	2S-1/2 H Alloy						Alumilite*			
Electrolyte	10% H_2SO_4						15% H_2SO_4			
Anodizing Time, min	10	20	30	40	50	60	10	20	30	60
Temperature, ^oC	35	35	35	35	35	35	21	21	21	21
Current Density, amp/dm^2	1.55	1.55	1.55	1.55	1.55	1.55	1.6	1.6	1.6	1.6
Coating Thickness, μm	4.1	7.6	11.7	15.2	13.7	14.0	6.5	11.5	18.0	39.8
Specific Abrasion Resistance, g/μm	8.0	11.3	14.5	15.5	16.3	14.9	12	15	17	14
Reference	[191]						[194]			

* 99.7% aluminum clad on 3S alloy.

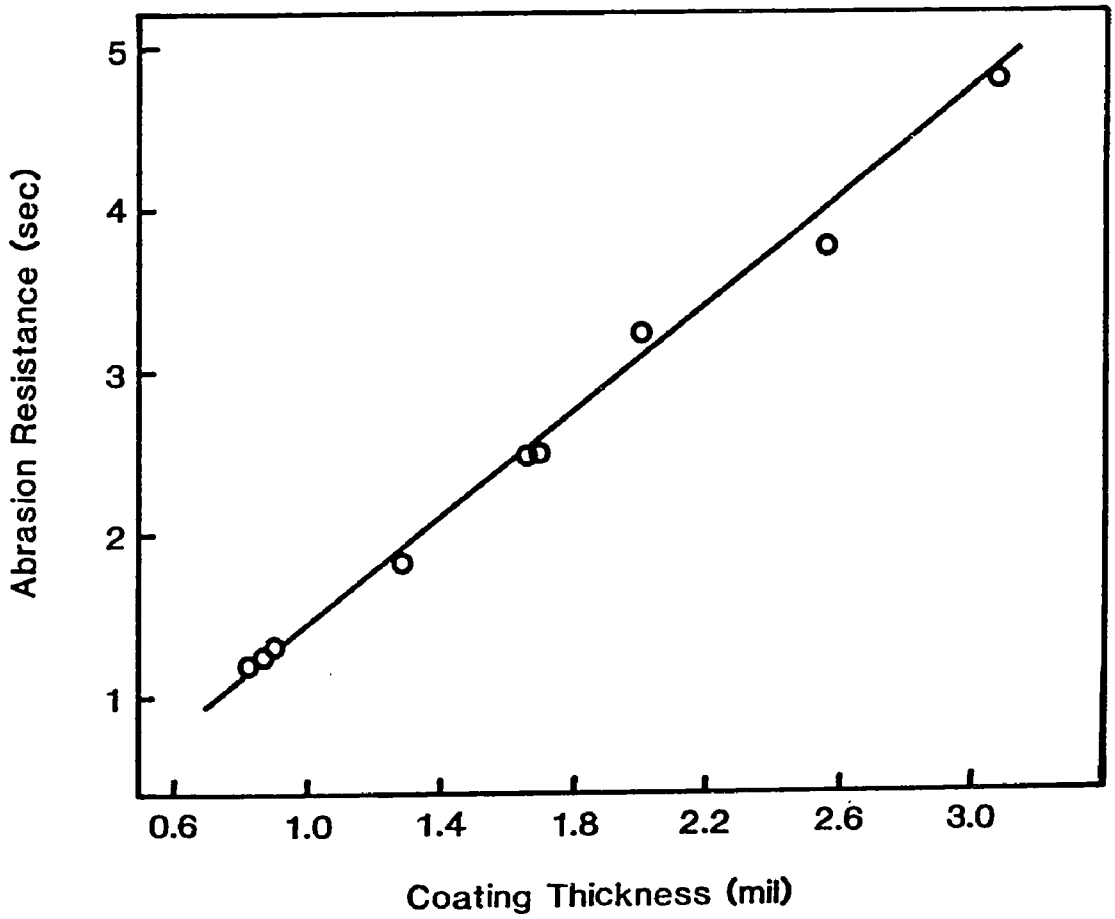

Figure 2-21. Linear dependence of abrasion resistance on the thickness of hard anodic coatings on 1100 alloy (taken from [196]).

Table 2-4. Effect of Electrolyte Temperature on the Specific Abrasion Resistance of Anodic Coatings on Commercial Purity (99.5%) Aluminum.

Electrolyte	4N H_2SO_4							3.3N H_2SO_4	
Temperature, ^oC	17	20	22	25	27	32	35	15.6	21.1
Current Density, amp/dm^2	1.0	1.0	1.0	1.0	1.0	1.0	1.0	1.6	1.6
Anodizing Time, min	30	30	30	30	30	30	30	20	20
Coating Thickness, μm	10.1	10.1	10.1	10.1	10.0	9.1	6.5	10	10
Specific Abrasion Resistance, g/μm	8.1	6.7	6.5	5.3	5.1	2.9	2.3	56	39
Reference	[192]							[197]	

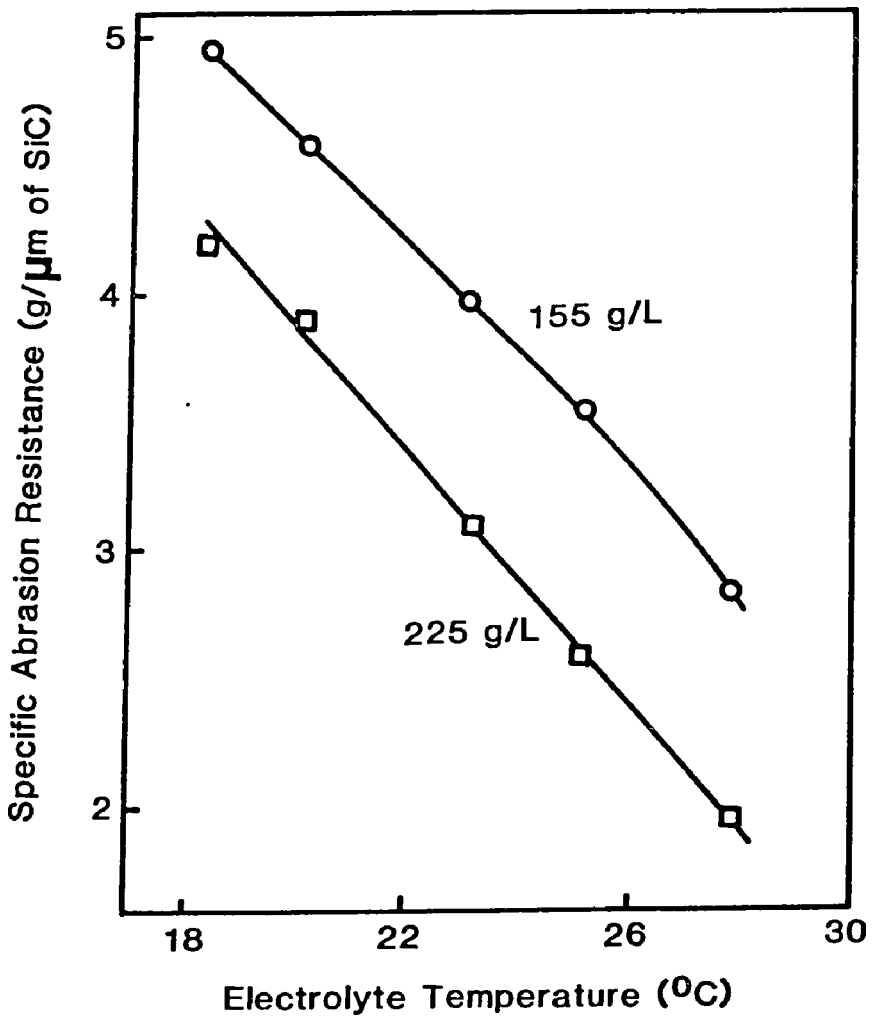

Figure 2-22. Effect of temperature and sulfuric acid concentration on the specific abrasion resistance of 25 μm sealed films on 5005 alloy. BS 1615 Jet Test method used at 70 L/min (taken from [8]).

Table 2-5. Specific Abrasion Resistance of Hard Anodic Coatings formed on Aluminum Alloys by Alumilite 726 process (taken from [198]).

Alloy	Coating Thickness, μm	Specific Abrasion Resistance, g/μm
1100	58.2	3.35
3003	56.6	3.43
2024-T	52.6	1.42
5052	64.0	2.83
6061-T6	50.0	3.11
7075-T6	60.7	2.48

Table 2-6. Specific Abrasion Resistance of 25 μm Films Formed in Four Major Acids under Constant Current Density and Constant Voltage Anodizing Modes Respectively (taken from [155]).

Anodizing Conditions	Acid Types			
	Sulfuric	Oxalic	Phosphoric	Chromic
Acid Concentration, M	1.5	0.25	0.25	0.25
Temperature, ^{o}C	20	20	20	60
Constant Current:				
Current Density, amp/dm^2	150	150	100	150
Anodizing Time, min	60	60	105	90
Specific Abrasion Resistance, g/μm	26.6	36.1	28.3	17.3
Constant Voltage:				
Voltage, V	19	70	160	150
Anodizing Time, min	38	30	60	60
Specific Abrasion Resistance, g/μm	34.4	52.1	53.9	45.4

sulfuric films [194] is shown in Figure 2-24.

2.4.2 Rubbing-type Methods

There are two abrasers, namely Taber and Erichsen, widely used for determining the abrasion resistance of anodized aluminum. The specimen is placed on the turntable of the Taber abraser and subjected to the rubbing action of a pair of freely rotating abrasive wheels that are weighted with a specific load. The number of revolutions required to penetrate the coating is a measure of wear resistance and the wear rate is generally expressed as the reduction in thickness or weight loss per 1000 revolutions. Erichsen abraser involves a to-and-fro motion, under a constant load, of an abrasive paper band fastened to the periphery of a metallic wheel against the specimen. The wheel indexes forward by a small amount after each double movement to bring a completely new abrasive surface into play so that each portion of the abrasive paper is used once only and the clogging of abrasive paper by abrasive wear debris is eliminated. The wear rate is generally recorded as the reduction in thickness or weight loss per 100 double movements and the wear resistance is defined as the reciprocal of wear rate.

2.4.2.1 Taber Test Results

Figure 2-25 illustrates an initial nonlinear region followed by a linear relation of weight loss against the number of revolutions for conventional and hard anodic coatings on aluminum alloy 6061-T6 [198]. This behavior is similar to that observed in Figure 2-5. The wear

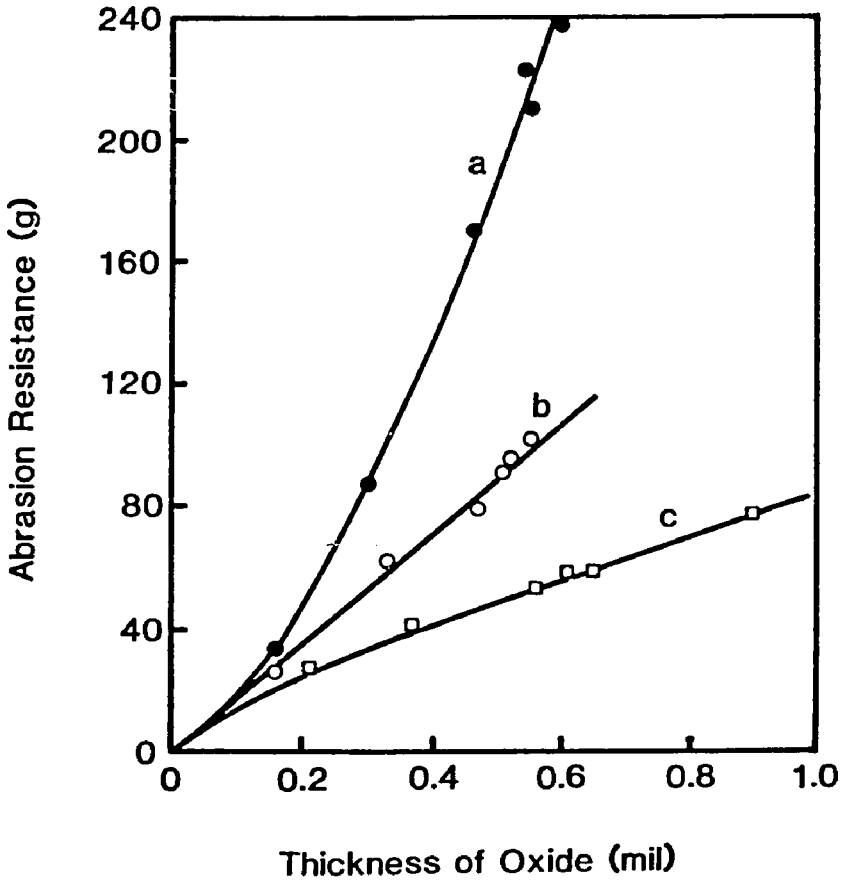

Figure 2-23. Relation of abrasion resistance to thickness for anodic coatings: (a) unsealed, (b) sealed in sodium dichromate solution, and (c) sealed in boiling distilled water. Anodic coatings were formed on 2S-1/2H alloy in a 10% H_2SO_4 bath at 95°F for various anodizing times (taken from [191]).

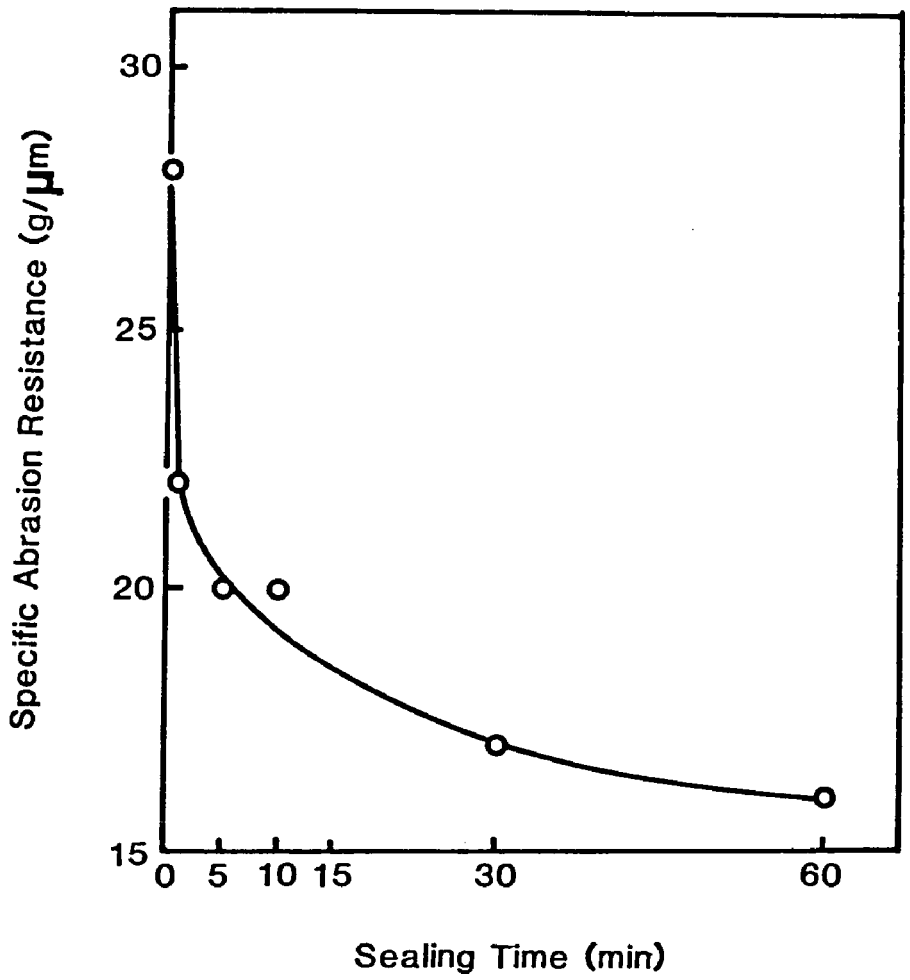

Figure 2-24. Effect of water sealing on the specific abrasion resistance of anodic films on Alumilite sheet formed in a 15% H_2SO_4 bath at 21°C and 1.6 amp/dm^2 for 30 minutes. Alumilite sheet is 99.7% aluminum clad on 3S alloy (taken from [194]).

rate of the conventional anodic coating is about twice as high as the hard coating. Results published by Hafer [199] illustrate the effects of alloy, electrolyte, and anodizing time on the wear rates of conventional coatings (Table 2-7). The highest wear rates were observed for chromic coatings on 2024 alloy and the lowest ones for sulfuric coatings on 3003 alloy. It is interesting to note that the wear rate decreases with increasing thickness, indicating an increase in the hardness of the coating with thickness. This behavior is in contradiction to Machlin and Whitney [200] who found that the wear rate increased with thickness for coatings obtained on aluminum alloys 2024-T3 and 6061-T6 (Figure 2-30a), and the effect was significantly greater for the former alloy than the latter. Koizumi, Ninagawa, and Ueda [201] used an electrolyte consisting of 100 g/L sulfuric acid and 15 g/L oxalic acid, covering temperature from -5 to 20°C and current density from 1 to 8 amp/dm^2. They found that the highest wear rate was obtained for the coating formed at the highest temperature and the lowest current density. Sealing reduces the wear resistance of hard anodic coatings by 10 to 20%, and the effect is more significant for water-sealed than for nickel acetate-sealed coatings [187].

2.4.2.2 Erichsen Test Results

The Erichsen abraser is usually used in conjunction with an eddy current operated film-thickness meter to exclude the influence of air humidity on the test results. An initial nonlinear region followed by a linear relationship in thickness reduction was again observed as a function of double movements under varying applied pressures and the

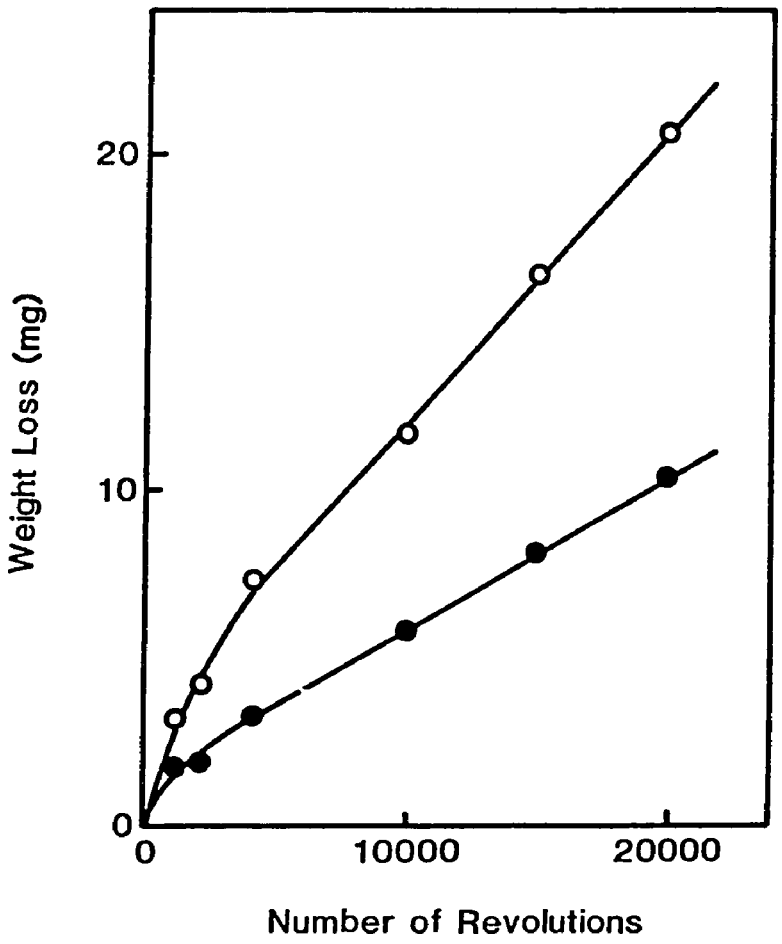

Figure 2-25. Dependence of weight loss on the number of revolutions of Taber abraser (CS-17 wheels, 100 g load) for conventional (open point) and hard (solid point) anodic coatings. Coatings were approximately 1.7 mils thick (taken from [198]).

Table 2-7. Dependence of Wear Rate on the Nature of Electrolyte and Anodizing Time. CS-17 Taber wheels used under 1000 g load (taken from [199]).

Alloy	Anodizing Time, min	Sulfuric Acid			Chromic Acid		
		Coating Thickness, mil	No. of Rev. to Failure	Wear Rate um/1000rev	Coating Thickness, mil	No. of Rev to Failure	Wear Rate um/1000rev
3003	20	0.24	855	7.13	0.04	57	17.82
	40	0.51	2480	5.22	0.08	143	14.21
	60	0.81	4748	4.33	0.14	278	12.79
2024	20	0.21	688	7.75	0.04	39	26.05
	40	0.46	1745	6.70	0.08	114	17.82
	60	0.73	3460	5.36	0.12	176	17.32

wear rate increased with contact pressure [202]. However, Witt and Gerken [203] found that the wear resistance of oxide films increases progressively from the coatings surface towards the metal/oxide interface. They also reported that the wear resistance of oxide films of equal thickness decreased in direct relation to increasing anodizing temperature.

Figure 2-26 shows the influence of anodizing temperature and sealing treatment on the wear resistance [202]. Oxide films sealed for 60 minutes exhibit higher wear rates than the unsealed ones and the effect is more striking at higher anodizing temperatures. The crossover of curves 2 and 3 was ascribed to the unsealed films consisting of a relatively soft exterior and a very hard inner zone. The reduction in the wear resistance of sealed oxide films also depends on the anodizing conditions, the effect being greater with increasing anodizing temperature and to a lesser extent with decreasing current density [202, 8]. Addition of oxalic acid to the sulfuric acid bath effectively increases the wear resistance of sealed oxide coatings, but the amount of added oxalic acid does not have any significant effect [202].

2.4.3 Scratch-type Methods

The method developed at the Siemens and Halske Research Laboratories [204] includes a hard metal pointer under a constant load moving to-and-fro on the surface of the oxide coating. When the film is penetrated, an electric relay circuit is closed which stops the motor operating the device. The number of double movements is taken

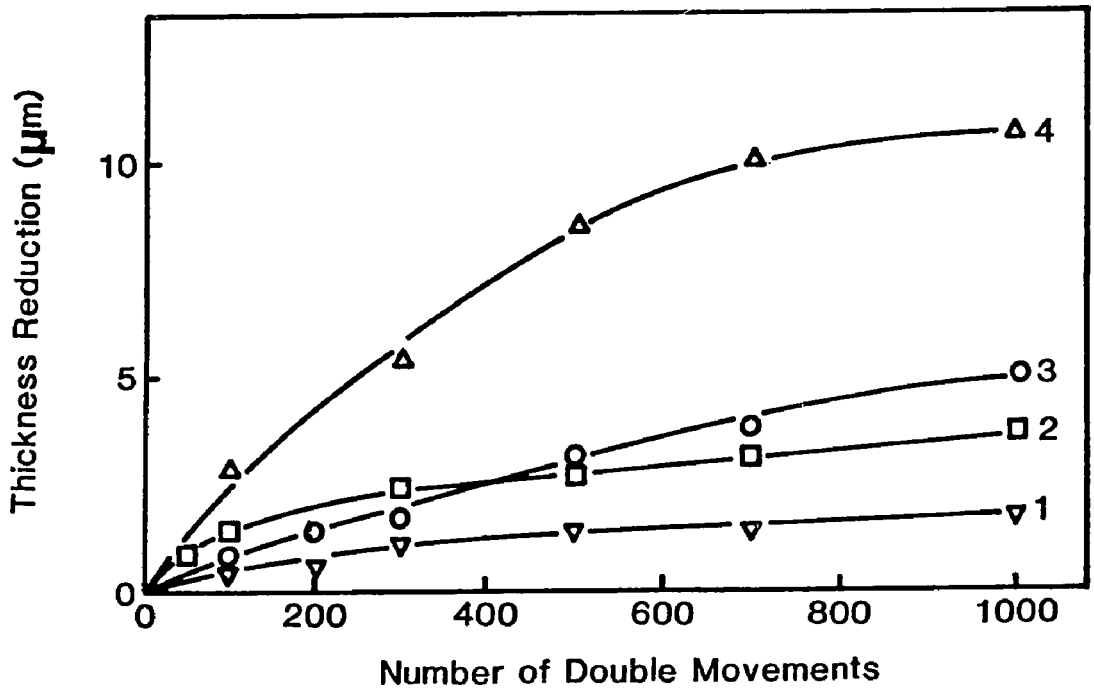

Figure 2-26. Influence of sealing on abrasion resistance. Basis material: AlMgl. Anodizing conditions: 200 g/L H_2SO_4, 1.5 amp/dm^2; (1) anodizing temperature 18°C, unsealed; (2) anodizing temperature 24°C, unsealed; (3) anodizing temperature 18°C, sealed in de-ion H_2O + 1g/L NH_4OAc; and (4) anodizing temperature 24°C, sealed in de-ion H_2O + 1g/L NH_4OAc (taken from [202]).

as the abrasion resistance. This value divided by the thickness of the coating is defined as the specific abrasion resistance. Taylor [205] has summarized the results obtained at Siemens and Halske as follows:

1. The abrasion resistance increases with film thickness.
2. The highest abrasion resistance is obtained by a d.c. dilute sulfuric acid process on 98-99% aluminum.
3. Oxide films produced in oxalic acid baths generally have low abrasion resistance.
4. The copper-containing alloys generally give lower abrasion resistance than copper-free alloys.
5. The presence of zinc and also high contents of silicon (13%) in the aluminum alloy lowers the abrasion resistance of oxide coatings.
6. In alloys of aluminum, where magnesium is the predominating constituent and a d.c. process is used, the abrasion resistance is generally high.

Campbell [188] has described an instrument for non-destructive testing of the scratch resistance of hard anodic coatings. The equipment consists of a diamond stylus with a 1 mil radius and a load of 70 g which travels a small area of about 0.01 in^2 until it raises debris at the end of the area. The shadow of the debris, as shown by a lamp set at a low angle, is used as a measure of wear resistance. This technique is, however, less objective and is rarely used.

2.4.4 Summary

There is no doubt that the wear resistance of anodized aluminum is dependent upon the anodizing and sealing conditions and the basis metal composition. Several investigators [2, 111, 199, 206, 207, 208] have suggested that the production of anodic oxide films on aluminum with increased specific abrasion resistance is favored by the following anodizing conditions: (a) low electrolyte temperature; (b) high current density or applied voltage; (c) low electrolyte concentration; and (d) addition of less aggressive electrolyte such as oxalic acid to sulfuric acid bath. In fact, these conditions minimize the amount of oxide dissolved into the solution during anodization by either reducing the dissolving power of electrolyte or by reducing the exposure time of the oxide film to the electrolyte. These conditions also increase the limiting thickness of oxide films and, thus, improve significantly the total abrasion resistance. Cooling the solution itself becomes the principal factor in these processes because of the tremendous Joule heating effect.

A pulse anodizing technique has been developed in Japan [209] for producing hard anodic coatings at normal temperatures. The applied voltage is initially kept high for a short period and, then, is decreased abruptly to a lower value for another period of time. The accumulated Joule heating is dispersed during the recovery period and the chemical dissolution of oxide film is, therefore, reduced significantly. This successive increase and decrease in the applied potential enables hard anodization to be carried out at room temperature and saves a large amount of capital cost spent in the

cooling system. The oxide films so obtained are thick and hard and their physical and mechanical properties are considerably improved.

Contradictory results observed in the literature are the relations of specific abrasion resistance with coating thickness. There are four cases obtained from the literature:

1. The specific abrasion resistance increases with thickness to a maximum value and then decreases for thicker coatings [191, 194], as seen in Table 2-3.
2. The specific abrasion resistance increases with thickness [199], as seen in Table 2-7.
3. The specific abrasion resistance decreases with thickness [8, 200, 203], as seen in Figure 2-30.
4. The specific abrasion resistance is independent of thickness for hard anodic coatings [196], as seen in Figure 2-21.

It seems that cases 3 and 4 are more reasonable as judged from the pore structure of oxide films. The pores of conventional oxide films are tapered because of the significant chemical dissolution rate. The solid content per unit volume of the coating increases from the exterior surface towards the metal/oxide interface and, thus, the specific abrasion resistance decreases with thickness. Hard anodic films consist of practically parallel pores. The density of oxide is considered to be almost uniform throughout the entire coating, since the chemical dissolution is minimized and in many instance is negligible. Therefore, the specific abrasion resistance of hard

anodic coatings is practically constant.

Sealing reduces the abrasion resistance of anodized aluminum, this effect being greater for hot water-sealed versus metal salt solution-sealed coatings. This phenomenon is most likely due to the precipitation of metal hydroxides into the pores which then contribute to the abrasion resistance. The abrasion resistance of oxide film decreases with increasing sealing time because of the increased degree of hydration. The effect of anodizing conditions on the abrasion resistance of sealed coatings is the same as that of unsealed coatings.

The alloy constituents such as copper, silicon, magnesium, manganese, zinc, etc., are generally added to aluminum to improve its mechanical strength. These alloy constituents can significantly affect the properties of anodic films because they are either dissolved ($CuAl_2$, $MgZn_2$, $NiAl_3$, Fe), oxidized (Mg, AlMg, Mg_2Si), or unaffected (Si, AlMn, $CuAl_7$) by the anodization process [199]. If they are dissolved, the anodic coating produced has low density and, hence, poor wear resistance. For example, the copper constituents of 2000 series aluminum alloys are dissolved by the anodic reaction, resulting in relatively poor wear resistant coatings (Tables 2-5 and 2-7 and Figure 2-30). If the alloy constituents are oxidized or unaffected by the reaction, coating density and abrasion resistance are not lowered appreciably. The maximum abrasion resistance is obtained on pure aluminum and Al-Mg alloys.

With a given type of electrolyte the acid concentration, the electrolyte temperature, the current density, and the anodizing

voltage are interrelated. No one of these variables can be changed without getting a change in the values of the others. The interrelation of concentration, temperature, and voltage to obtain a constant current density of 12 amp/ft^2 [210] is shown by Figure 2-27. The anodizing voltage increases with decreasing temperature or concentration and with an increase in the current density as the other variables are fixed. Figure 2-28 shows the variation of abrasion resistance of 0.3 mil thick coatings with the anodizing voltage which is changed by varying temperature, current density, and concentration [210]. In all cases the abrasion resistance increases with anodizing voltage due to the corresponding increase in the apparent density of oxide coatings as proposed by Keller et al. [112] and Brace [206]. Because the cell size increases linearly with the applied voltage, the number of pores per unit area decreases and hence the apparent density increases with the anodizing voltage.

A correlation between the abrasion resistance and anodizing conditions seems unlikely. Deal [196] has found that the specific abrasion resistance increases almost linearly with apparent density of oxide coatings (Figure 2-29). The wear rates were found to increase with a decrease in the hardness of coating [195, 200]. An example is given in Figure 2-30. However, a quantitative correlation of the specific abrasion resistance with physical and/or mechanical properties of oxide coatings is still lacking. The material removal mechanisms of anodic films and the dependence of wear rates on the entired interacting system have not been explored yet.

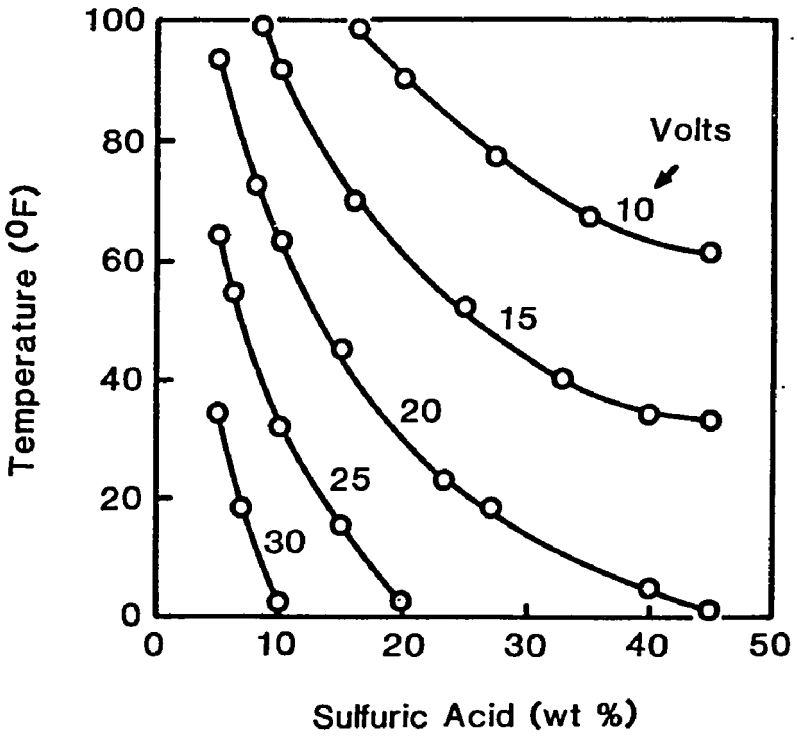

Figure 2-27. Relation of temperature, concentration, and voltage for a current density of 12 amp/ft^2 in a sulfuric acid type electrolyte for anodic coatings formed on 99.99% aluminum sheet (taken from [210]).

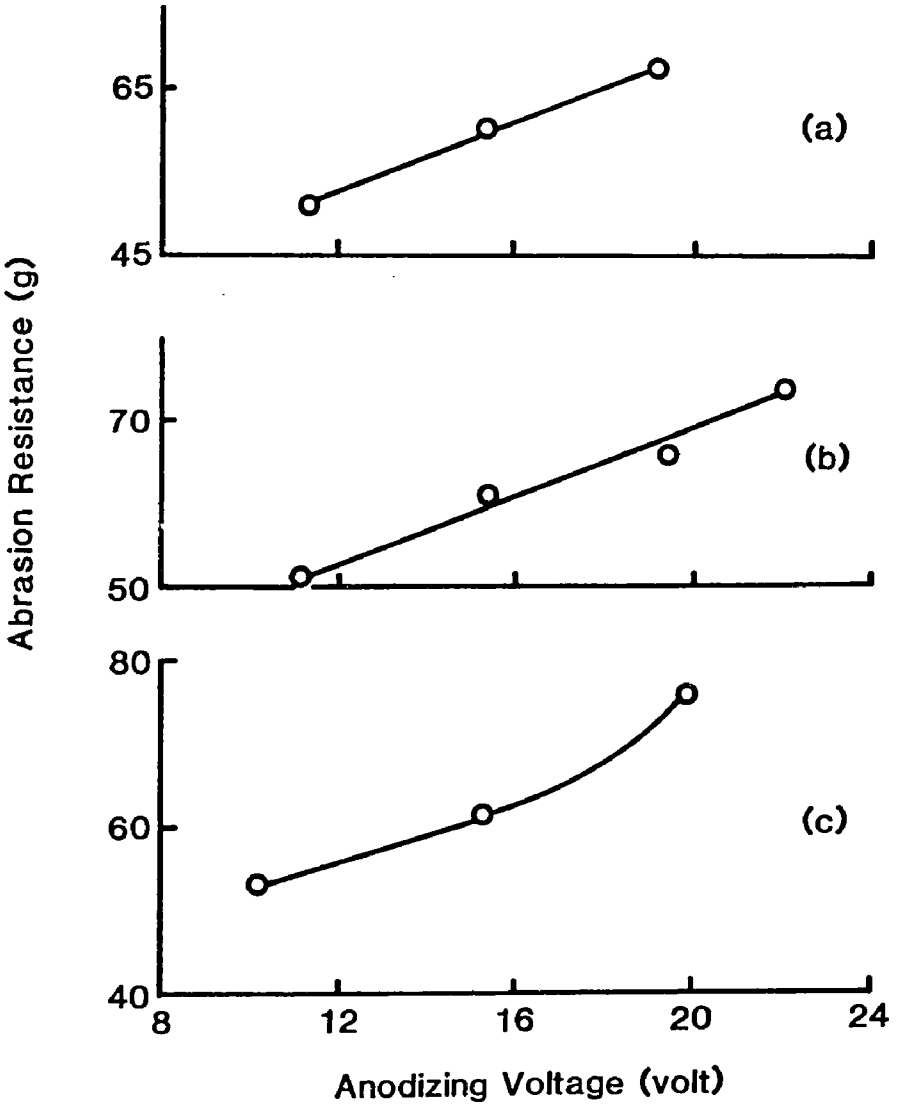

Figure 2-28. Effect of anodizing voltage on abrasion resistance of 0.3 mil thick coatings on 5557-H25 alloy. Voltage is changed by varying (a) electrolyte temperature; (b) current-density; and (c) acid concentration (taken from [210]).

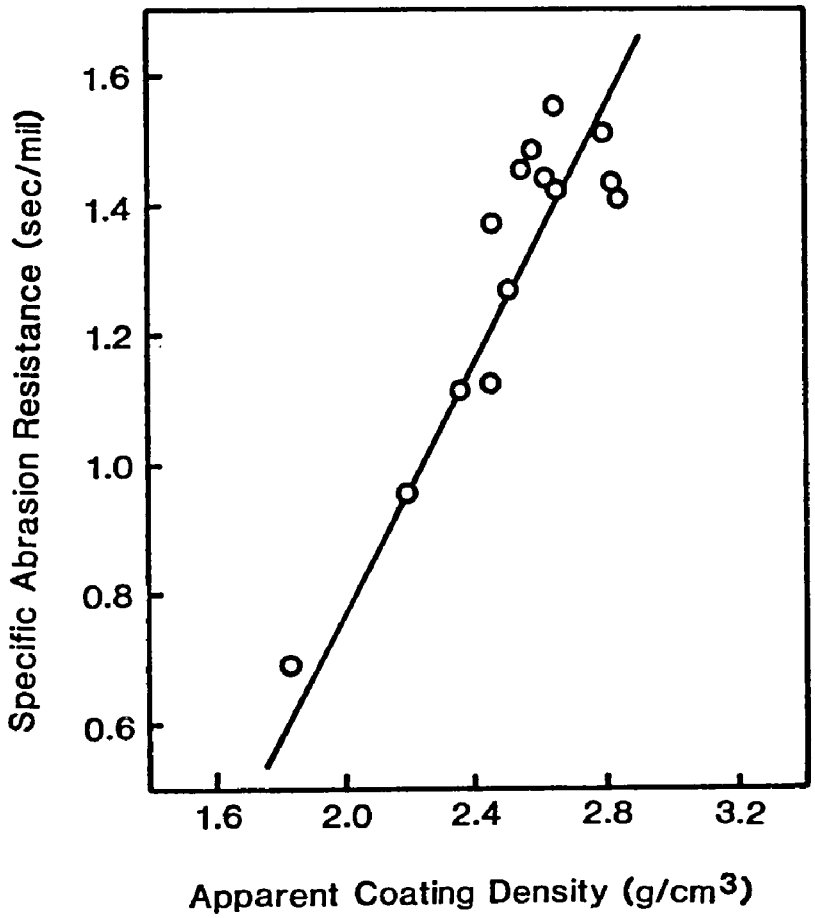

Figure 2-29. Variation of specific abrasion resistance with apparent density of anodic coatings formed on several alloys by both conventional and hard anodizing processes (taken from [196]).

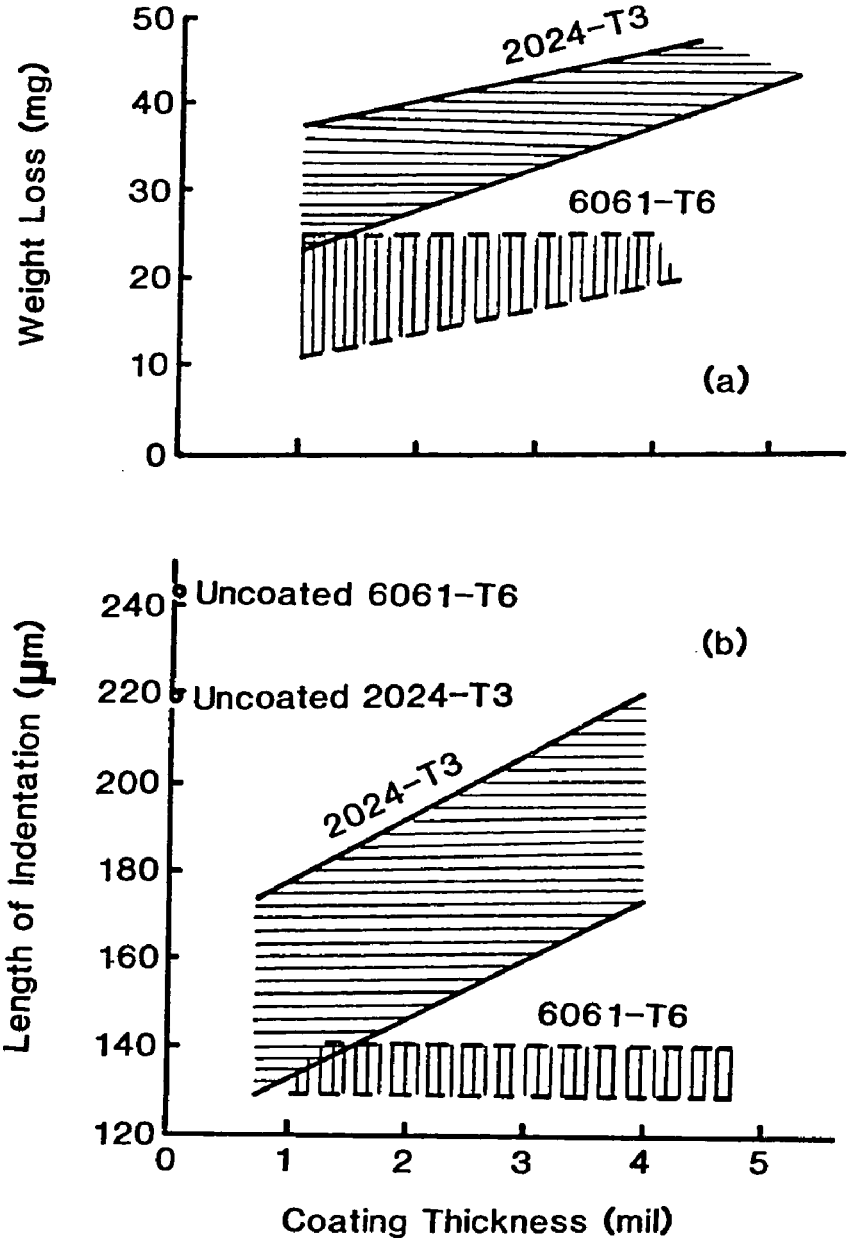

Figure 2-30. (a) Wear rate and (b) hardness as a function of coating thickness for hard anodic coatings formed on 2024-T3 and 6061-T6 alloys. Wear rate is measured by the weight loss of sample after 10,000 revolutions of CS-17 Taber wheels under 500 g load. Hardness is determined by the indentation length of long diagonal using a Knoop indenter under 500 g load (taken from [200]).

CHAPTER 3

EXPERIMENTAL SECTION

The aluminum used in this study was an 1100 alloy expressly anodized for use as a lithographic plate. The anodic coating was removed by immersing the plate in a mixture of 2% CrO_3 and 5% H_3PO_4 at 95°C for 5 to 10 minutes (ASTM Standard B 137). The metal was then etched in a 8% NaOH electrolyte, desmutted in HNO_3, chemically polished in H_3PO_4-HNO_3 solution, and thoroughly washed with distilled water immediately before anodizing. The anodization was carried out in 15% H_2SO_4 under different conditions of electrolyte temperature and anodizing voltage. The thickness of oxide coating was controlled by varying the anodizing time. Commercial electrolysis grade lead was used as the cathode. Electrolyte circulation was produced by compressed air and the temperature of the anodizing solution was controlled by a water bath. The anodized sample was immersed in a 5% $NaHCO_3$ solution for 10 seconds to neutralize the residual acid, thoroughly washed with distilled water and, then, stored in a desiccator before testing.

Polymer coatings were applied from solution using a spinning disk applicator. The thickness was controlled by varying the velocity of rotation and the polymer solution concentration. Polystyrene and poly-n-butylmethacrylate were applied from a toluene solution. The polymer-coated sample was left in air for an hour before baking in an oven at 80°C for at least 10 hours.

Four different aqueous solutions were utilized for sealing the aluminum oxide coatings: distilled water, nickel acetate solution, potassium dichromate solution, and sodium silicate solution. Distilled water sealing was carried out at the boiling point. The nickel acetate solution contained 6 g/L of nickel acetate and 8 g/L of boric acid: the pH was 5.6 and the sealing temperature was 90 $\pm$ 5 ^{o}C. The potassium dichromate solution contained 15 g/L potassium dichromate and 3 g/L NaOH: the pH was 6.9 and the sealing temperature was 90 $\pm$ 5 ^{o}C. The sodium silicate solution contained 5% by weight sodium silicate ($Na_2O:SiO_2$ = 1:3.3): the pH was 11.4 and the sealing temperature was 90 $\pm$ 5 ^{o}C.

The coated plates were worn by a procedure outlined previously [211]. The wear procedure involves a back-and-forth motion of a weighted block against the sample plate immersed in an aqueous solution of SiC abrasives. The average particle size of the abrasive was about 1 μm. 2 grams of SiC abrasive dispersed in 40 mL distilled water was used in all tests except where otherwise indicated. Contact pressure was adjusted by either changing the block or adding dead weight to the shaft.

Three techniques were used to evaluate the wear rate: (a) weight loss measurements; (b) surface roughness measurements; and (c) specular reflectance measurements. The weight loss measurements were made using a Gram-Atic balance. The weight of oxide films prior to and after wear was determined to 0.1 mg according to the ASTM Standard B 137 method. The weight of an anodic coating was obtained from the weight difference between the anodized sample and bare substrate and

was expressed in units of mg/dm^2. Chromic/phosphoric acid solution was used to strip off the oxide film without attacking the metal substrate. Roughness measurements were made using a Talor-Hobson Surtronic 3 profilometer. Surface roughness is recorded as the average height above and below a center line.

A summary of specular reflectance measurements for determining film thickness has been published [10]. The infrared specular reflectance spectra were obtained using a Perkin-Elmer Model 186-0373 specular reflectance accessory on a Perkin-Elmer Model 283 infrared spectrophotometer. Since the angle of incident radiation at the coating surface is 6.5^{o} for this reflectance accessory, coating thickness could be calculated by equation (12) or (13).

$$t = [m - 1/2 - (\Phi_1 - \Phi_2)/2\pi] \; / \; 2\, n_1\, \nu_m \tag{12}$$

and

$$t = x \; / \; [2\, n_1\, (\nu_{m+x} - \nu_m)] \tag{13}$$

Figures 3-1 to 3-3 exhibit typical interference fringe patterns of anodic coatings produced at $30^{o}C$ and 15 V for 15, 35, and 45 minutes, respectively. A linear relationship between the order and the corresponding wavenumber of interference fringe minima in the spectral region from approximately 2000 to 3000 cm^{-1} was observed in each case (Figure 3-4), indicating that the total phase change $(\Phi_1 - \Phi_2)$ and the refractive index (n_1) for these systems are independent of the wavenumber in this spectral region according to equation (12). The

total phase change could be obtained from the intercept at the ordinate. 1.62 and 1.59 were used as the refractive indices for anodic oxide [212] and polystyrene [213] coatings, respectively. The average values of thickness as calculated by equations (12) and (13) are summarized in Tables 3-1 to 3-3. The interference fringe minimum centered at 2326.6 cm^{-1} for the 35-min coating, which is distorted by the CO_2 absorption band at 2349 cm^{-1} (antisymmetric stretch) due to the path difference in sample and reference beams (Figure 3-2), was not included in thickness calculation. A resolved CO_2 absorption band is seen in Figure 3-1, where this absorption band decreases the intensities of a fringe minimum in Figure 3-2 and a fringe maximum in Figure 3-3. The arrows on these figures show the wavenumber location involved. Only one interference fringe is involved in thickness calculation by equation (12), but two are required by equation (13). There is an intrinsic error in indexing the wavenumber of each fringe. The film thickness as calculated by equation (12) would therefore have a smaller standard error than that determined from equation (13). Examples of this are seen in Tables 3-1 to 3-3. Since 18 spectra do not improve the accuracy in thickness calculation, six spectra and equation (12) were used to determine the thickness of coatings.

Figure 3-5 gives an example showing the changes in the interference fringe pattern of the anodic coating on aluminum as a consequence of reduced thickness by wear. The anodic coating was produced in 15% H_2SO_4 at 30°C and 15 V for 35 minutes. The specular reflectance spectrum exhibiting the interference fringes is shown as the solid line in Figure 3-5. The dotted line in the spectrum was

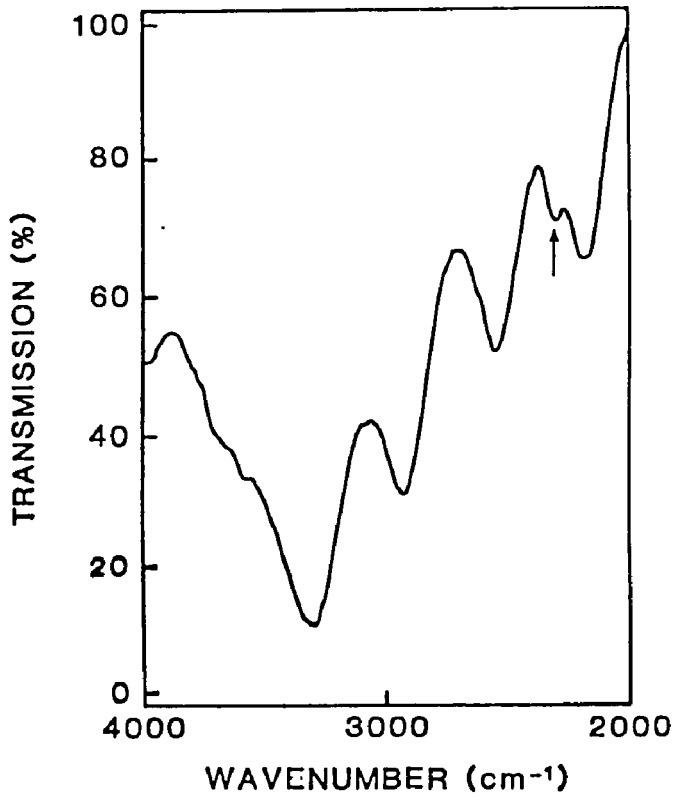

Figure 3-1. Typical interference fringe pattern of the anodic coating formed in 15% H_2SO_4 at 30°C and 15 V for 15 minutes.

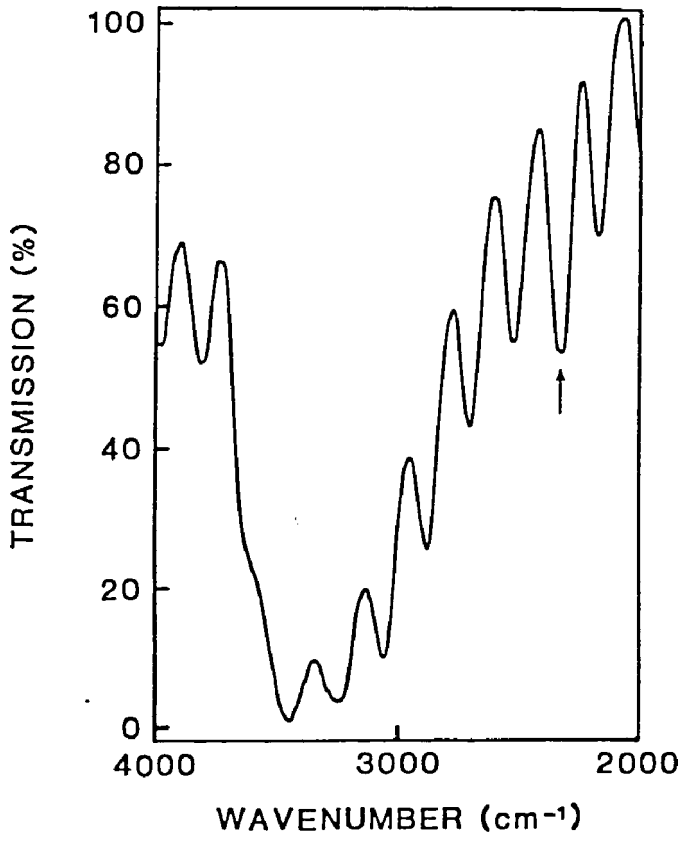

Figure 3-2. Typical interference fringe pattern of the anodic coating formed in 15% H_2SO_4 at 30°C and 15 V for 35 minutes.

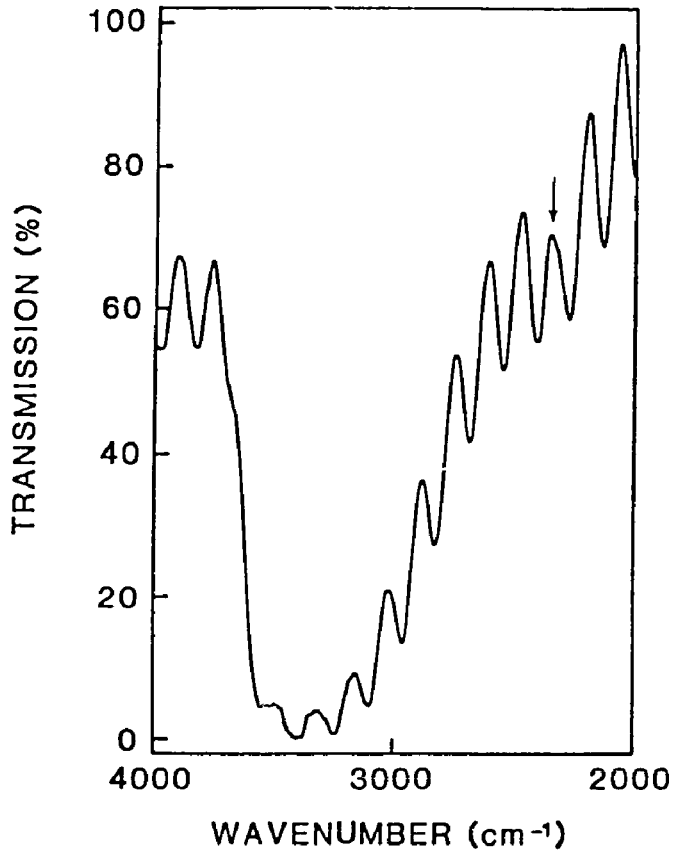

Figure 3-3. Typical interference fringe pattern of the anodic coating formed in 15% H_2SO_4 at 30°C and 15 V for 45 minutes.

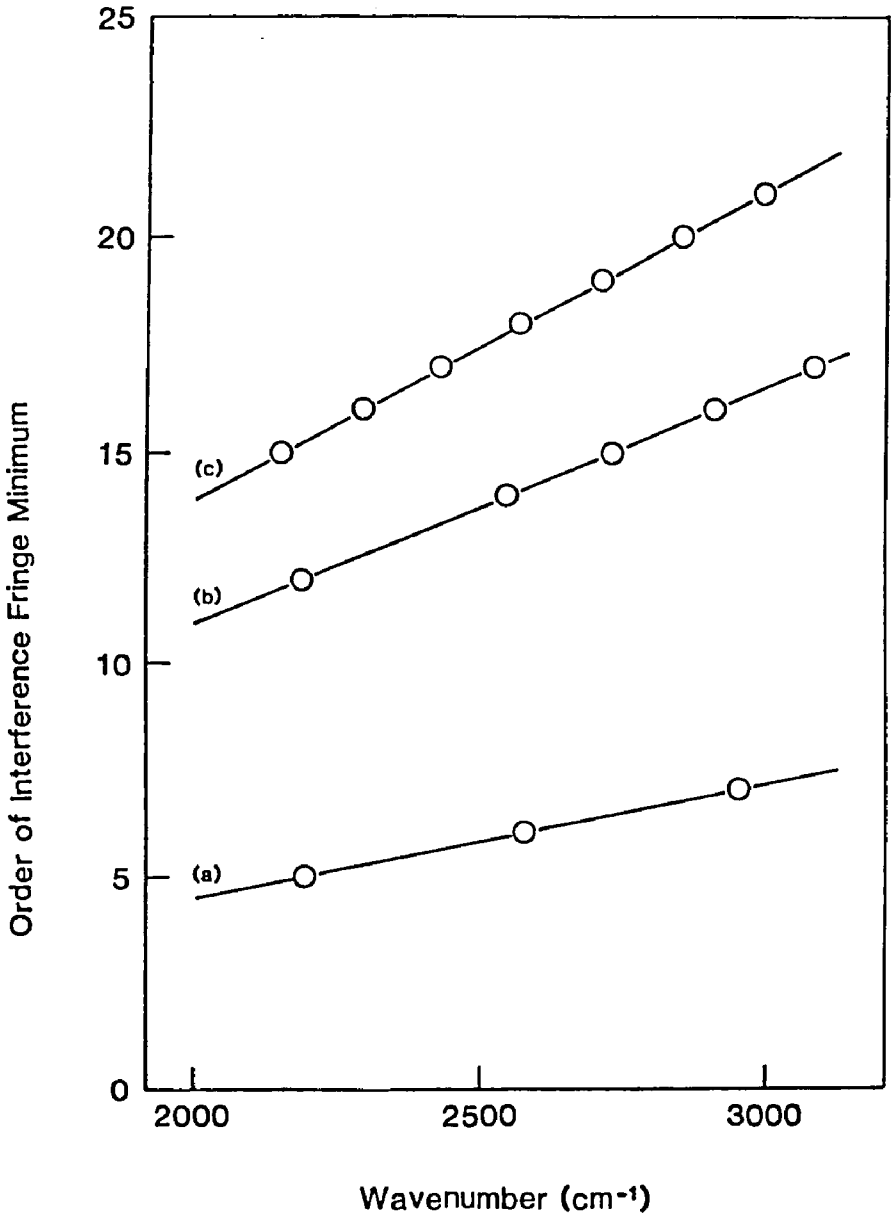

Figure 3-4. Linear dependence of the order of interference fringe minima on the corresponding wavenumber for interference fringe patterns given in (a) Figure 3-1, (b) Figure 3-2, and (c) Fifure 3-3.

Table 3-1. Thickness of a 15-min Anodic Coating as Calculated by Equations (12) and (13).

$\bar{\nu}_m(6)^*$, cm^{-1}	$\bar{t}_m(6)$, μm	$\bar{t}_m(18)$, μm
2952.3 ± 6.0	8.134 ± 0.016	8.140 ± 0.022
2565.5 ± 4.8	8.157 ± 0.015	8.156 ± 0.019
2194.2 ± 10.4	8.131 ± 0.039	8.126 ± 0.034
$\bar{t}$, μm	8.140 ± 0.027	8.141 ± 0.028
$\bar{t}'$, μm	8.144 ± 0.097	8.181 ± 0.127

* number in the parenthesis is the number of spectra used in thickness calculation.

$\bar{t}_m$: average value of the m-th order fringes calculated by equation (12).

$\bar{t}$: average value of all fringes calculated by equation (12).

$\bar{t}'$: average value calculated by equation (13) using the first and last fringes in the table.

Table 3-2. Thickness of a 35-min Anodic Coating as Calculated by Equations (12) and (13).

$\bar{\nu}_m(6)$, cm^{-1}	$\bar{t}_m$, μm(6)	$\bar{t}_m(18)$, μm
3083.8 ± 7.0	17.175 ± 0.039	17.165 ± 0.047
2906.2 ± 8.9	17.162 ± 0.053	17.165 ± 0.046
2724.9 ± 8.4	17.172 ± 0.053	17.173 ± 0.045
2543.4 ± 6.7	17.183 ± 0.045	17.186 ± 0.040
2336.6 ± 5.6	---	---
2186.5 ± 6.7	17.165 ± 0.052	17.161 ± 0.048
$\bar{t}$, μm	17.171 ± 0.046	17.170 ± 0.045
$\overline{t'}$, μm	17.199 ± 0.057	17.175 ± 0.087

Table 3-3. Thickness of a 45-min Anodic Coating as Calculated by Equations (12) and (13).

$\bar{\nu}_m(6)$, cm^{-1}	$\bar{t}_m(6)$, μm	$\bar{t}_m(18)$, μm
2990.8 ± 4.1	22.043 ± 0.030	22.046 ± 0.030
2848.7 ± 2.4	22.059 ± 0.019	22.050 ± 0.021
2706.9 ± 3.0	22.075 ± 0.024	22.069 ± 0.025
2565.2 ± 3.1	22.091 ± 0.027	22.087 ± 0.027
2425.5 ± 3.1	22.091 ± 0.029	22.082 ± 0.023
2292.3 ± 3.0	22.027 ± 0.029	22.024 ± 0.033
2150.2 ± 1.5	22.048 ± 0.016	22.050 ± 0.018
$\bar{t}$, μm	22.062 ± 0.033	22.058 ± 0.033
$\bar{t}'$, μm	22.030 ± 0.096	22.035 ± 0.082

obtained after 4000 cycles in the wear apparatus. The shifts in the fringe maxima and minima are readily apparent.

Thickness of a thin coating may also be determined by the absorption measurement utilizing equation (15).

$$\Delta A = \log(T_s / T_c) \tag{15}$$

The "ring-breathing" mode bands of polystyrene appearing in the 700 to 800 cm^{-1} region were used. Figure 3-6 shows a calibration curve of the ΔA vs. thickness by weight in the case of high molecular weight polystyrene on anodized aluminum. This calibration curve, and one similar to it for poly-n-butylmethacrylate coatings, were used to determine coating thickness directly from the ΔA measurements. Figure 3-7 shows an absorption band for polystyrene as a function of the number of wear cycles. The decrease in the intensity of the absorption band as a function of the number of wear cycles is striking. Absorption measurement is applicable to thickness determination.

The apparent density, d_a, of an anodic coating was determined by weight and specular reflectance measurements.

$$d_a = (w_a - w_s)/t\ A_s \tag{26}$$

where w_a and w_s are weights of anodized sample and bare substrate, respectively; t is the thickness of oxide film as determined by the interference fringe technique and A_s the specimen size.

Wettability measurements were made by placing a drop of doubly

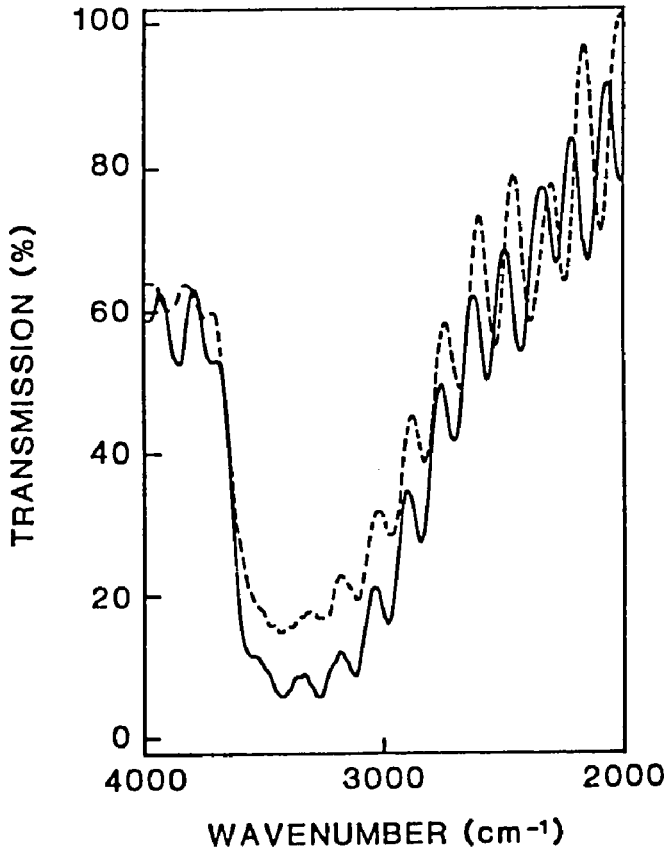

Figure 3-5. Typical interference fringe patterns of anodized samples prior to (solid curve) and after 4000 cycles (dotted curve) in the accelerated wear apparatus at a contact pressure of 22.9 g/cm^2.

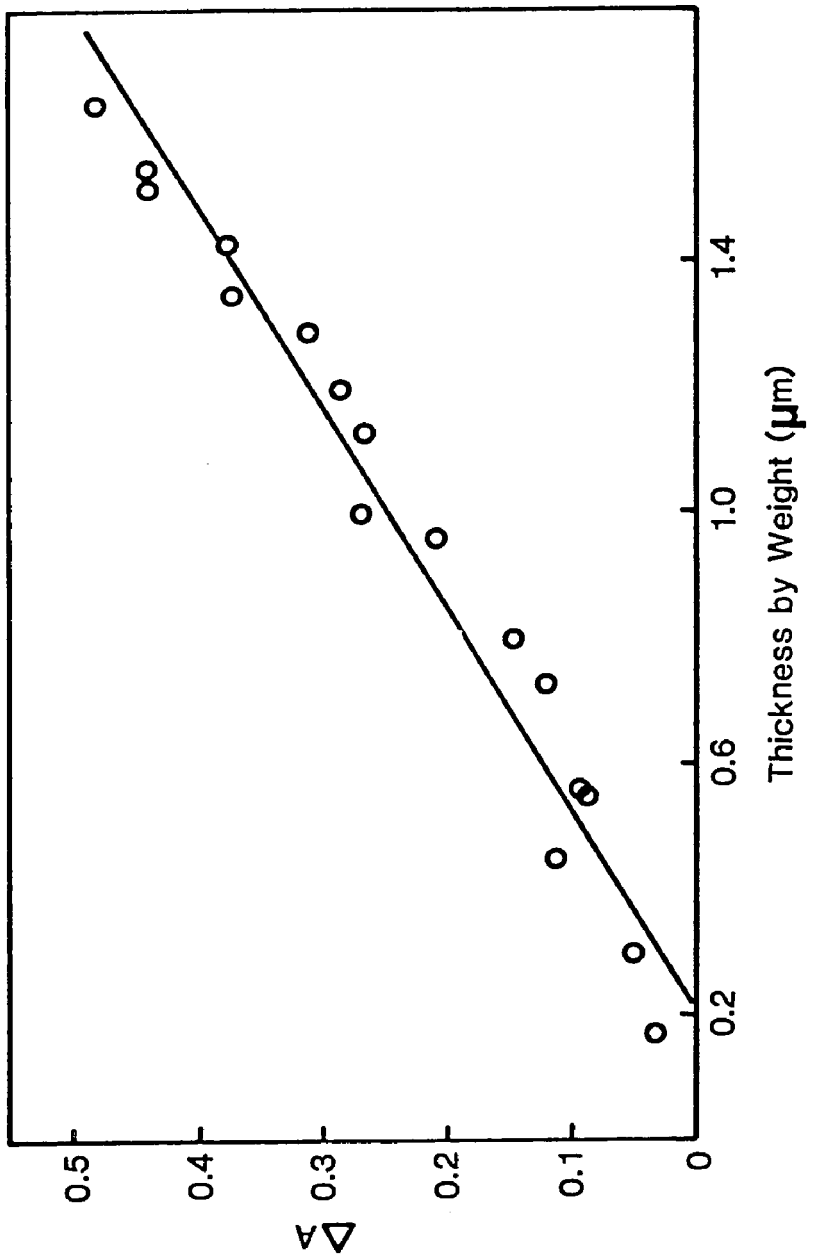

Figure 3-6. Comparison between ΔA and the film thickness of high molecular weight polystyrene on anodized aluminum as determined by weight (taken from [10]).

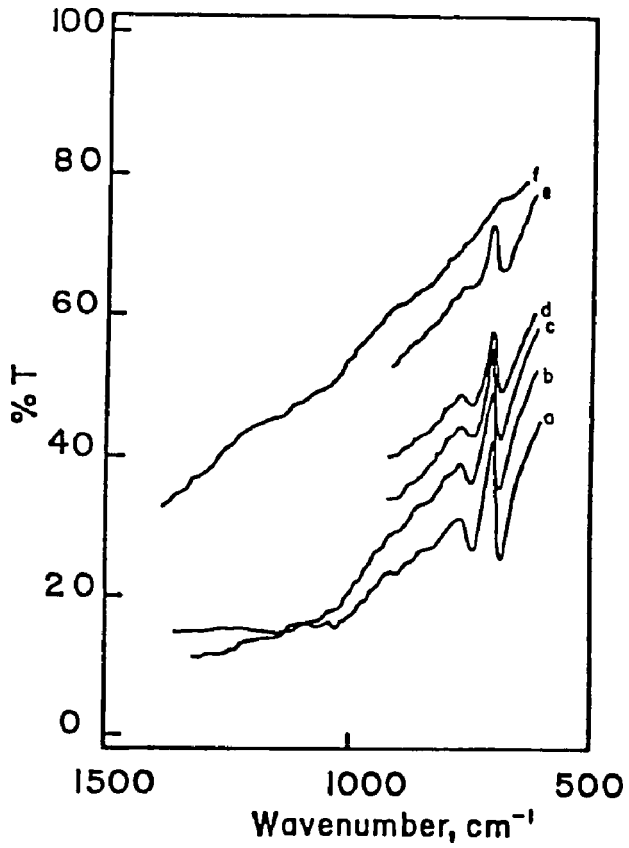

Figure 3-7. Specular infrared reflectance spectra of high molecular weight polystyrene on a commercial plate anodized in sulfuric acid as a function of the number of wear cycles: (a) 1800, (b) 2100, (c) 2300, (d) 2500, (e) 2700 cycles, and (f) uncoated and unworn (taken from [10]).

distilled water on the sample surface and measuring the contact angle by means of an NRL Contact Angle Goniometer Model A-100. A container of doubly distilled water was placed in the environmental chamber in order to establish a high humidity and minimize the rate of evaporation. Contact angle measurements were made 2 minutes after a water drop of 5 μL was placed on the substrate. The average value of 4 different droplets was taken as the contact angle.

CHAPTER 4

EXPERIMENTAL RESULTS

4.1 Rates of Formation of the Anodic Film on Aluminum

The rate of formation of the anodic coating as a function of anodizing conditions was determined by the interference method and gravimetric means. At least three measurements were made to obtain the average values of the thickness, weight and apparent density of the anodic coating. Figure 4-1 shows that the thickness of the anodic coating prepared under different anodizing voltages and electrolyte temperatures increases linearly with anodizing time. In order to avoid the initial current surge in the constant voltage mode (Figure 2-14) which may result in nonuniform oxide film growth, the anodizing voltage during anodization was initially kept low then gradually increased to its desired value. Consequently, there existed an initial coating at zero anodizing time, i.e. when the anodizing voltage is reached. The formation rates are summarized in Table 4-1. Formation rates of the anodic coating as determined by gravimetric means decreased progressively with the anodizing time (Figure 4-2). The effect is more significant at higher electrolyte temperatures when the anodizing voltage is kept constant, and at lower anodizing voltages under isothermal conditions. This behavior is more clearly exhibited if the apparent density of anodic coatings is plotted against the film thickness, as shown in Figures 4-3 and 4-4. Apparent density falls off progressively with film thickness in all cases.

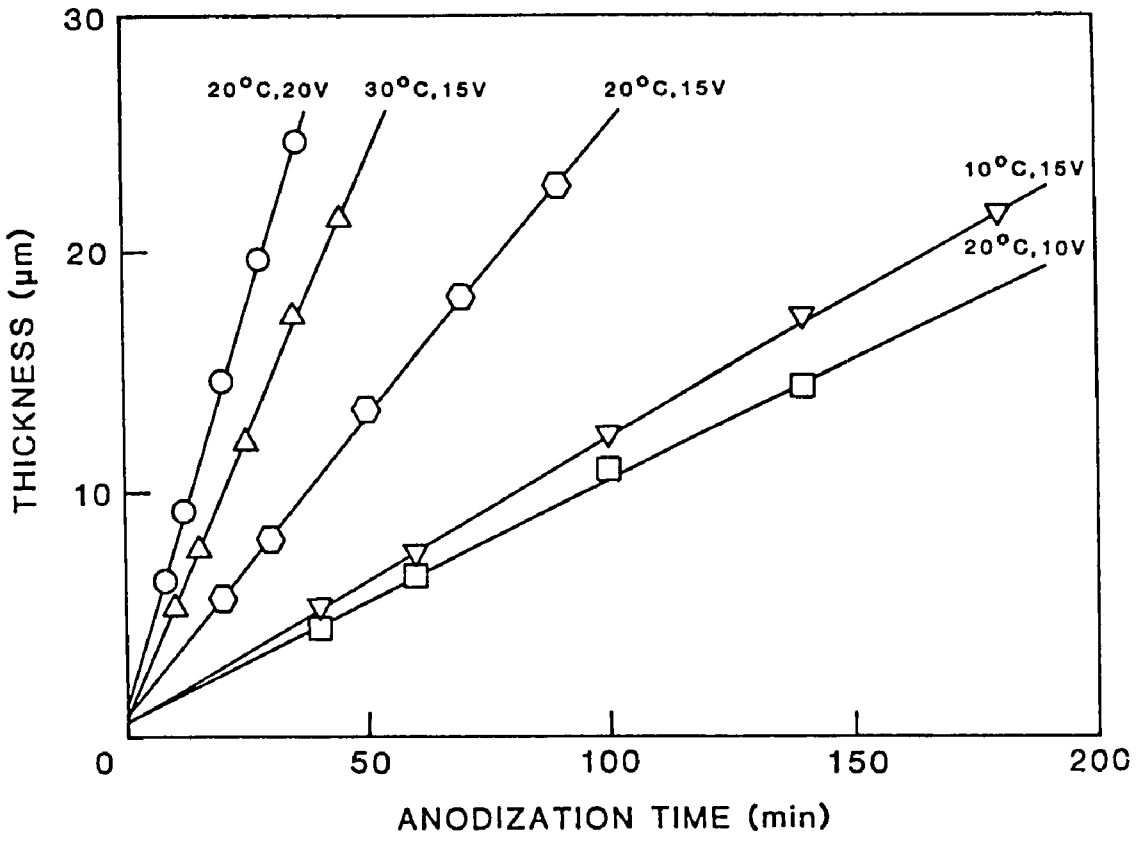

Figure 4-1. Rates of formation of the anodic coatings on aluminum determined by the interference method as a function of anodizing conditions.

Table 4-1. Rate of Formation of the Anodic Coatings on Aluminum as a Function of Anodizing Conditions.

Electrolyte	Anodizing voltage, V	Electrolyte Temp., ^{o}C	Formation Rate, μm/min
15% H_2SO_4	15	10	0.12
	15	20	0.26
	15	30	0.46
	10	20	0.10
	20	20	0.65

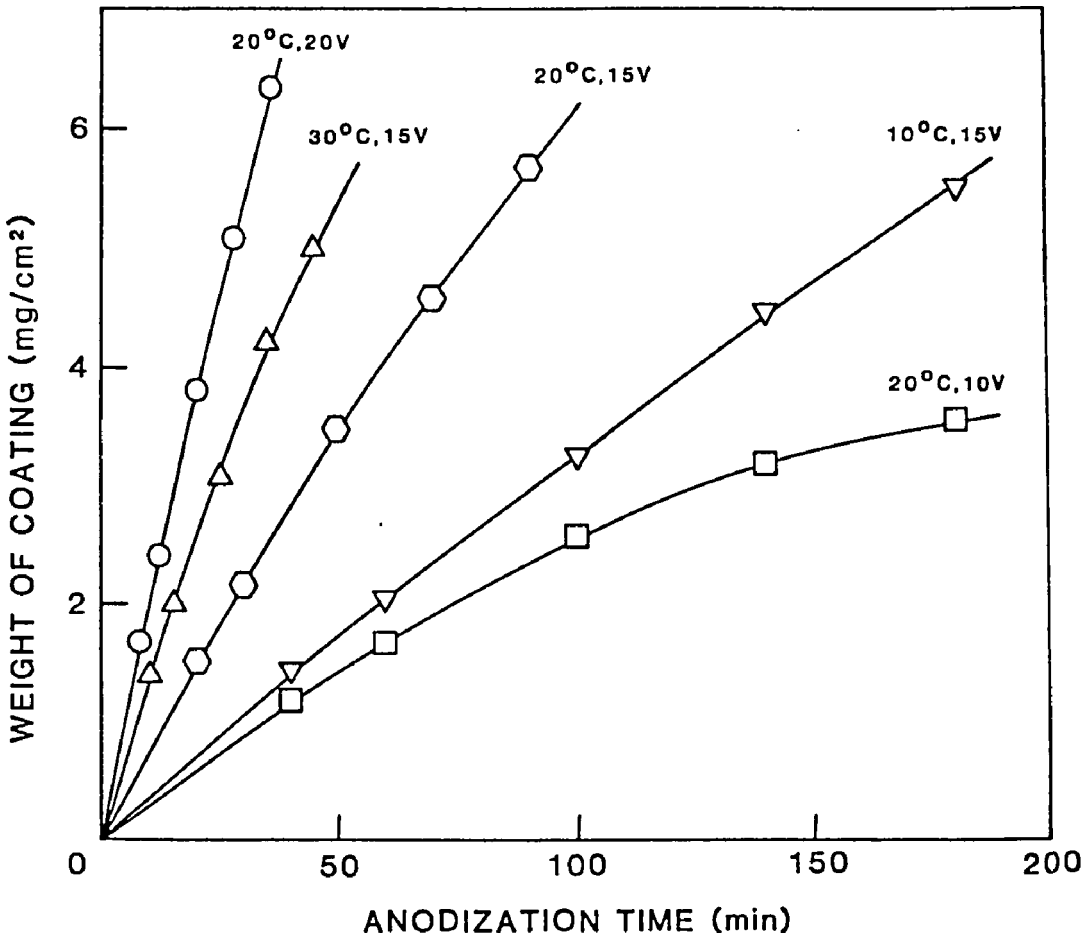

Figure 4-2. Rates of formation of the anodic coatings determined by the gravimetric means as a function of anodizing conditions.

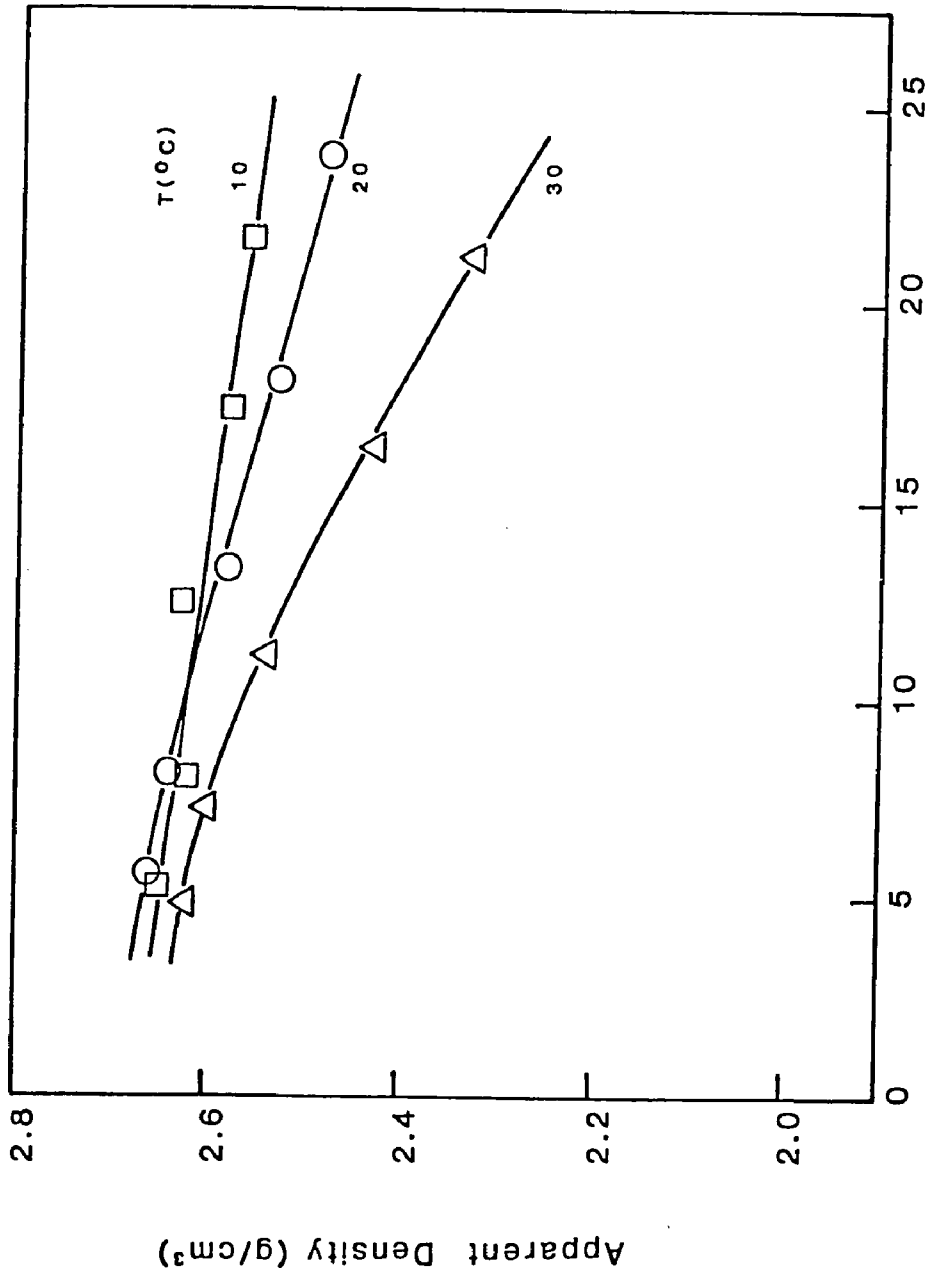

Figure 4-3. Dependence of the apparent density of anodic coatings on the film thickness as a function of the electrolyte temperature in the constant voltage (15 V) mode.

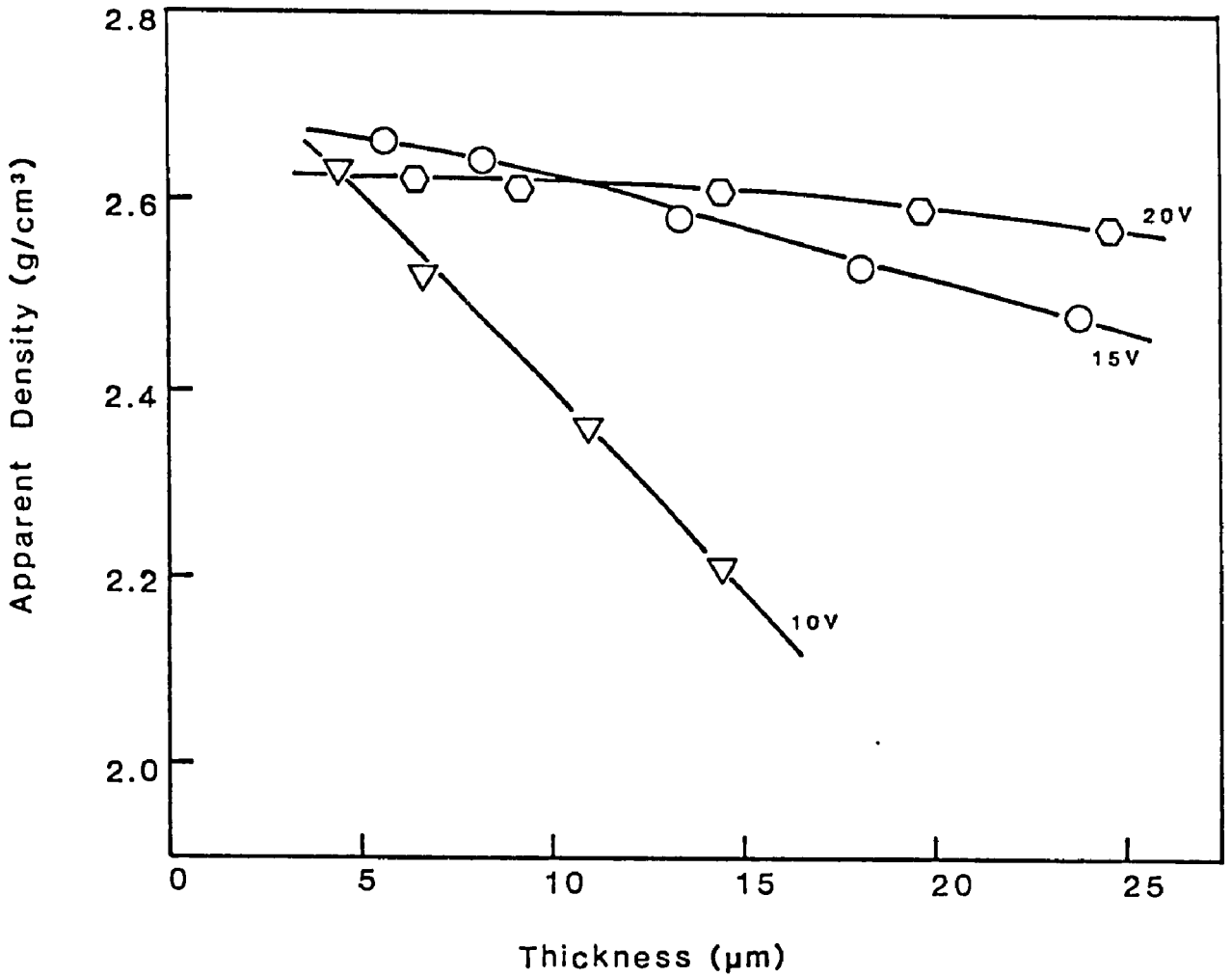

Figure 4-4. Dependence of the apparent density of anodic coatings on the film thickness as a function of the anodizing voltage under isothermal (20°C) conditions.

4.2 Determination of Wear Rates

Three techniques have been used to evaluate the wear rate: (a) weight loss measurements; (b) surface roughness measurements; and (c) specular reflectance measurements. Figure 4-5 shows an example of a wear test by weight measurements. The anodized aluminum sample gains instead of losing weight as wear proceeds. Weight loss measurements appear inapplicable to a study of wear of anodized aluminum.

An example of wear rate determination by surface roughness measurements is shown in Figure 4-6. The anodic coating was produced in 15% H_2SO_4 at 20°C and 20 V for 30 minutes. Higher contact pressures result in greater wear rates. As the number of wear cycles increases, the surface becomes smoother and the wear rate progressively decreases. The continuously changing rate values obtained from surface roughness measurements makes this technique less than suitable for quantitative analysis of wear.

A constant wear rate was obtained from specular reflectance measurements. Figure 4-7 gives an example of a wear test by the interference fringe technique. The thickness of oxide film was determined after 0, 800, 1600, 2400, 3200, 4000, and 5000 wear cycles. At each contact pressure, there is an initial increase in the thickness, but after 800 cycles the coating thickness decreases linearly with wear cycles. The initial increase in the thickness was observed for all anodic coatings on aluminum abraded by SiC powders. The wear rate could be obtained from the slope of the latter linear relationship between thickness and wear cycle and expressed in units of μm/cycle. Specular reflectance is therefore a useful technique for

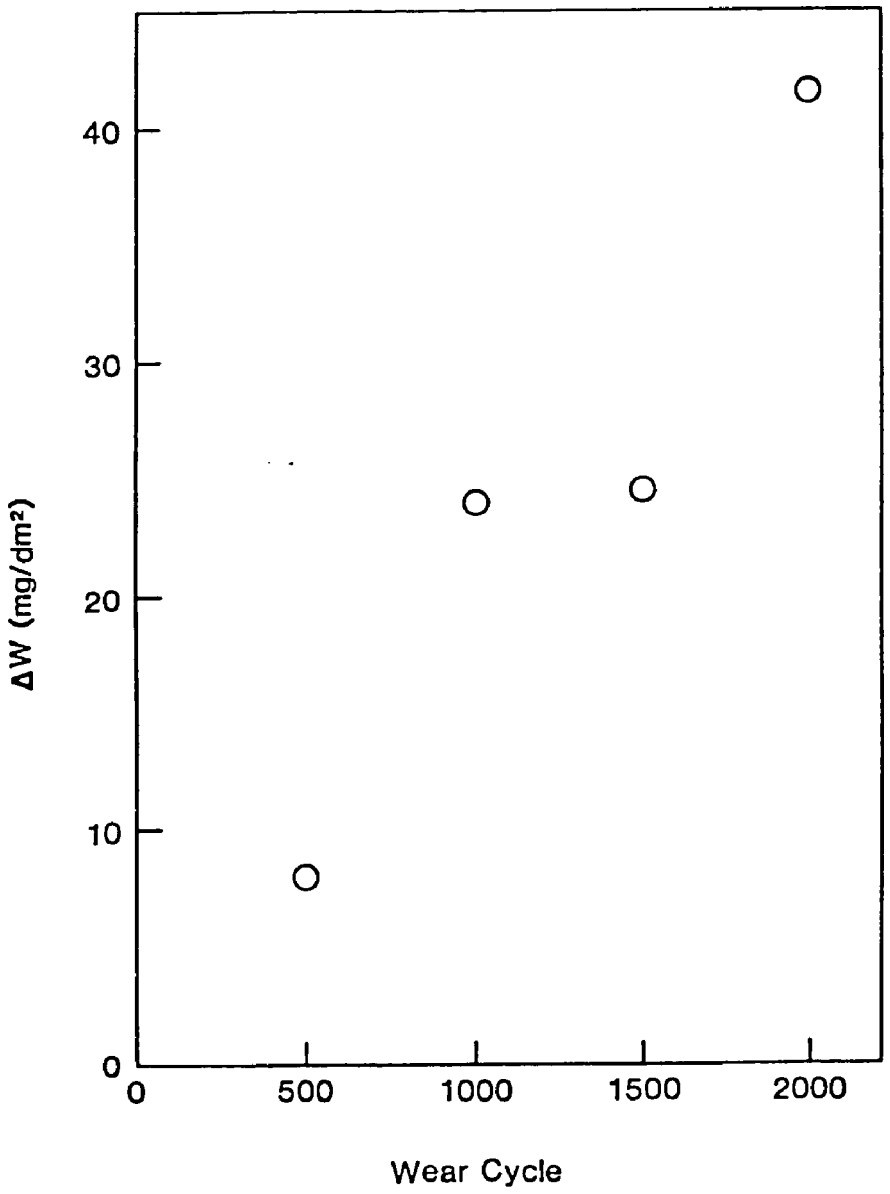

Figure 4-5. Measurement of wear by weight loss. Anodic coating was prepared in 15% H_2SO_4 at 20°C and 20 V for 30 minutes. 1 μm SiC abrasive and 22 g/cm^2 contact pressure were used in the test.

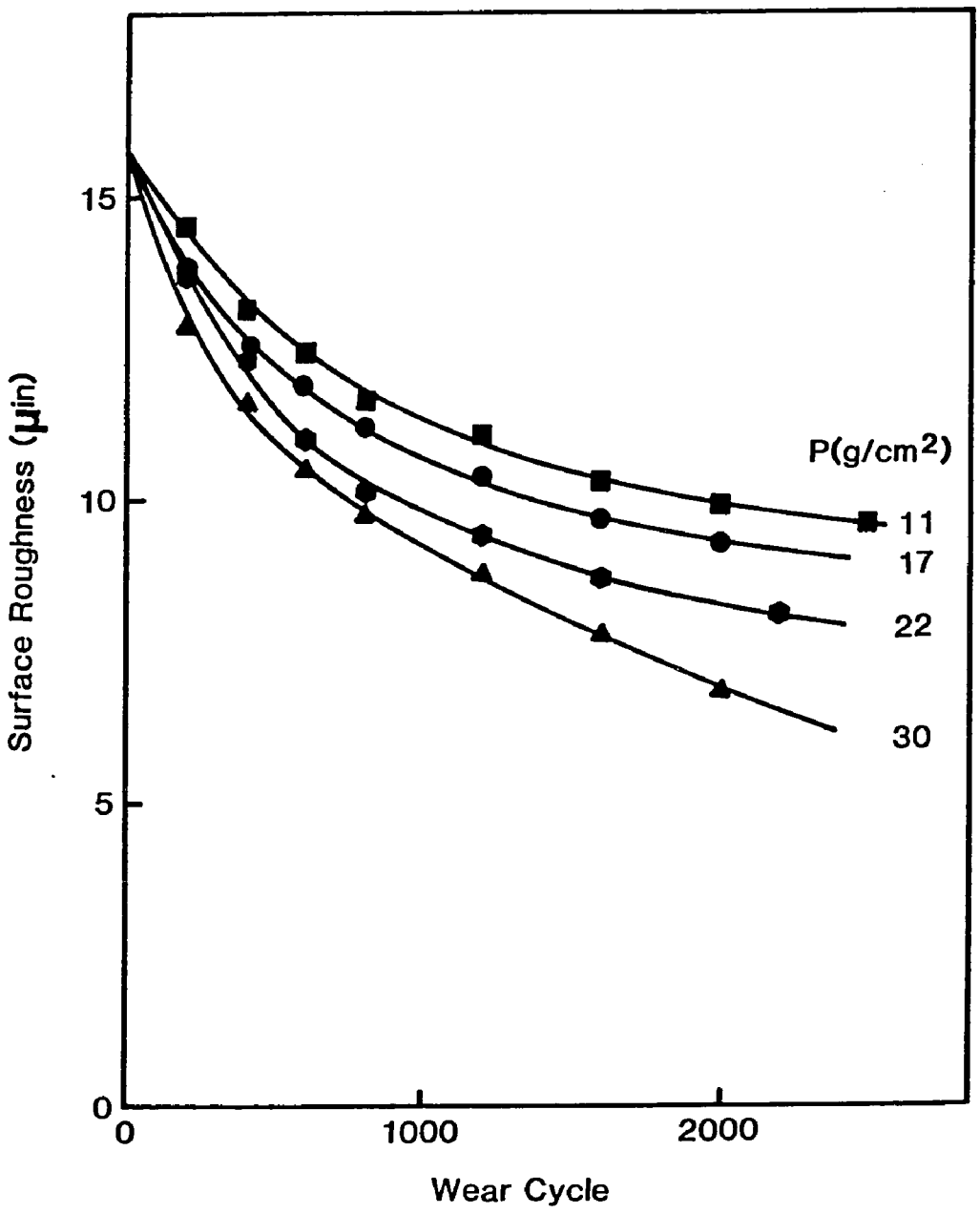

Figure 4-6. Influence of contact pressure on the wear of anodized aluminum as determined by surface roughness measurements. 0.3 μm alumina abrasives were used in the test.

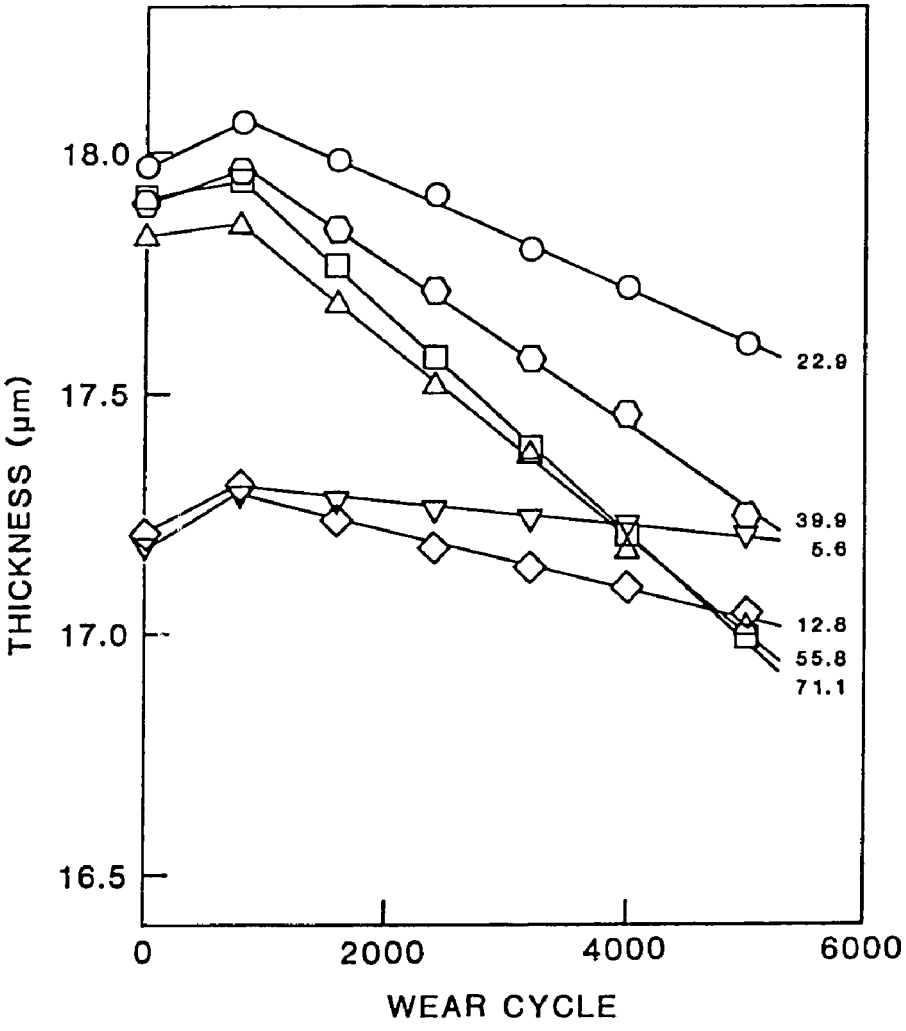

Figure 4-7. Changes in the film thickness by wear under different contact pressures as determined by the interference fringe method for anodic coatings formed in 15% H_2SO_4 at 30°C and 15 V for 35 minutes.

wear study.

4.3 Rates of Wear of the Anodic Coating on Aluminum

Since the wear resistance of a material is not an intrinsic property, but dependent upon the material itself and the wear environment, a series of experiments was carried out to determine the effect of contact pressure and abrasive concentration on the wear rate of anodized aluminum. Figures 4-8 and 4-9 show that the wear rate is directly proportional to the contact pressure for anodic coatings formed in 15% H_2SO_4 at 15 V for different anodizing times at 30°C for the former case and 20°C for the latter. The contact pressures were 5.6, 12.8, 22.9, 39.9, 55.8, and 71.1 g/cm^2. A transition was observed in each case. The contact pressure at the transition point shifts to higher values for coatings exhibiting lower wear rates. The experimental results for the wear rate as a function of abrasive concentration are shown in Figure 4-10. The test solutions consisted of 2, 4, 7, 10, 15, and 20 grams of SiC abrasive powder dispersed in 40 mL distilled water. The wear rate increases very rapidly at low concentrations and tends to level off at higher concentrations. It was found that the experimental data fitted an equation of the Langmuir adsorption isotherm type (solid curves) quite well for both cases.

The effect of anodizing conditions on the wear rate of anodic coatings on aluminum is summarized in Figures 4-11 and 4-12. Wear rate increases with the thickness of anodic coatings, the effect being more significant at higher electrolyte temperatures (Figure 4-11) or

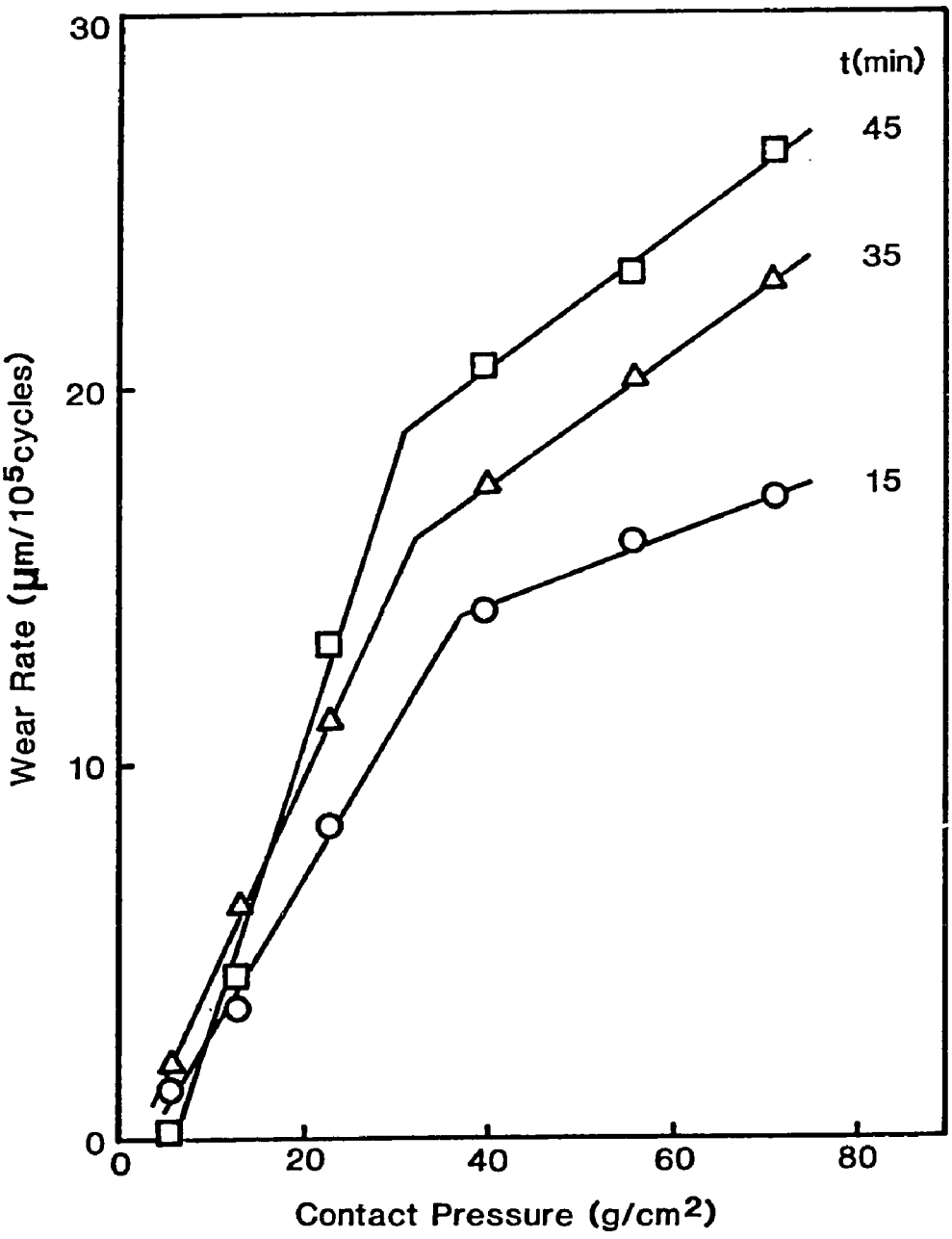

Figure 4-8. Effect of contact pressure on the wear rate of anodic coatings produced in 15% H_2SO_4 at 30°C and 15 V for different anodizing times.

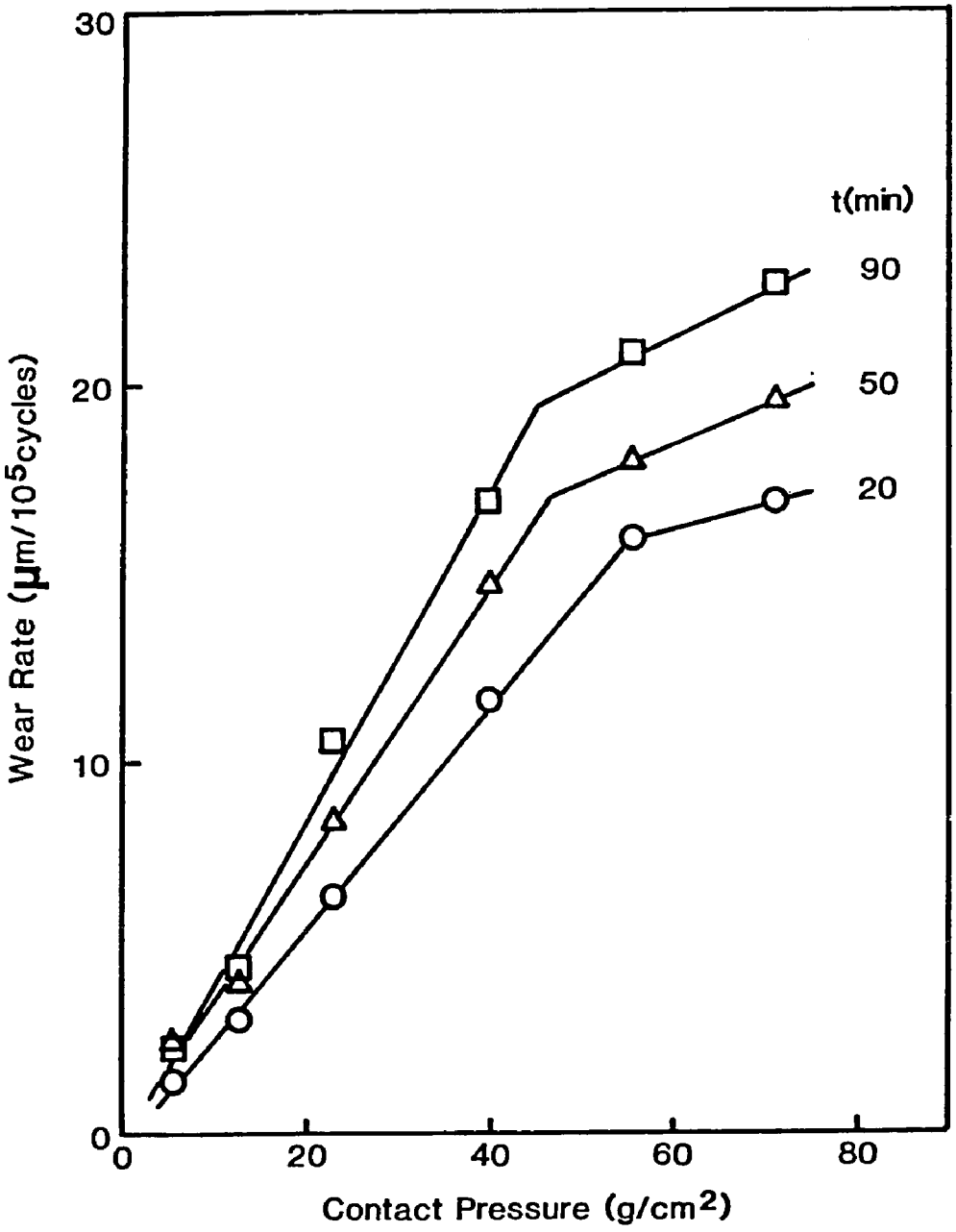

Figure 4-9. Effect of contact pressure on the wear rate of anodic coatings produced in 15% H_2SO_4 at 20°C and 15 V for different anodizing times.

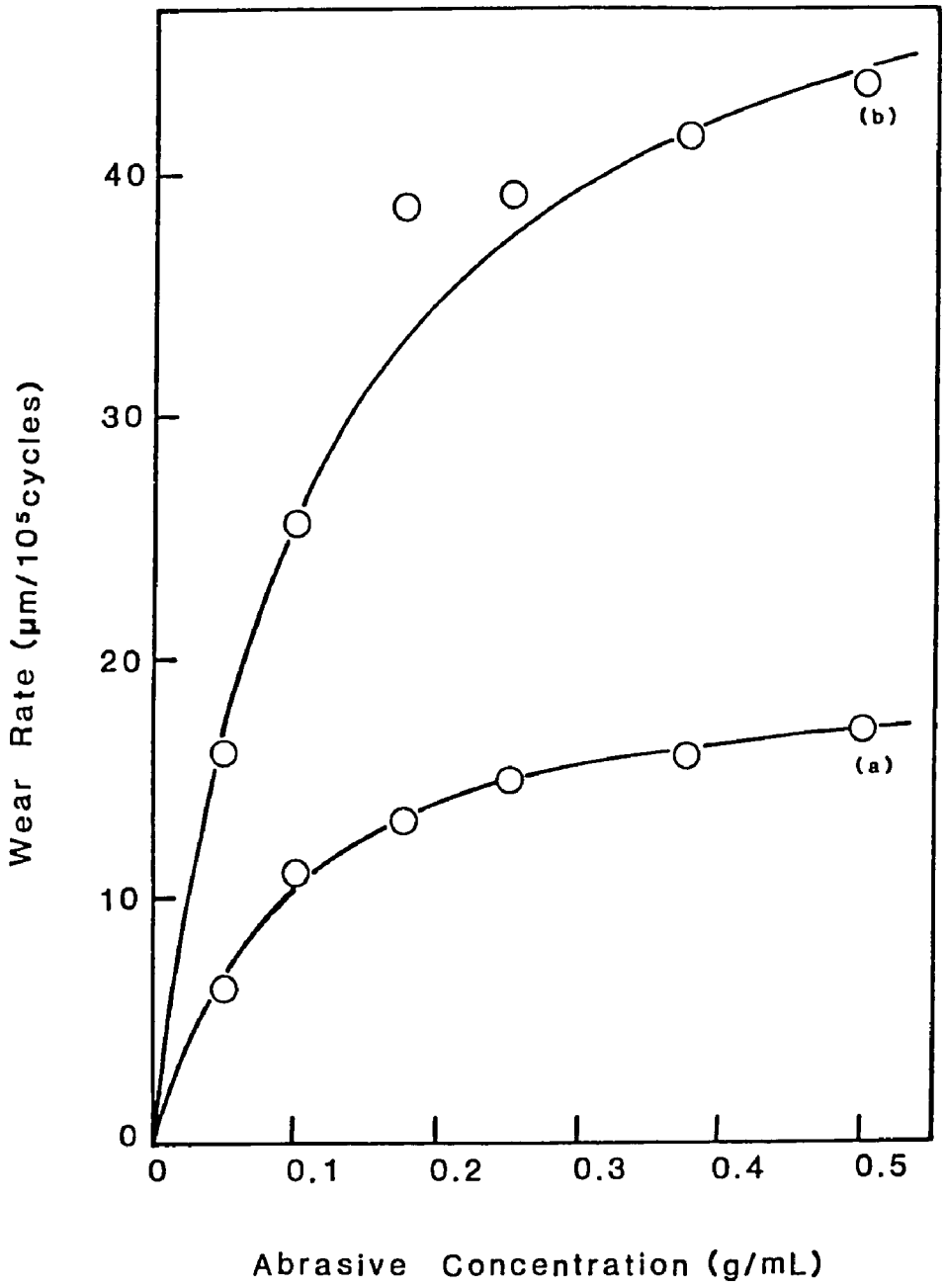

Figure 4-10. Effect of abrasive concentration on the wear rate of anodized aluminum. Anodic coatings were prepared: (a) at 20°C and 15 V for 20 minutes and (b) at 20°C and 10 V for 140 minutes. The contact pressure was 22.9 g/cm^2.

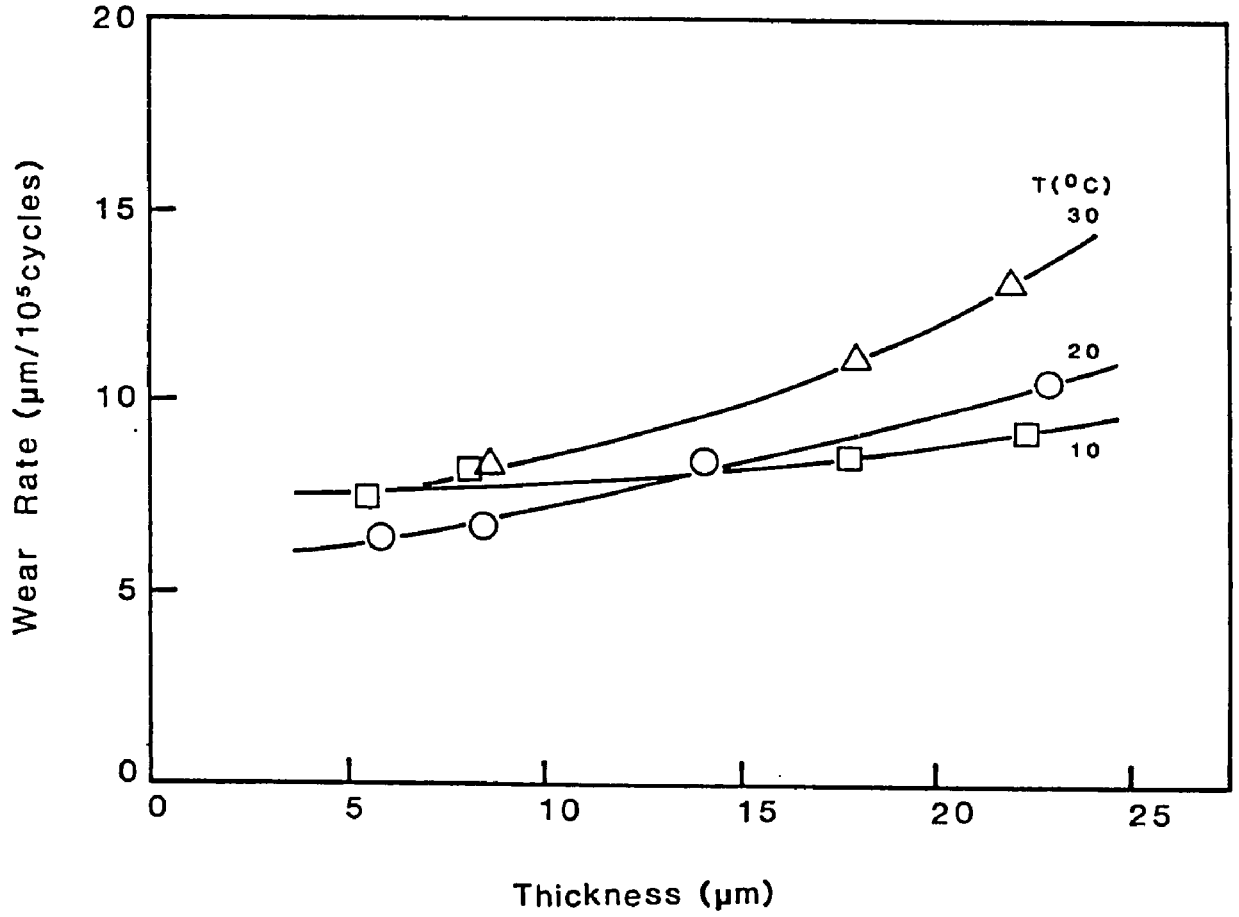

Figure 4-11. Rate of wear of the anodic coatings formed in 15% H_2SO_4 at 15 V and different electrolyte temperatures as a function of film thickness. Contact pressure was 22.9 g/cm^2.

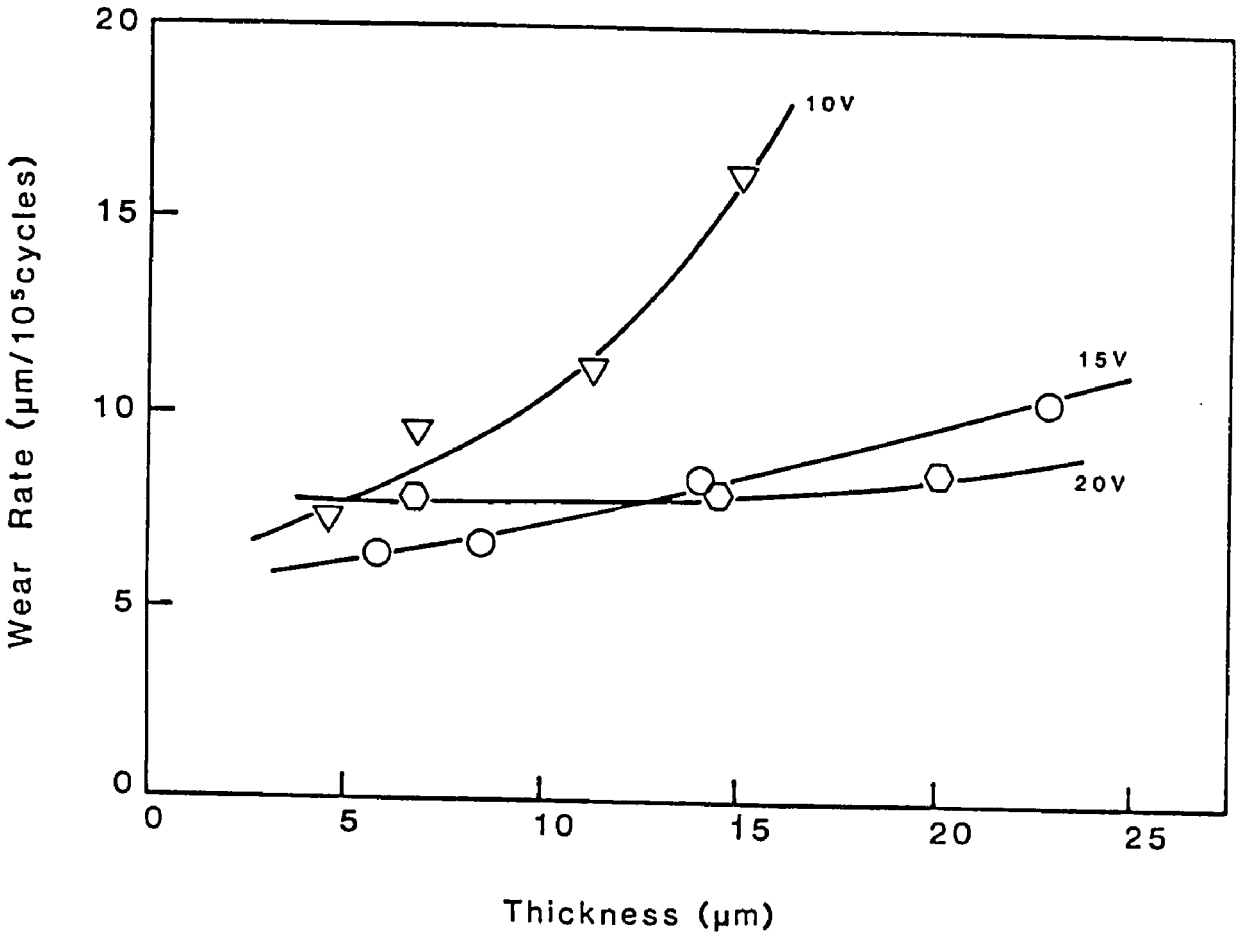

Figure 4-12. Rate of wear of the anodic coatings formed in 15% H_2SO_4 at 20°C and different anodizing voltages as a function of film thickness. Contact pressure was 22.9 g/cm^2.

lower anodizing voltages (figure 4-12). This behavior is very similar to that for the apparent density of oxide films as a function of film thickness.

4.4 Rates of Wear of Sealed Anodic Coatings on Aluminum

The wear behavior of the sealed coatings was very different from that of the unsealed coatings in that there was a rapid rate of wear during the very early stages, followed by a much lower rate of wear. The data for the four different sealing solutions are summarized in Figures 4-13 to 4-17 for sealing times of 1, 2, 10, 30, and 60 minutes. Anodic coatings were prepared in 15% H_2SO_4 at 20°C and 15 V for 18 minutes. The abrasive concentration was 1 g SiC in 50 mL distilled water and the contact pressure was 22 g/cm^2. It will be noted that the oxide sealed in sodium silicate exhibited the greatest rate of wear over long time periods and that the wear rate was approximately constant over the entire time period, whereas the other sealants led to a high rate of wear during the early stages, falling off with wear time.

The wettability of the anodized surface by water after sealing was determined for all the aqueous environments at 1, 2, 5, 10, 20, 30, and 60 min sealing time. These data are plotted in terms of contact angle of the water droplet with the anodized surface in Figure 4-18. Coatings sealed in the nickel acetate, potassium dichromate, and distilled water exhibited reduced wettability after short sealing times and good wettability after long sealing times. The sodium silicate sealant was unique in that excellent wettability was

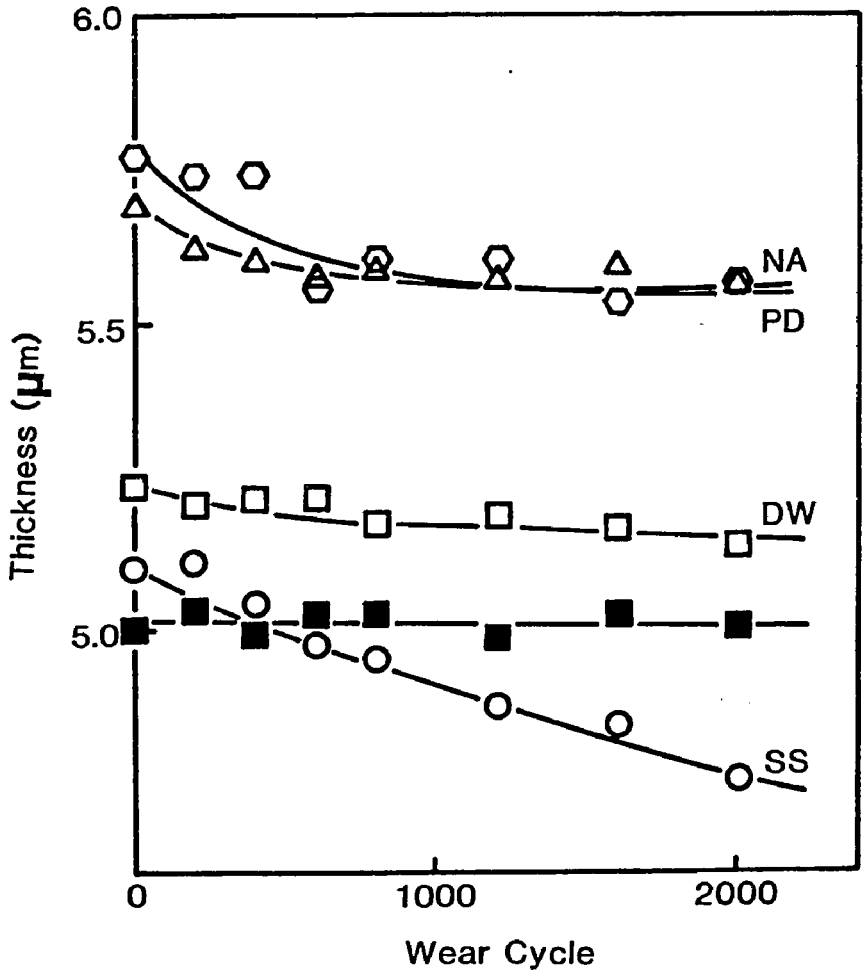

Figure 4-13. Rates of wear of anodized aluminum sealed in nickel acetate solution (NA), potassium dichromate solution (PD), distilled water (DW), and sodium silicate solution (SS) for 1 min. Reference curve for an unsealed anodized aluminum is also given (solid squares).

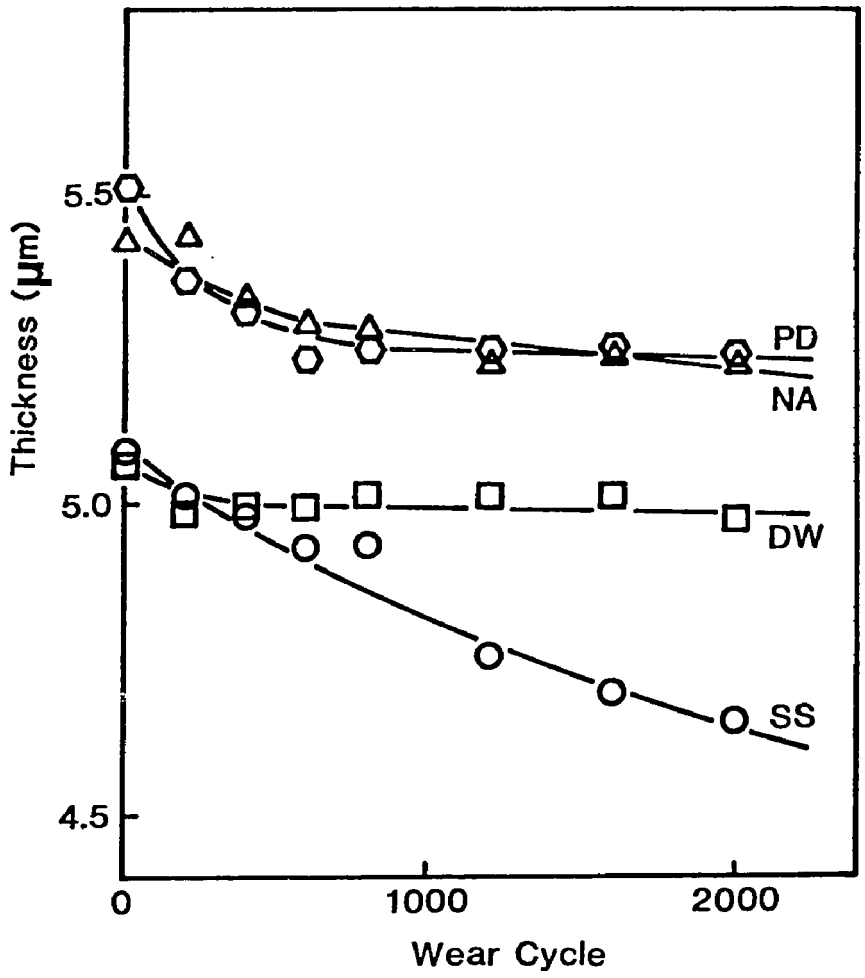

Figure 4-14. Rates of wear of anodized aluminum sealed in nickel acetate solution (NA), potassium dichromate solution (PD), distilled water (DW), and sodium silicate solution (SS) for 2 min.

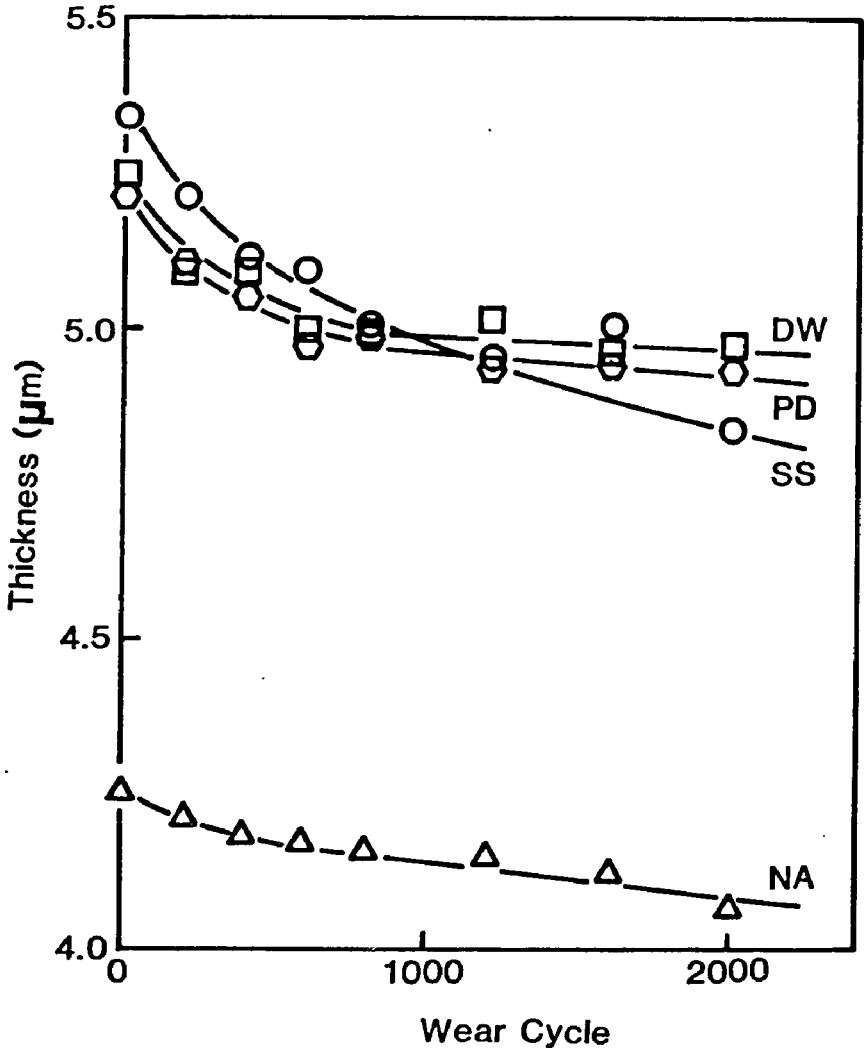

Figure 4-15. Rates of wear of anodized aluminum sealed in nickel acetate solution (NA), potassium dichromate solution (PD), distilled water (DW), and sodium silicate solution (SS) for 10 min.

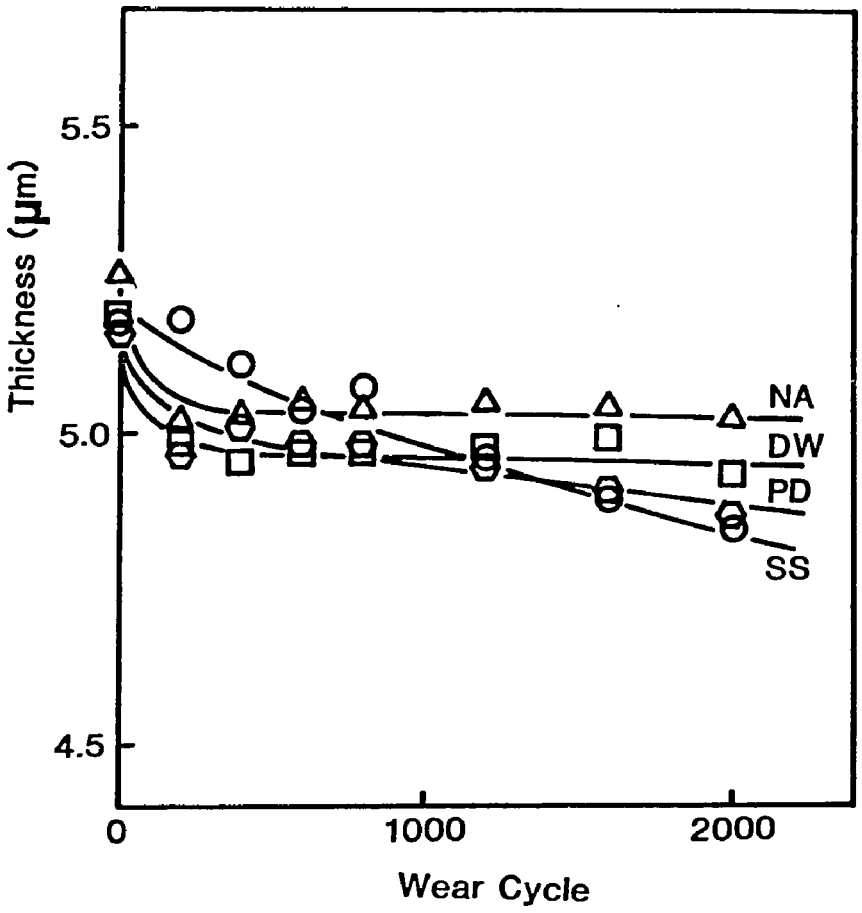

Figure 4-16. Rates of wear of anodized aluminum sealed in nickel acetate solution (NA), potassium dichromate solution (PD), distilled water (DW), and sodium silicate solution (SS) for 30 min.

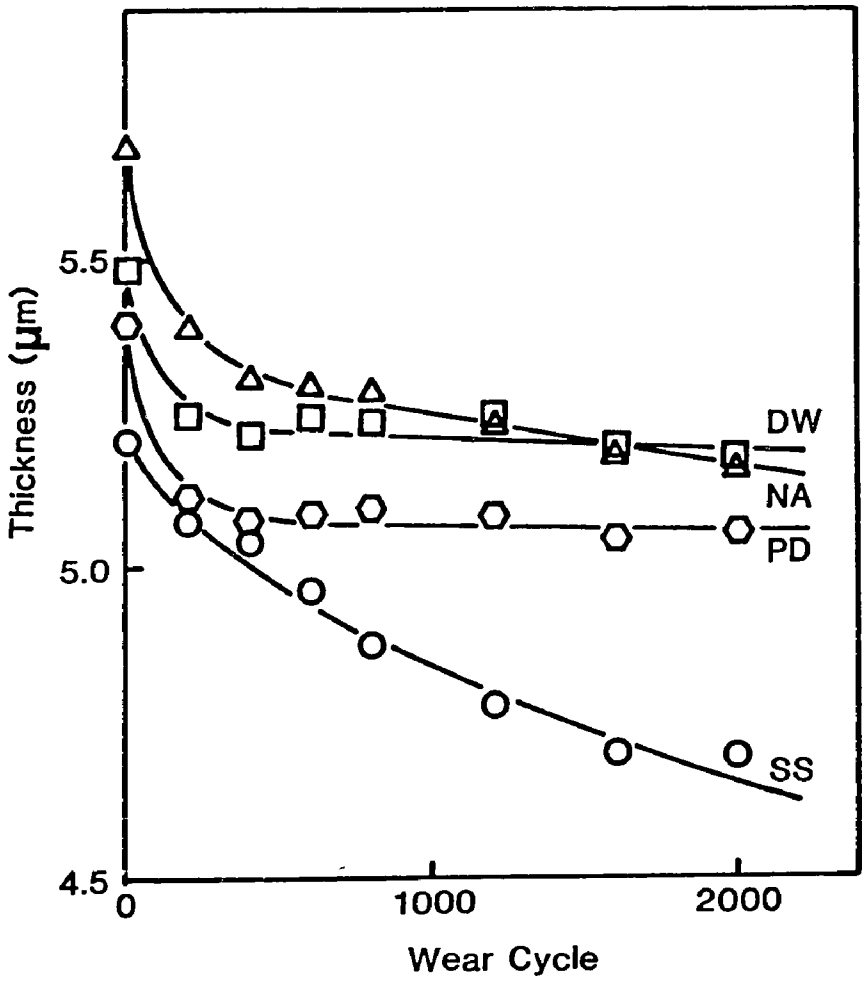

Figure 4-17. Rates of wear of anodized aluminum sealed in nickel acetate solution (NA), potassium dichromate solution (PD), distilled water (DW), and sodium silicate solution (SS) for 60 min.

exhibited at all sealing times. All sealing treatments results in very small contact angles (good wettability) at sealing times in excess of 10 minutes.

The tendency of an ink (Red GA 80-1421) to wet the anodized and sealed aluminum surface was determined concurrently with the contact angle measurements. Ink, when applied with a hand roller, readily stuck to all the aluminum surfaces when the surface was dry because of the inherent roughness of the surface (Figure 4-19). When the surface was wetted with distilled water, ink wet the anodized aluminum surface sealed in boiling distilled water, nickel acetate solution or potassium dichromate solution to a certain degree (Figure 4-20). The anodized surface was not wetted by ink when sealed in sodium silicate solution, even at short (one minute) sealing times. When the surface was wetted with a commercial fountain solution, ink did not wet all the aluminum surfaces, either sealed or unsealed (Figure 4-21).

Another two series of experiments were conducted to determine the effect of the nature of the anodized aluminum on the wettability of the surfaces sealed in boiling distilled water and sodium silicate solution. Anodic coatings were formed in 15% H_2SO_4 at 20°C and 15V for 20 min and at 20°C and 10V for 140 min. After anodization, the anodized specimen was immersed in the anodizing solution at 35°C for 0, 10, and 35 minutes and then sealed. The oxide film was completely removed from the 140-min sample after 35 min immersion. Experimental data of the contact angle of water with the anodized surfaces sealed in distilled water are shown as a function of the sealing and immersion times in Figure 4-22 for 20-min coatings and Figure 4-23 for

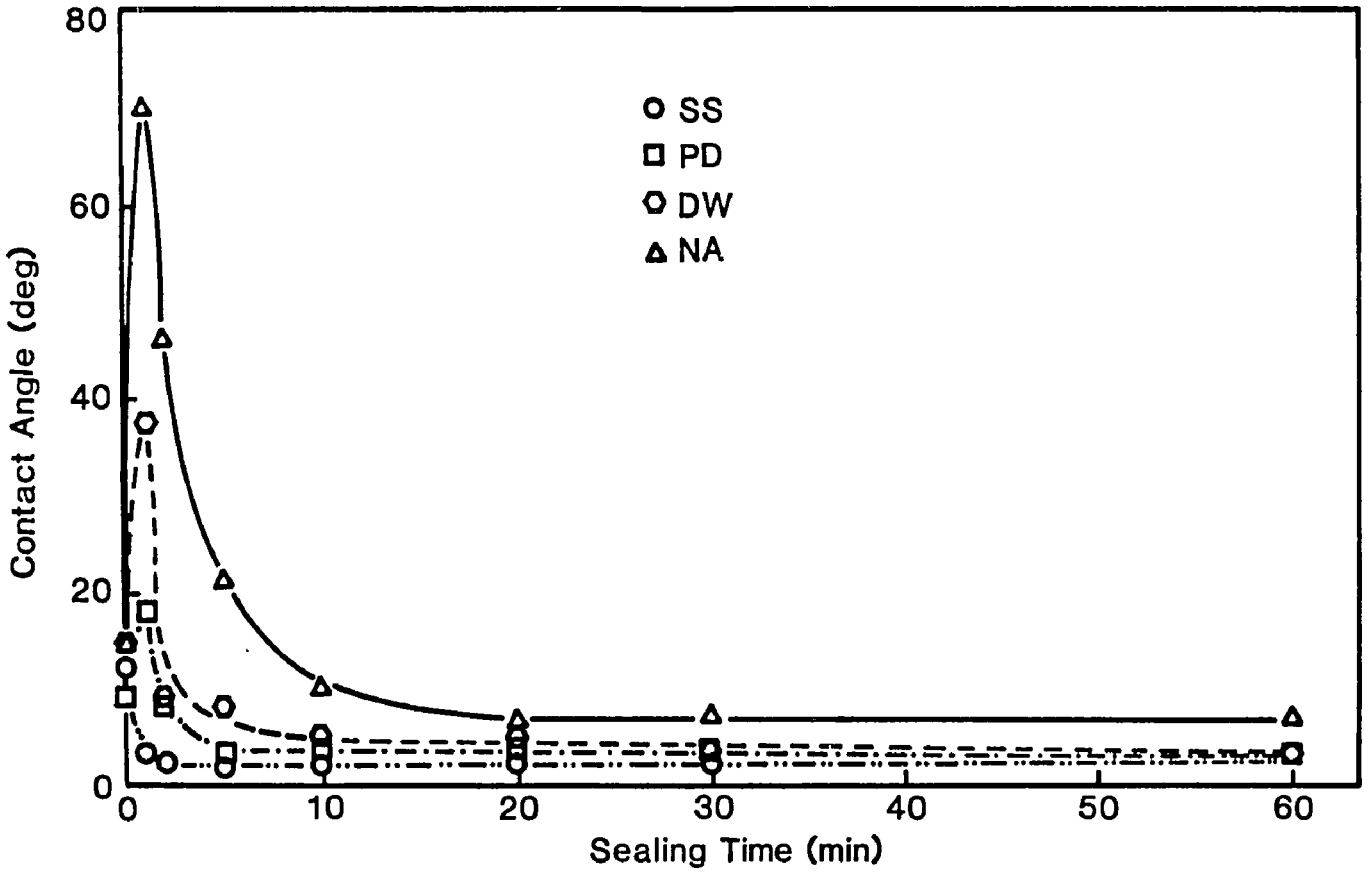

Figure 4-18. Contact angle of water with anodized aluminum surfaces sealed in sodium silicate solution (SS), potassium dichromate solution (PD), distilled water (DW), and nickel acetate solution (NA) for times up to 60 minutes.

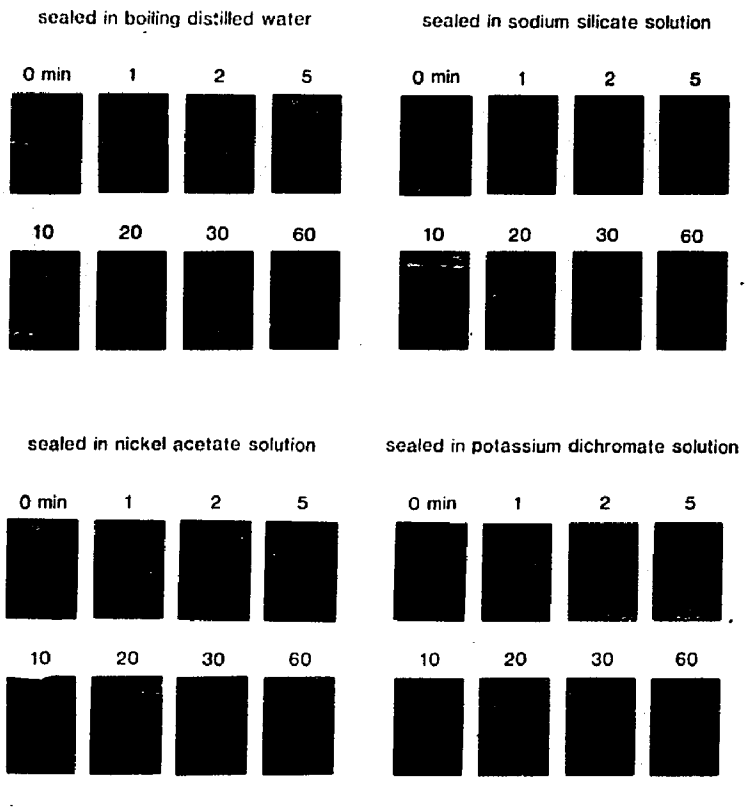

Figure 4-19. Tendency of an ink to wet the anodized aluminum surfaces sealed in sodium silicate solution, nickel acetate solution, potassium dichromate solution, and distilled water for various times. The aluminum surface was dry.

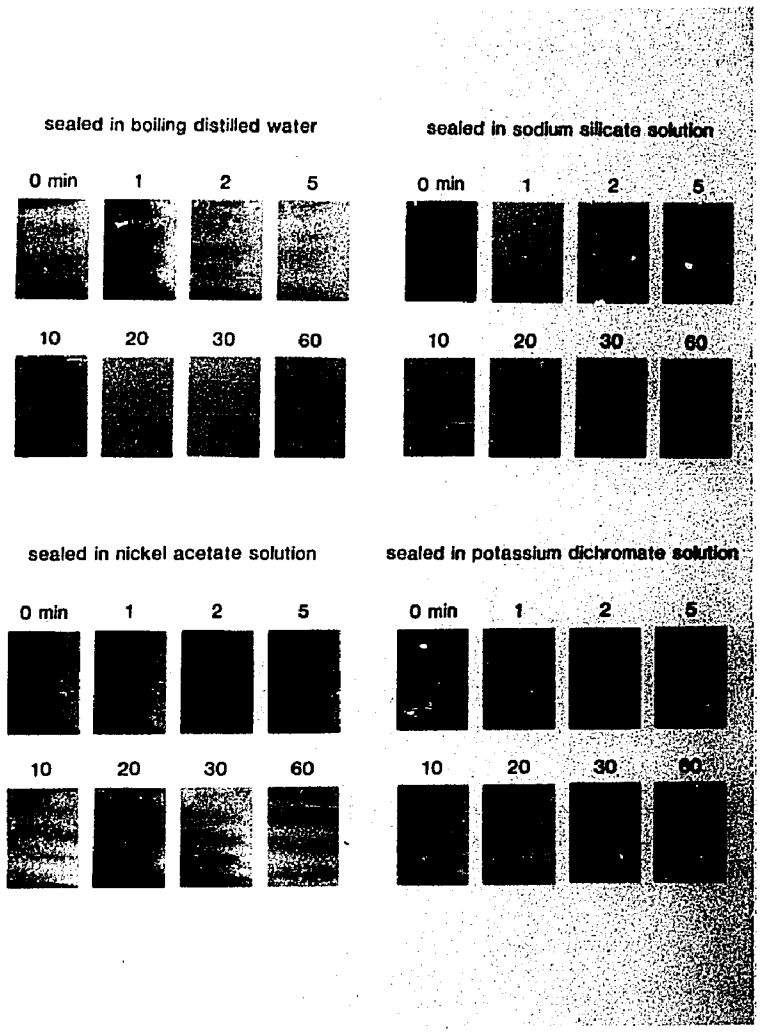

Figure 4-20. Tendency of an ink to wet the anodized aluminum surfaces sealed in sodium silicate solution, nickel acetate solution, potassium dichromate solution, and distilled water for various times. The aluminum surface was wetted with distilled water before the application of ink.

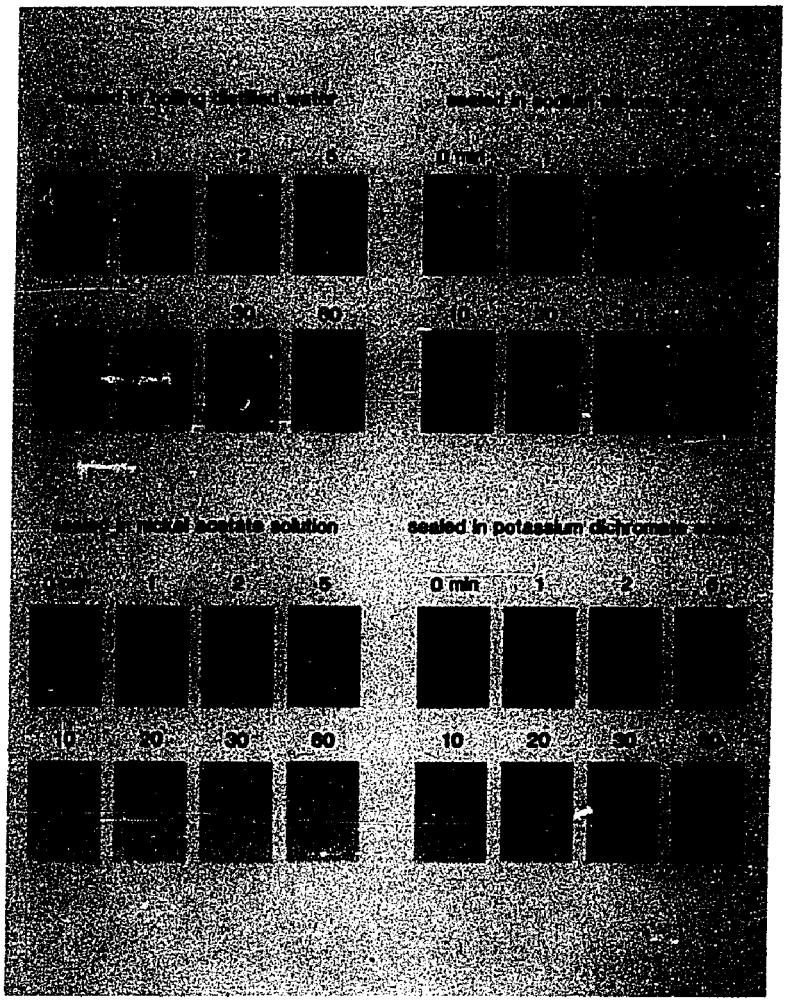

Figure 4-21. Tendency of an ink to wet the anodized aluminum surfaces sealed in sodium silicate solution, nickel acetate solution, potassium dichromate solution, and distilled water for various times. The aluminum surface was wetted with a commercial fountain solution before the application of ink.

140-min coatings. The 20-min anodized surfaces after both 0 and 10 min immersions exhibited reduced wettability after short sealing times and good wettability after long sealing times, the effect being less significant in the latter case. The anodized surfaces after 35 min immersion were completely wetted with distilled water at all sealing times. No reduced wettability after sealing was observed for 140-min coatings (Figure 4-23). The 140-min coatings after 10 min immersion again exhibited excellent wettability. The behavior of the water contact angle for the anodized surfaces sealed in sodium silicate solution for all coatings studied was similar to that shown in Figure 4-18.

4.5 Wear of Polymer Coatings on Anodized Aluminum

Wear test conditions for polymer coatings were: 1 g SiC in 50 mL distilled water and 22 g/cm^2 contact pressure. Figure 4-24 shows infrared specular reflectance spectra for high molecular weight polystyrene coated on a commercial anodized aluminum plate, before abrasion and after 100 cycles in the wear testing apparatus. The interference fringes are superimposed upon the spectrum of the polystyrene, but a number of fringes are visible which can be used for thickness measurements. An example of changes of the film thickness of high molecular weight polystyrene with the number of wear cycles is given in Figure 4-25. Polymer film thickness decreases linearly with wear cycles. There is no initial increase in thickness at the early stages of wear, which is different from that of anodic coatings (Figure 4-7).

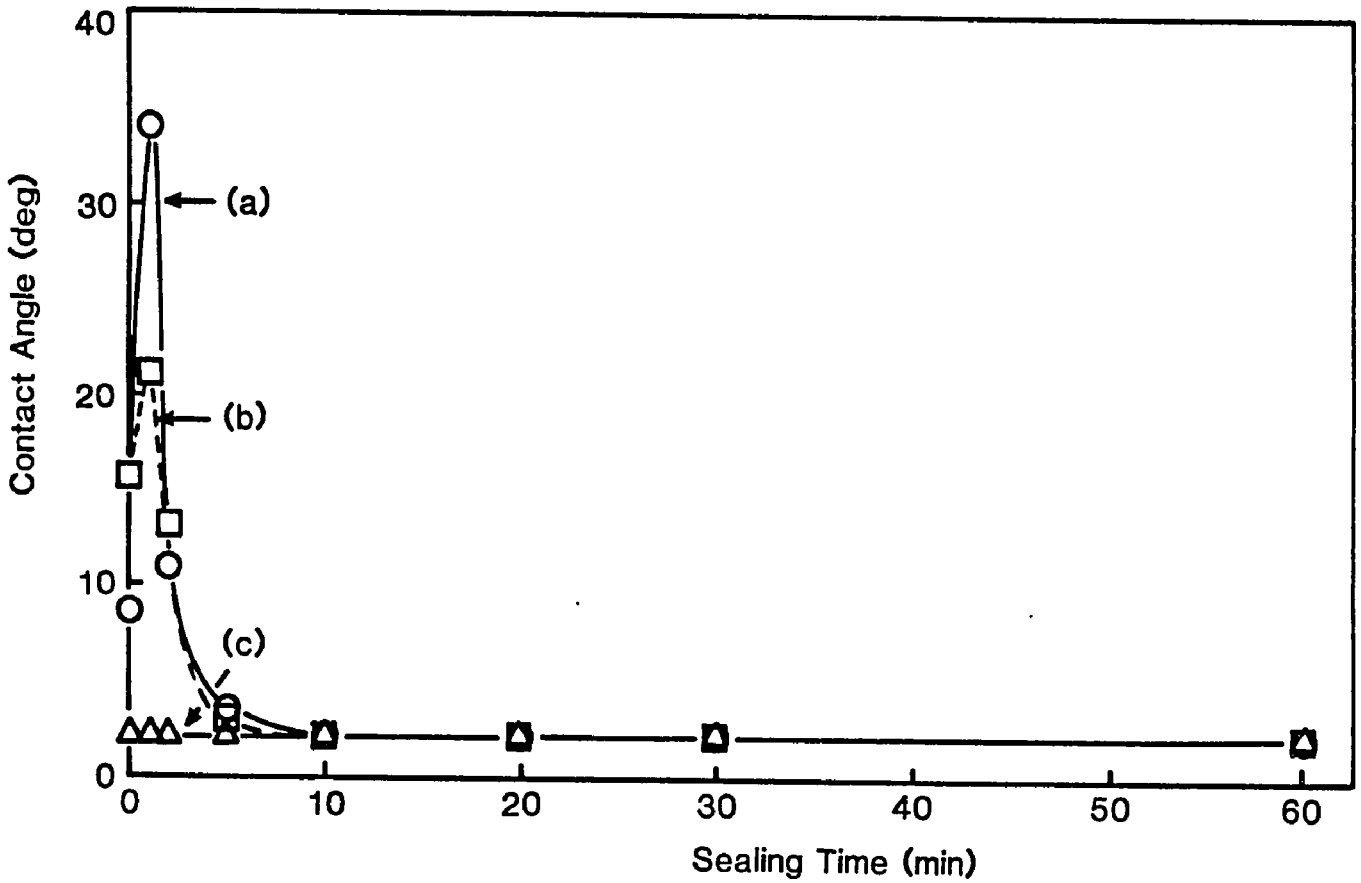

Figure 4-22. Contact angle of water with anodized aluminum surface sealed in boiling distilled water up to 60 min. Anodized aluminum was prepared in 15% H_2SO_4 at 20°C 15V for 20 min and immersed in the same electrolyte at 35°C for (a) 0 min, (b) 10 min, and (c) 35 min.

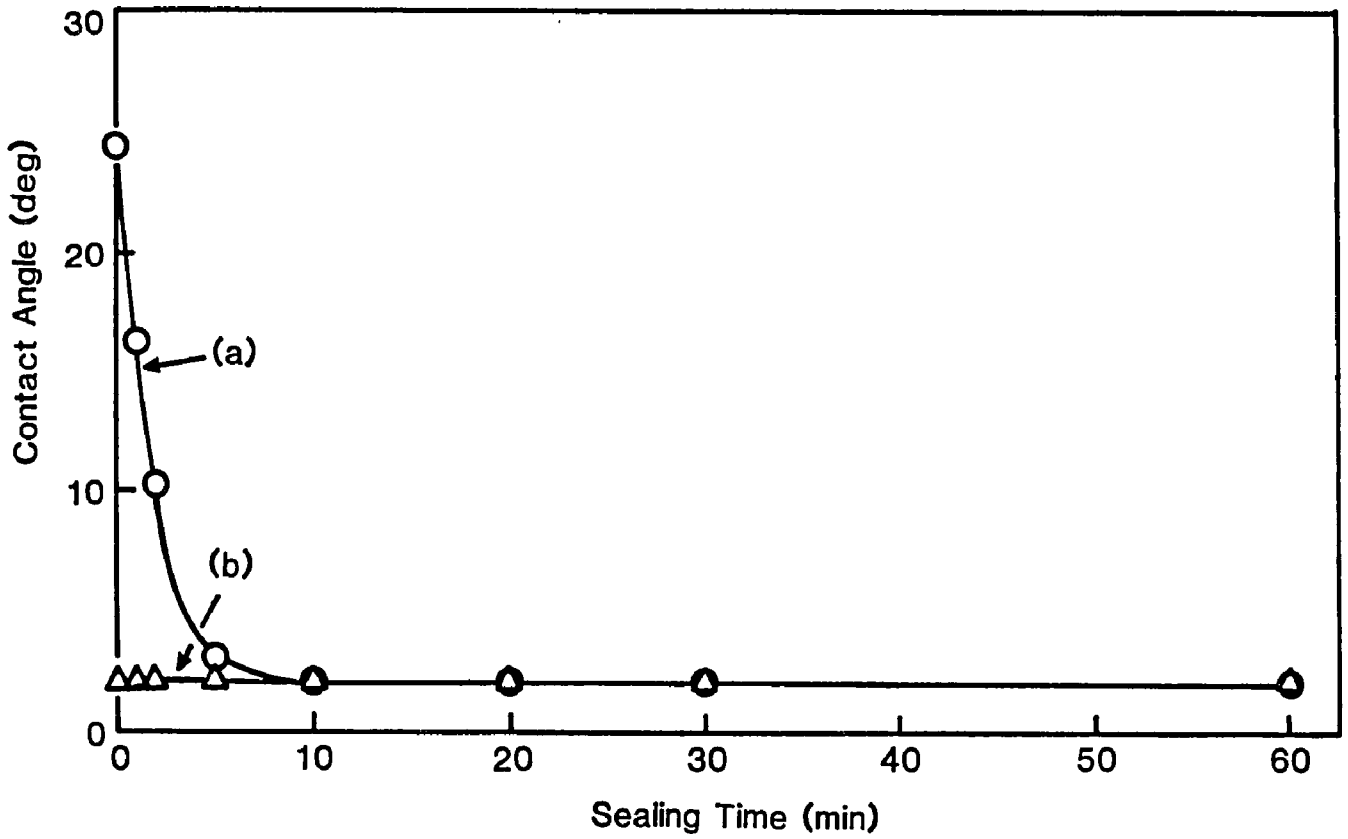

Figure 4-23. Contact angle of water with anodized aluminum surface sealed in boiling distilled water up to 60 min. Anodized aluminum was prepared in 15% H_2SO_4 at 20°C 10V for 140 min and immersed in the same electrolyte at 35°C for (a) 0 min and (b) 10 min.

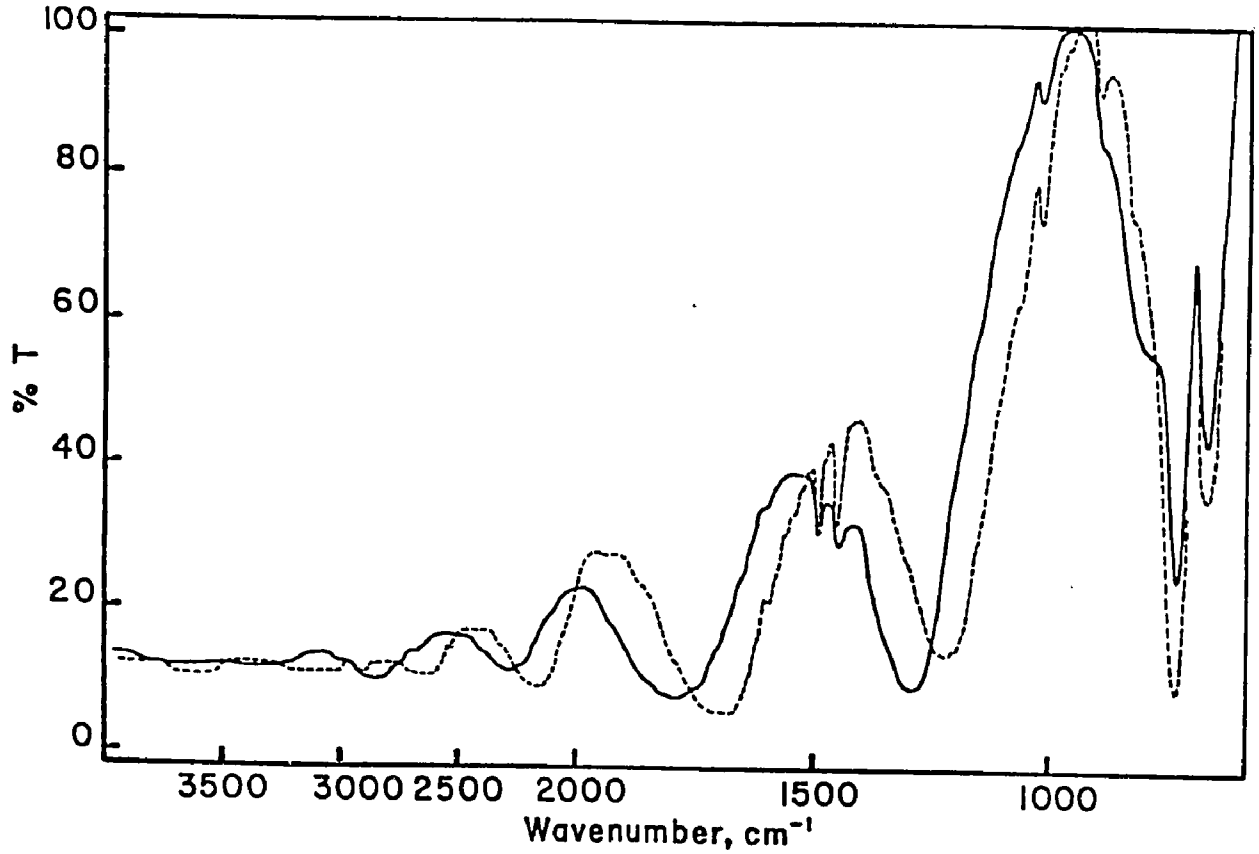

Figure 4-24. Specular infrared reflectance spectra of high molecular weight polystyrene on a commercial plate anodized in sulfuric acid. Dotted line represents unworn coating and solid line represents spectrum form coating after 100 wear cycles (taken from [10].

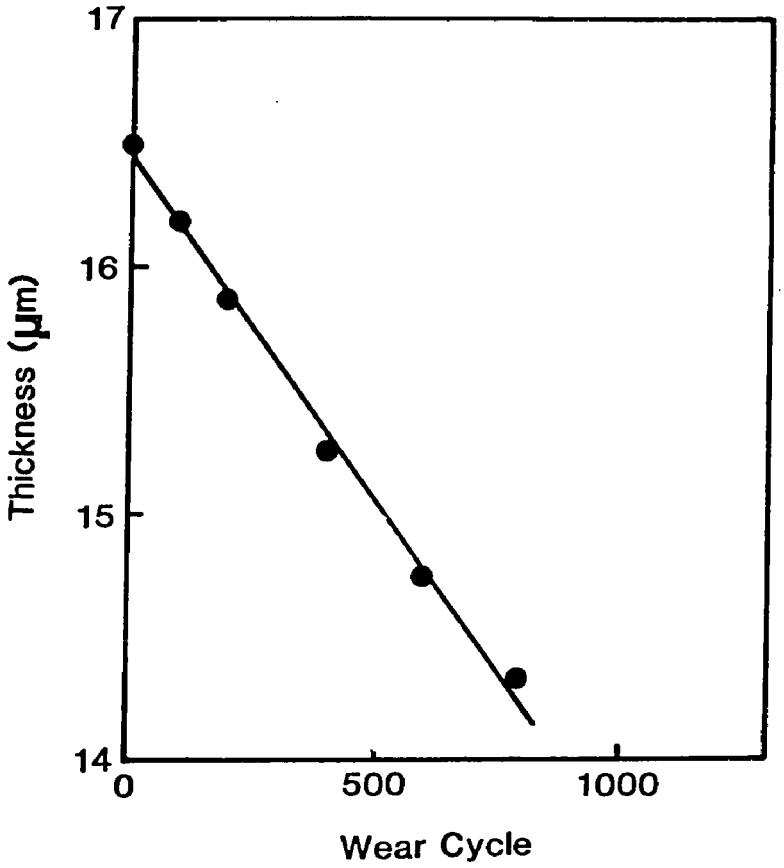

Figure 4-25. The rate of wear of a polystyrene coating on an anodized aluminum formed in 15% H_2SO_4 at 10V and 20°C and sealed in boiling distilled water for 30 min.

A series of experiments was carried out to determine if the rate of wear of a polymeric coating is appreciably influenced by the manner in which the anodized aluminum substrate is prepared. Anodized aluminum was prepared in 15% H_2SO_4 at different anodizing voltages and electrolyte temperatures. The anodized substrate was used in both the sealed and unsealed states. Sealing was carried out for 30 min in boiling distilled water. The thickness of the anodic oxide was approximately 2 μm in all cases and the thickness of high molecular weight polystyrene coatings was 12-17 μm. The results of these experiments are summarized in Table 4-2.

As the polymer coatings become thinner than about 2.5 μm the interference fringes no longer appear in the normal infrared region. The empirical relationship $\Delta A = \log T_s/T_c$ permits the determination of polymer film thickness to small values, provided that an absorption band of sufficient intensity is present in the spectrum of the polymer coating. The "ring-breathing" mode bands of polystyrene appearing in the 700-800 cm^{-1} region are excellent for this purpose. The applicability of this empirical equation to the thickness determination and an example showing the changes of the absorption band by wear have been presented in chapter 3. Plots of the rates of wear of low molecular weight polystyrene, high molecular weight polystyrene, and poly-n-butylmethacrylate on a commercial plate anodized in sulfuric acid and a laboratory plate anodized in 5% phosphoric acid are given in Figures 4-26 to 4-28.

Table 4-2. Rates of Wear of Polystyrene Coatings on Sealed and Unsealed Anodized Aluminum, 2 μm in Thickness.

Electrolyte	Anodizing voltage, V	Anodizing temp, °C	Polystyrene coating thickness unsealed	sealed	Wear rate in μm/10^4 cycles unsealed	sealed
15% H_2SO_4	10	20	12.1	16.5	9.6	27.4
	15	10	12.8	15.8	11.1	17.2
	15	20	13.1	--	13.9	--
	15	30	12.1	15.6	11.5	26.6
	20	20	11.9	15.7	14.1	19.3

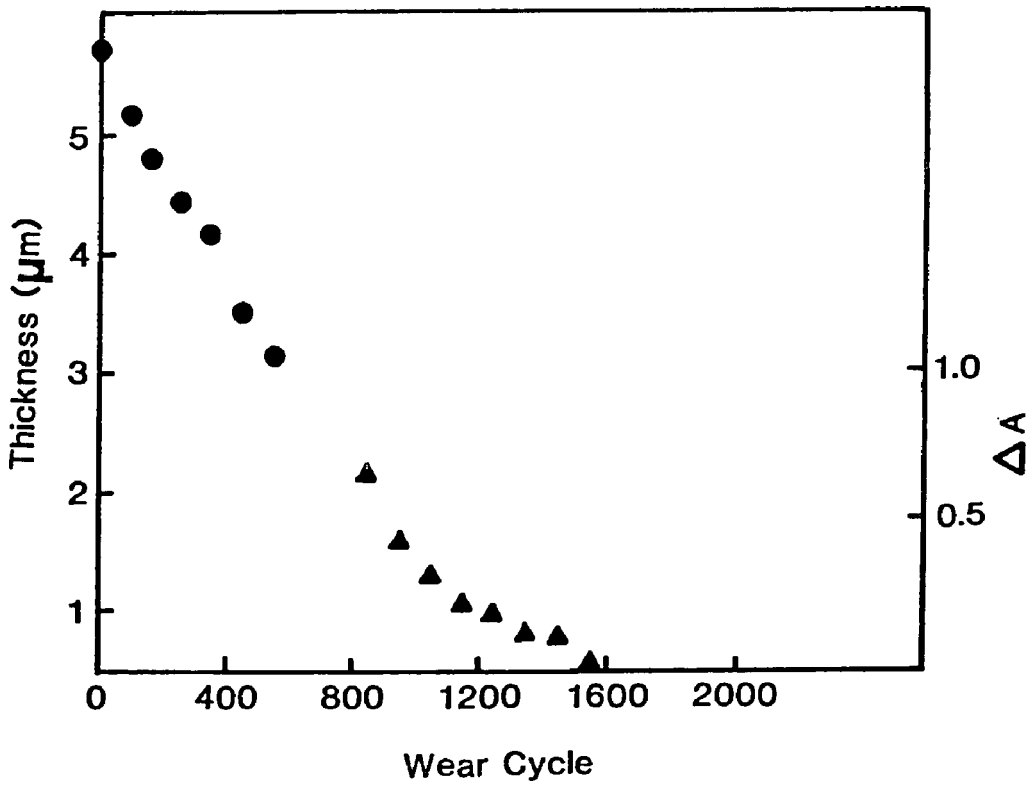

Figure 4-26. Wear of low molecular weight polystyrene on a commercial plate anodized in sulfuric acid. Circles represent measurements made by interference fringe technique and triangles by the absorption technique (taken from [10]).

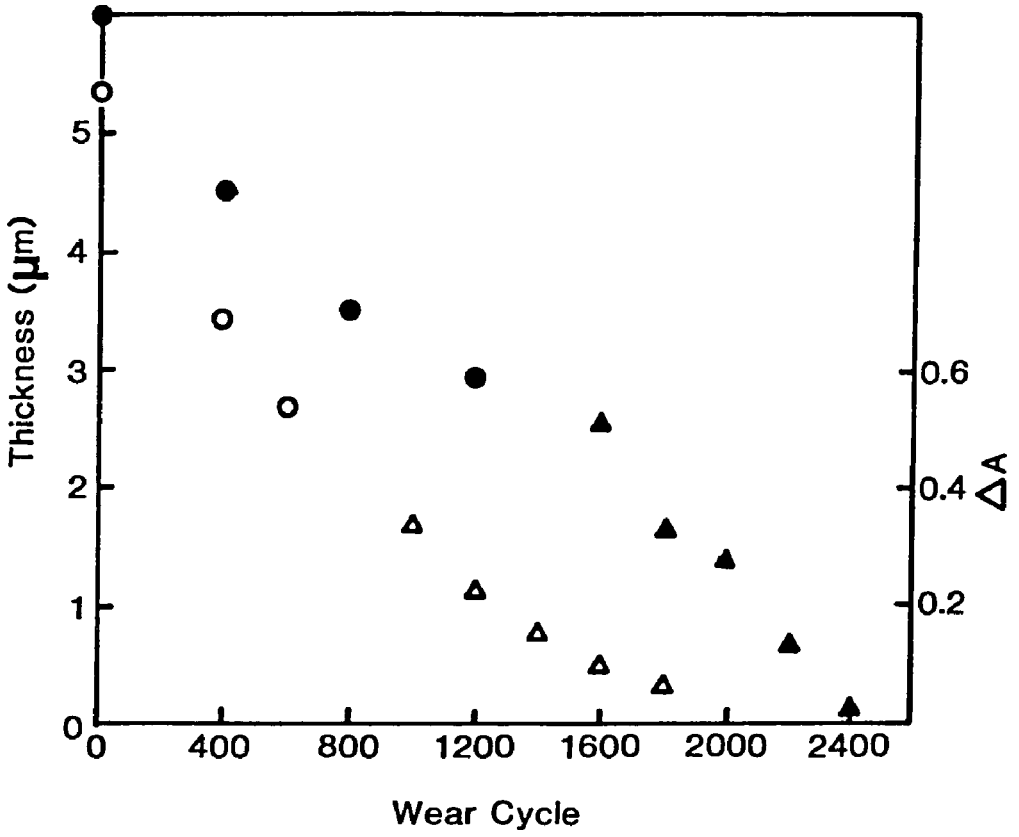

Figure 4-27. Wear of high molecular weight polystyrene on a commercial plate anodized in sulfuric acid (open points) and in 5% H_3PO_4 (solid points). Circles represent measurements made by interference fringe technique and triangles by the absorption technique (taken from [10]).

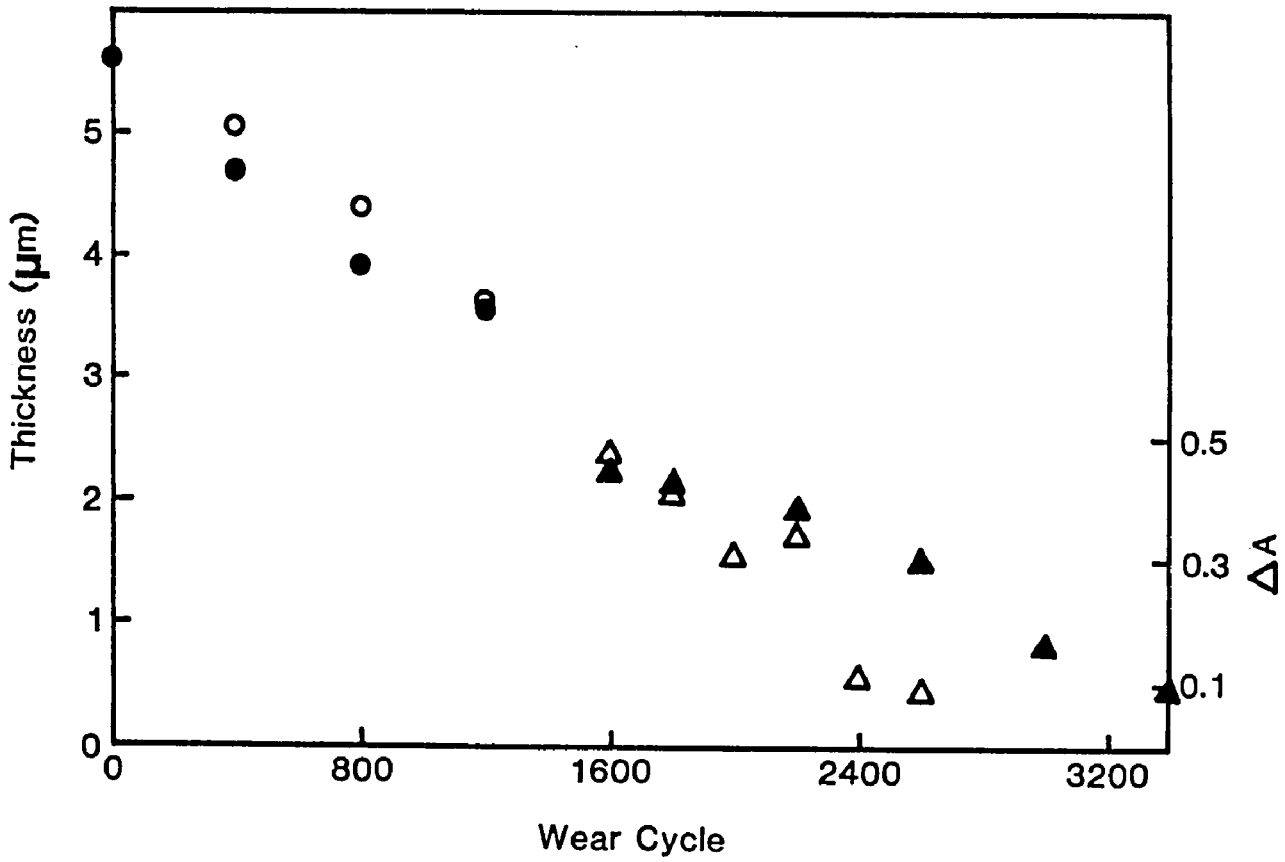

Figure 4-28. Wear of poly-n-butylmethacrylate on a commercial plate anodized in sulfuric acid (open points) and in 5% H_3PO_4 (solid points). Circles represent measurements made by interference fringe technique and triangles by the absorption technique (taken from [10]).

4.6 Changes of the Surface Wettability due to Wear

A series of experiments was carried out to determine if the wettability of both anodized aluminum and polymer surfaces is appreciably influenced by wear. Two anodized aluminum samples were used. One was formed at 20°C and 15 V for 20 min, which has the lowest wear rate in the range of anodizing conditions employed, and a second, exhibiting the highest wear rate, prepared at 20°C and 10 V for 140 min. High molecular weight polystyrene was coated to these two anodized substrates. The coating thickness of polystyrene was approximately 12 μm. Figures 4-29 and 4-30 show the changes of the water contact angle as a function of the number of wear cycles for anodized aluminum and polystyrene surfaces, respectively. Wear increases the hydrophilicity of the 140-min anodized surface, while the contact angle on water of the 20-min anodized surface increased with wear. Polymer surfaces became slightly more hydrophilic with wear and the influence of the underlying substrate appeared negligible.

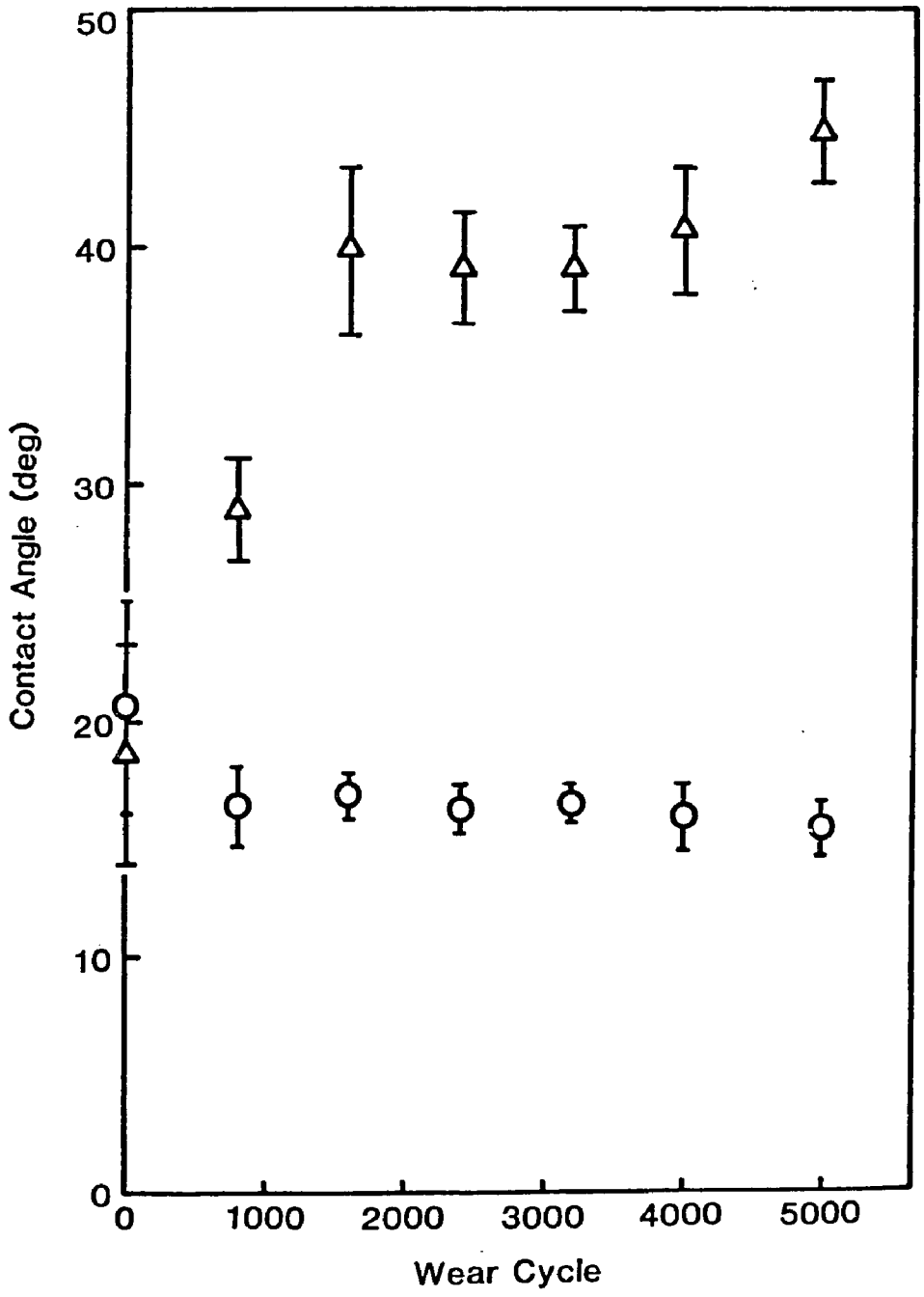

Figure 4-29. Contact angle of water with surfaces of a 20-min coating (△) and a 140-min coating (o) as a function of the number of wear cycles.

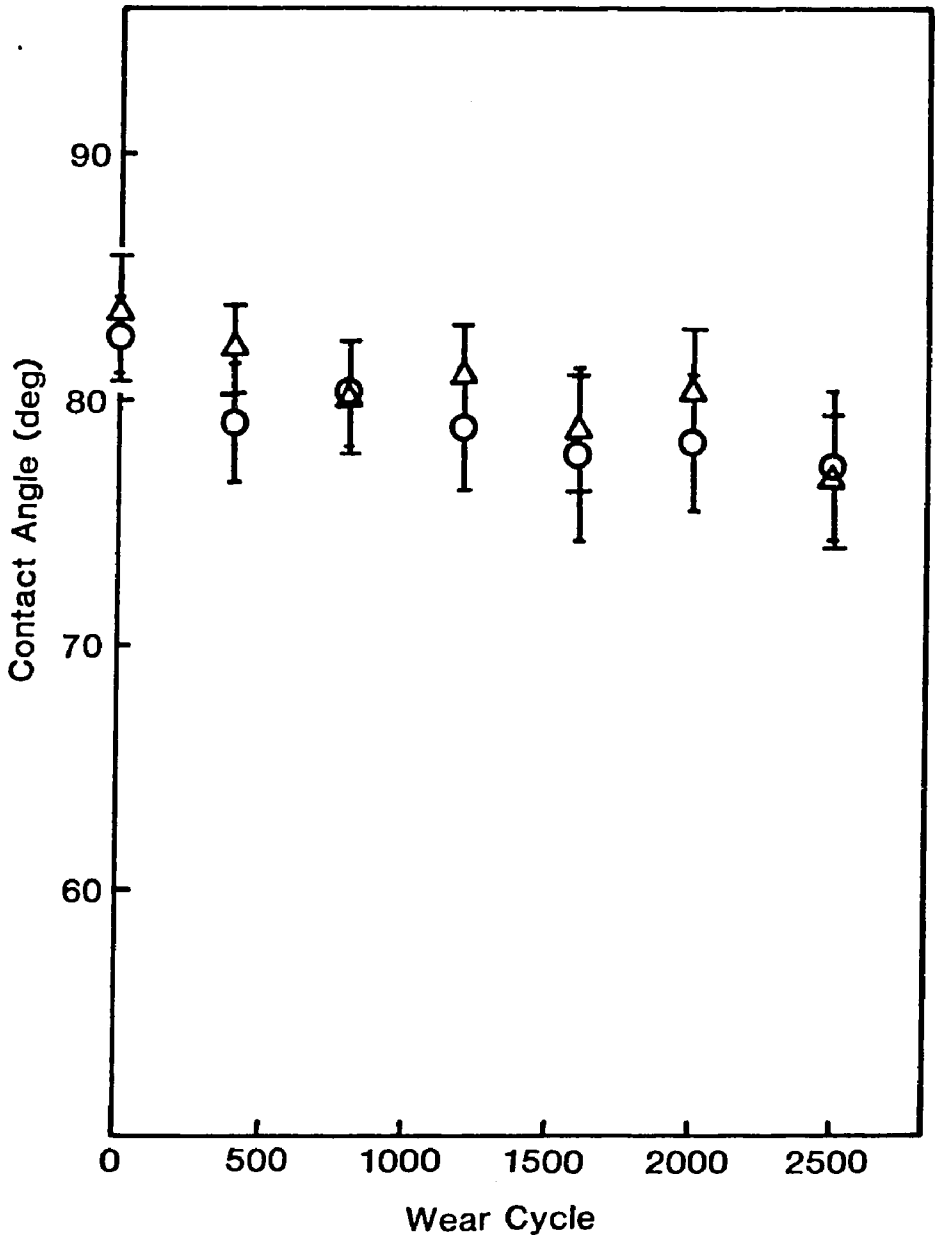

Figure 4-30. Contact angle of water with polystyrene surfaces as a function of the number of wear cycles. Anodized aluminum substrates were a 20-min coating (△) and a 140-min coating (o).

CHAPTER 5

DISCUSSION

5.1 Use of Anodized Aluminum as the Substrate for Lithographic Printing Plates

Salgo [214] has pointed out that high quality printing and long run life can only be achieved by offset printing plates which possess the following properties:

1. Both printing and non-printing areas must possess a high degree of resistance against mechanical and chemical actions.
2. Ink-receptive areas must strongly adhere to the base, must readily receive and give off the ink in order to reduce loads on these parts during printing.
3. Maximum selectivity of the printing and non-printing areas must be ensured.
4. The plate surface must be as smooth as possible while retaining a large specific surface area.

The best candidates for offset printing are the bimetal plates. However, bimetal plates cannot be employed economically in all fields. Aluminum has filled an important need in the lithographic printing industry because of its light weight, ease of graining and surface treatment, and economy in moderate and long term use [214, 215, 216, 217]. The anodizing process converts the soft aluminum metal to a hard yet porous surface. The high resistance of this oxide surface to wear and corrosion adds significantly to the run

life of the plate and provides protection from mechanical damage and corrosion during shipment and storage. Moreover, the porous structure of oxide layers is almost the same as that of lithostone which has high water holding capacity at the surface and shows good adhesion of the image area to the surface.

Graining is a very important process in the lithographic printing plate manufacture. It improves the adhesion of photosensitive coatings and water holding capacity [218, 219, 220, 221]. Graining can be accomplished in various ways [218]: (1) ball graining, (2) brush graining, (3) blasting, (4) electrochemical graining, and (5) chemical graining. Coarser grains hold more water in the non-image areas, making the water balance on the press less critical [218, 222] and improving adhesion of image areas to the substrate [218]. The image areas are more susceptible to penetration by the underlying metal substrate, increasing the risk of dot loss [223]. Coarse-grained plates also require a higher printing force than fine-grained plate, resulting in a reduced run life [214]. Finer grains provide higher resolution images and more faithful reproductions [218, 222, 223]. A compromise must be reached to obtain satisfactory printing performance. Graining is generally carried out prior to the anodization, since the anodizing process does not change the surface topography significantly. Scanning electron micrographs in Figure 5-1 show the surface topography of a chemically grained metal surface and two anodized aluminum surfaces. The surface topography of a brush-grained metal surface prior to and after anodization are shown in Figure 5-2. The anodic coating faithfully duplicates the

underlying metal surface.

Hydrophilicity of the anodized aluminum surface can be improved by sealing treatments which ensure maximum differentiation between the image and non-image areas. Good wettability of the anodized surface by water can be achieved by sealing for about 10 min in distilled water, nickel acetate solution, or potassium dichromate solution, or at any sealing time in sodium silicate solution (Figure 4-18). Many commercial lithographic plates receive a silicate treatment of a proprietary nature. The probable reason for this treatment is dramatically shown in Figure 4-18. Coatings treated in sodium silicate solution do not exhibit the reduced wettability (high contact angle with water) at short sealing times which occurs when the anodized aluminum is sealed in boiling distilled water, nickel acetate solution, or potassium dichromate solution. A sodium silicate treated anodized surface is able to repel inks even when it is wetted with distilled water only (Figure 4-20). Of course, commercial lithographic printing utilizes a fountain solution with optimum water wetting conditions (Figure 4-21).

Dean and Ford [216] studied the mode of failure of commercial lithographic printing plates by running these plates on a printing press. Anodized aluminum substrates were obtained from two batches. The voltage employed in producing the anodized substrate for the first batch was higher than that for the second batch. Plates from the second batch failed by loss of image or blinding out after less than 300,000 impressions, while failure was not observed for those plates from the first batch even after 500,000 impressions. They concluded

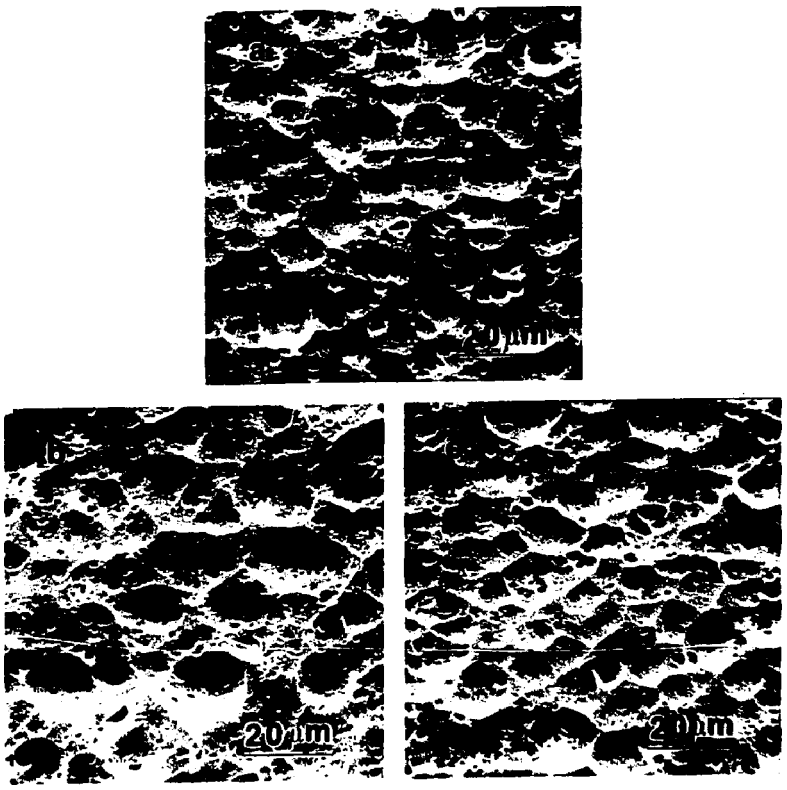

Figure 5-1. Surface topography of (a) a chemically grained aluminum metal surface, (b) an anodized aluminum surface produced in 15% H_2SO_4 at 30°C and 15 V for 45 min, and (c) an anodized aluminum surface produced in 15% H_2SO_4 at 20°C and 15 V for 20 min.

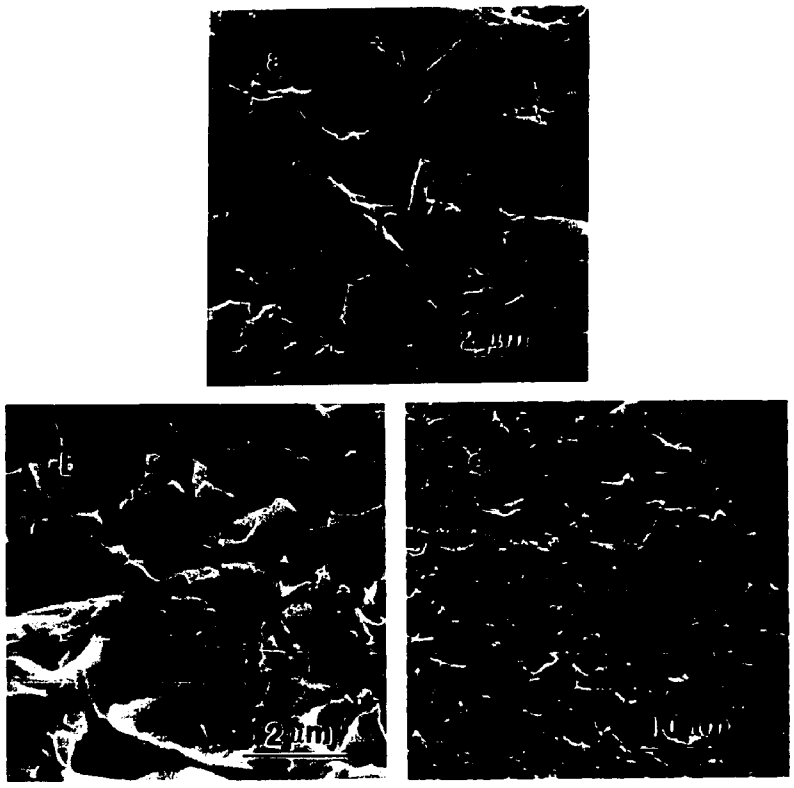

Figure 5-2. Surface topography of (a) a brush-grained aluminum metal surface and (b) and (c) an anodized aluminum surface produced in 15% H_2SO_4 at 20°C and 20 V for 30 min at two magnifications.

that the failure mechanism of plates from the second batch involved abrasive removal of the anodic coating. Plates produced at the higher anodizing voltage showed better resistance to abrasive wear. The wear property of anodic coatings will be discussed in further detail later.

5.2 Structure of the Anodic Oxide Film on Aluminum

The thickness of the oxide film increases linearly with the anodizing time (Figure 4-1). The weight increase of this oxide is not linear with time (Figure 4-2) due to the chemical dissolution of cell wall by the anodizing electrolyte during the anodizing process which results in the oxide having a tapered pore structure. The amount of oxide dissolved into the anodizing solution depends on the aggressiveness of the electrolyte and the anodizing time. The higher the electrolyte temperature, the more aggressiveness the electrolyte. The longer the anodizing time, the greater the amount of oxide dissolved away. Since the current density, the electrolyte temperature, and the anodizing voltage are interrelated with a given electrolyte (Figure 2-27), high electrolyte temperatures at constant anodizing voltage or high anodizing voltages under isothermal conditions provide high formation rates of the oxide coating (Table 4-1), reducing the anodizing time required to achieve a desired thickness. However, both conditions cause a significant temperature rise on the anode because of the Joule heating. The chemical dissolution rate is therefore enhanced. Optimum conditions for producing the densest and hardest are expected to exist. Figures 4-3 and 4-4 show the apparent density of oxide coatings formed under

various conditions as a function of the coating thickness. The densest coating, approximately 5 μm thick, was obtained at 20°C and 15 V for 20 min, while thick coatings of high apparent density, i.e. hard anodic coatings, could be obtained from the conditions of high anodizing voltage and low electrolyte temperature, e.g. at 20°C and 20 V in the range studied.

Figures 4-3 and 4-4 also show that the apparent density falls off progressively with the anodizing time or film thickness. It is because of the increased chemical dissolution rate with film thickness due to the increased surface area of the oxide coating and the temperature rise on the anode. It is more difficult for the Joule heating generated at the pore base to transport through the pore to the bulk solution as the oxide film thickness increases.

It has been found [123, 121] that when the anodized aluminum specimen is immersed in an aggressive solution, usually the anodizing electrolyte, the thickness of the oxide coating remains almost constant up to a certain time of dissolution. Appreciable thinning of the oxide coating was observed as the pore mouths merged into each other at the surface. The dissolution time at the transition point depends on the slant of the pore in the coating; the greater the taper of the cell wall the more rapid the dissolution. The nearly constant thickness of the coating at the early stages of dissolution is a result of the chemical dissolution which takes place primarily on the cell wall because of the much greater surface area of the pore wall than the apparent surface area of the specimen. The mechanism of dissolution is generally referred to as pore-widening and is

responsible for the tapered pore structure of the oxide coating. Figures 5-3 and 5-4 show the scanning electron micrographs of surface topography of the coatings produced at 20°C and 15 V for 20 min and at 20°C and 10 V for 140 min, respectively, which were then immersed in a 15% H_2SO_4 at 35°C for 0, 10, and 35 minutes. No significant change of the surface structure of the 20-min coating was observed after 10 min of immersion (Figure 5-3b), while the pore structure was completely destroyed after 35 min immersion (Figure 5-3c). 10 min immersion was long enough to destroy the surface structure of the 140-min coating (Figure 5-4b). The extremely rough surface of these samples accounts for the excellent wettability. The tapered pore wall is clearly seen in Figures 5-3c and 5-4b, which further confirms the structure of the anodic coating. It is also interesting to note that the surface structure of the 10 V coating (Figure 5-4b) is finer than that of the 15 V coating (Figure 5-3c), indicating that the cell size is smaller for the oxide coating formed at lower anodizing voltage.

5.3 Applicability of Optical Techniques to the Study of Wear

The wear apparatus [211] was originally developed in order to compare the ability of commercial lithographic plates to withstand the abrasive nature of many printing inks. The method has proven to be adequate for this task, with satisfactory correlations being obtained between commercial experience and the accelerated test data. In the present study, emphasis has been placed on the use of the wear apparatus as a tool for determining the wear resistance of anodic coatings on aluminum prepared in different ways and the resistance of

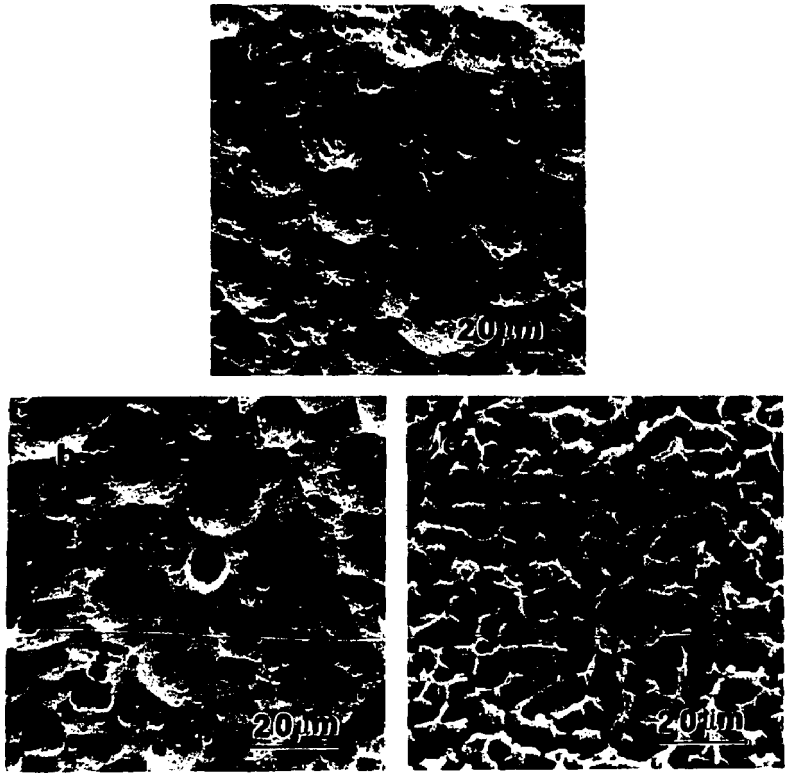

Figure 5-3. Surface topography of anodized aluminum surface produced at 20°C and 15 V for 20 min and immersed in 15% H_2SO_4 at 35°C for (a) 0, (b) 10, and (c) 35 min.

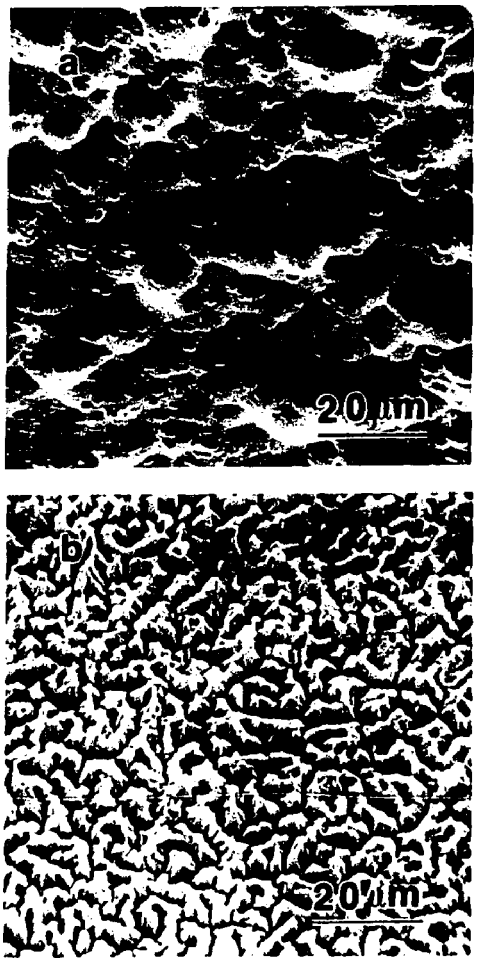

Figure 5-4. Surface topography of anodized aluminum surface produced at 20°C and 10 V for 140 min and immersed in 15% H_2SO_4 at 35°C for (a) 0 and (b) 10 min.

polymer coatings to lateral abrasion. Optical techniques have proven to be superior in determining the rate of wear as compared with both the weight loss and surface roughness measurements. The method explored in this study should have applicability to the selection of (1) the optimum surface preparation method for the substrate and (2) polymeric coatings with satisfactory resistance to abrasive wear for systems in which high abrasive resistance is important.

The infrared specular reflection technique adopted for determining the coating thickness of both anodized aluminum and polymer coatings on aluminum proved useful in the thickness approximations for 4 to 25 μm anodic coatings and 2.5 to 25 μm polymer coatings. The relative intensity of a specific absorption band in the polymers studied allowed the measurement of coatings down to approximately 0.5 μm. It is probable that the cited coating thickness range might be extended to higher and lower values, but this study did not require such an extension and no effort was made to expand the range.

The optical techniques have the restriction that the coatings must be sufficiently transparent to develop the interference fringes. Also, calibration curves are required for those polymer systems in which the intensity of the absorption band is used to determine the coating thickness. The technique has the major advantage that the thickness measurement is non-destructive and measurements on the same sample may be readily made as a function of the wear time.

5.4 Mechanisms of Material Removal under Three-body Abrasion Conditions

Surface material of a brittle solid may be removed by plastic deformation or indentation fracture, depending on the material itself and wear environments [11]. Heavy plastic deformation associated with the abrasion process was observed for brittle materials such as polycrystalline alumina [224, 225], polycrystalline rutile [226], polycrystalline $BaTiO_3$ [227], or MgO [228]. These observations suggest that the material removal mechanism in brittle solids is similar to that in metals, i.e. material removal involves cutting and plowing actions rather than brittle fracture. Cutter and McPherson [225] suggested that temperatures in the range 800 to 1200°C are experienced during abrasion of alumina, which are sufficiently high to allow considerable plasticity of the near surface region to occur. Swain [229] observed that in addition to the cutting grooves, grain boundary cracking and occasional grain pullout occurs during the abrasive wear of polycrystalline alumina. The material removal mechanism in the latter process is very similar to the delamination mechanism proposed by Suh [230]. Sin et al. [63] found a great number of grooves on abraded polymethylmethacrylate and that cutting action was responsible for the material removed.

Figure 5-5 shows the surface topography of the anodized surface and polystyrene coating on anodized aluminum abraded by 1 μm SiC abrasives under three-body conditions. The anodized aluminum was produced in 15% H_2SO_4 at 20°C and 10 V for 140 min. Scanning electron micrographs of the same samples abraded with a 600 grit (14.5 μm) SiC

abrasive paper, i.e. under two-body abrasion conditions, are shown in Figure 5-6 for comparison. A great number of grooves on the worn surfaces and the absence of surface cracking for all cases suggest that the material removal for the system studied under either two-body or three-body abrasion conditions involves cutting and plowing actions. It is interesting to note that a number of cavities are clearly seen in the anodized aluminum surface abraded under three-body conditions, while this phenomenon was not observed for the other cases. These cavities result from the embedded abrasive particles which were knocked out by other abrasive particles during wear testing. A survived SiC particle is shown in the center of Figure 5-7a as indicated by an arrow. The embedded SiC was confirmed by the energy-dispersive analysis of X-rays (Figure 5-7b). The embedded SiC particles in the anodized surface account for the weight gain of worn sample (Figure 4-5) and the increase in the apparent oxide film thickness at the early stages of wear (Figure 4-7). The refractive index of SiC was reported to be 2.654 and 2.697 for hexagonal and cubic crystals [231], respectively. SiC abrasives picked up by the oxide surface changed the apparent refractive index of the coating, resulting in an increase in the apparent film thickness as calculated by equation (12). As soon as the pick-up of abrasives reaches its equilibrium condition, a steady reduction in the thickness with wear time was observed.

The pick-up of abrasive particles by the wearing surface is less possible for both anodized aluminum and polymer coatings under two-body conditions, because the abrasive particles are firmly bonded to

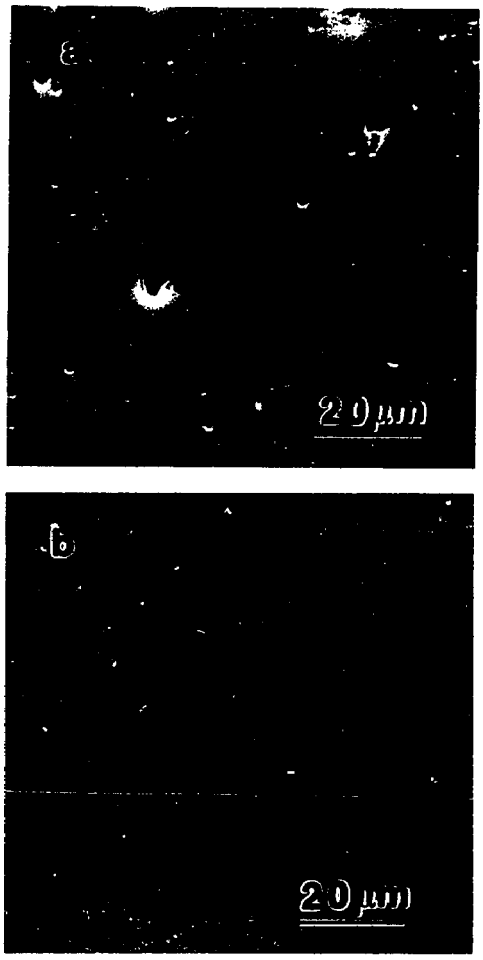

Figure 5-5. Surface topography of the surfaces abraded by 1 μm SiC abrasive powder under three-body abrasion conditions: (a) anodized aluminum surface after 5000 cycles in the accelerated wear apparatus and (b) polystyrene surface after 2500 cycles.

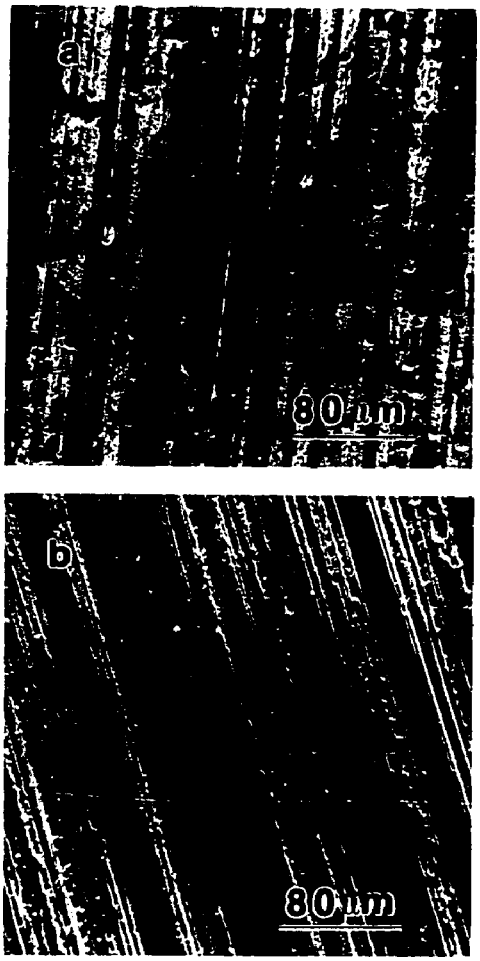

Figure 5-6. Surface topography of the surfaces abraded by 600 grit SiC papers under two-body abrasion conditions: (a) anodized aluminum surface after 400 cycles in the accelerated wear apparatus and (b) polystyrene surface after 200 cycles.

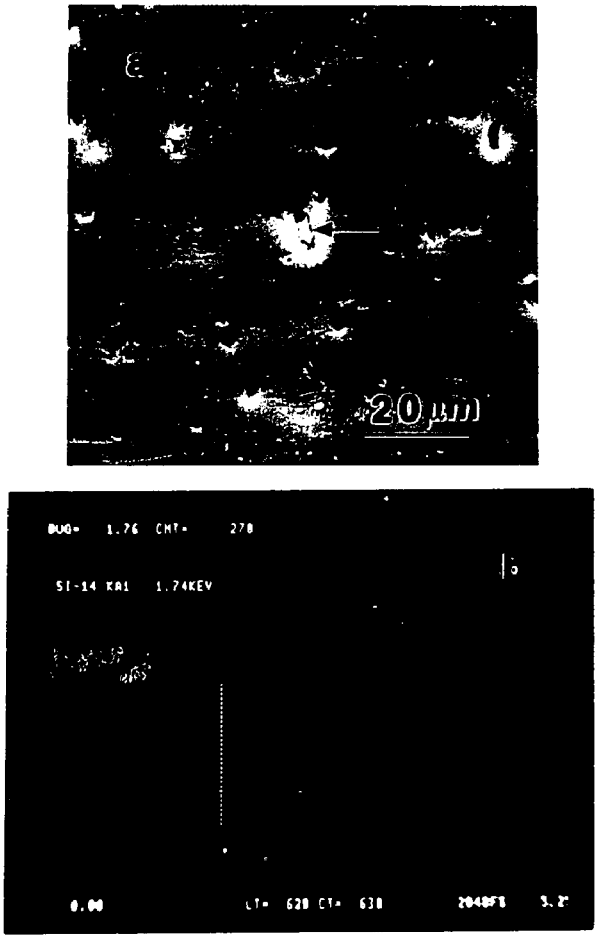

Figure 5-7. (a) SEM photograph showing an embedded SiC abrasive as indicated by an arrow on the anodized surface produced at 20°C and 10 V for 140 min and (b) energy dispersive spectrum of the embedded abrasive: the left, center, and right peaks corresponding to Al, Si, and S, respectively.

the paper by resins. The absence of a cavity in the worn polymer surface under three-body conditions (Figure 5-5b) is due to the resilient nature of polymers. The thickness of the polymer coating decreases linearly throughout the entire wear range, as shown in Figure 4-25.

Some surface reactions also occur concurrently with the wear process. Tremendously high frictional heat is evolved by the abrasion action, causing high temperatures near the surface region. A temperature rise of approximately 2°C of the abrasive solution was observed during the testing. The localized high temperature may facilitate the sealing of anodized aluminum and oxidation of polymer surface. Water contact angles of two worn anodized surfaces (Figure 4-29), which are roughly equivalent to those of sealed surfaces carried out in distilled water for one minute (Figures 4-22 and 4-23), suggest that the anodized surface was sealed to a certain degree by the wear process. The reduced water contact angle of polystyrene surfaces by wear (Figure 4-30) results from the oxidized products on the polymer surface. Figures 5-8 to 5-10 illustrate typical X-ray photoelectron spectra of polystyrene coatings on an anodized aluminum substrate after 0, 1000, and 2000 wear cycles in the accelerated wear apparatus. There exists only one major peak characteristic of carbon in the spectrum of polystyrene before wear (Figure 5-8). Figures 5-9 and 5-10 are spectra of polystyrene coatings after 1000 and 2000 wear cycles, respectively. In both of these spectra a peak due to oxygen at 535 e.v. is visible. The complete absence of peaks due to aluminum suggests that the oxygen signal does not result from aluminum

oxide on the substrate. It is more likely that the oxygen peak originates from superficial oxidation of the polystyrene.

5.5 Wear of Anodized Aluminum

The generalized wear equation, $dV/dS=(k/3)L/H$, predicts that the wear rate is proportional to the applied load or contact pressure and inversely proportional to the surface hardness. Experimental evidence supporting these relationships were presented in section 2.2.2. Figures 4-8 and 4-9 show that the wear rate of anodized aluminum is directly proportional to the contact pressure. A transition was observed in each case. Wear rates at high contact pressures were lower than expected. The indentation depth and hence the wear rate increases with contact pressure up to a critical value. With further increase in the contact pressure, only a slight increase in the indentation depth and wear rate will be affected due to the limiting size of abrasive particles. The contact pressure at the transition point, which shifts to higher values for harder coatings, may also account for this effect.

All of the wear equations appearing in section 2.2.2 do not include the factor of abrasive concentration, because these equations were derived based on the two-body abrasion conditions, in which the number of abrasive particles per unit area is fixed and determined by the size of abrasive. The abrasive particles are, however, not bonded under three-body abrasion conditions and the number of abrasive particles abrading the surface is dependent upon the concentration of abrasive suspension. Valdma [232] observed that there was an optimum

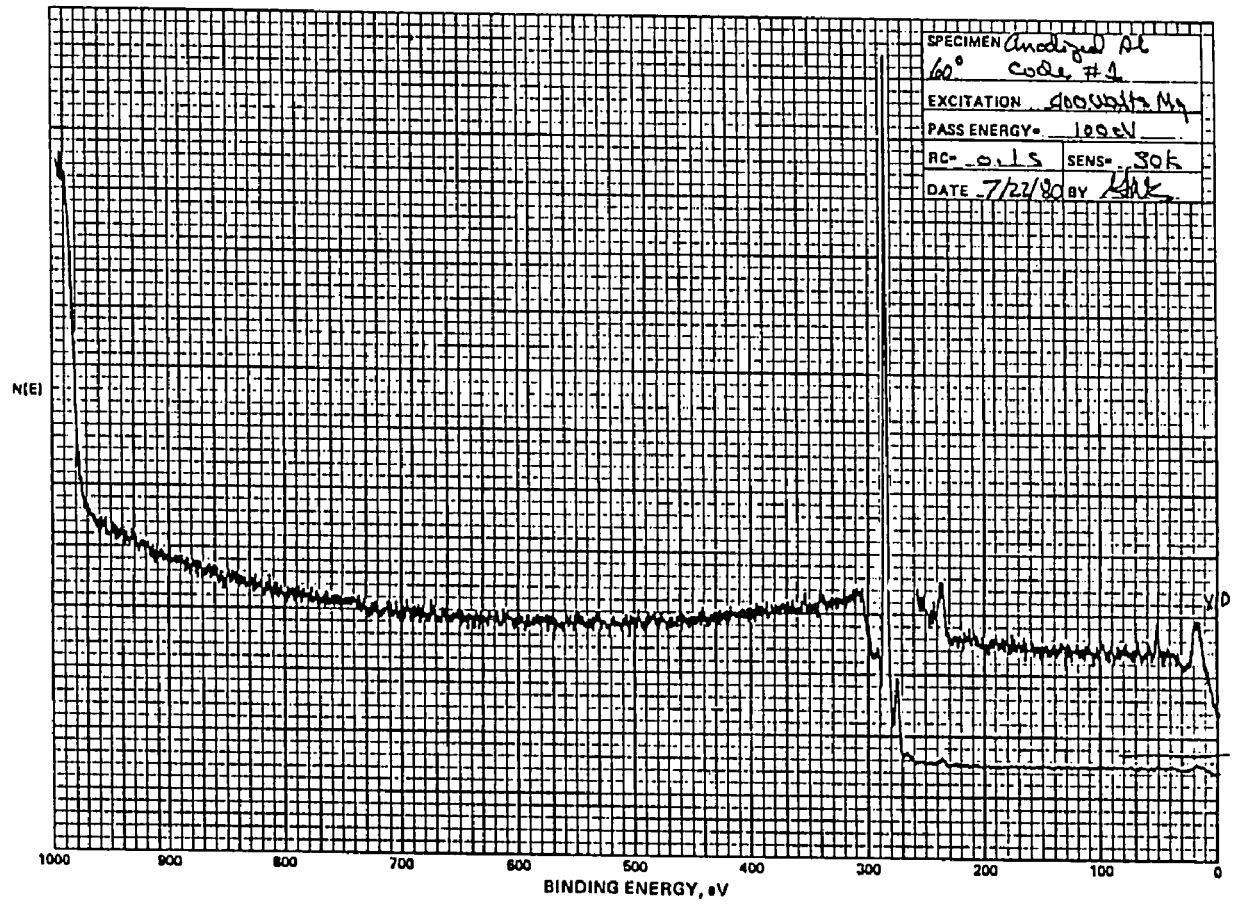

Figure 5-8. X-ray photoelectron spectrum of a polystyrene coating on an anodized aluminum substrate.

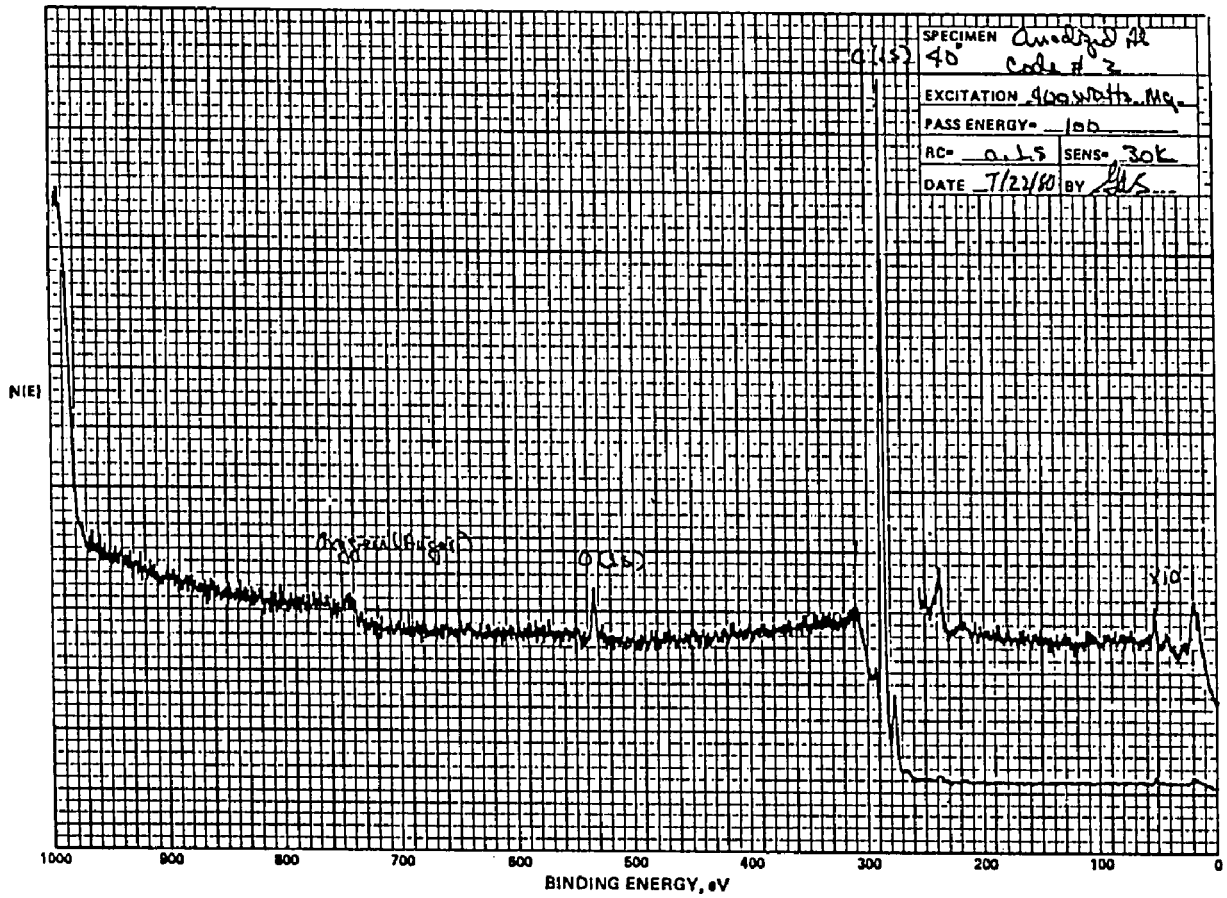

Figure 5-9. X-ray photoelectron spectrum of a polystyrene coating on an anodized aluminum substrate after 1000 cycles in the wear test.

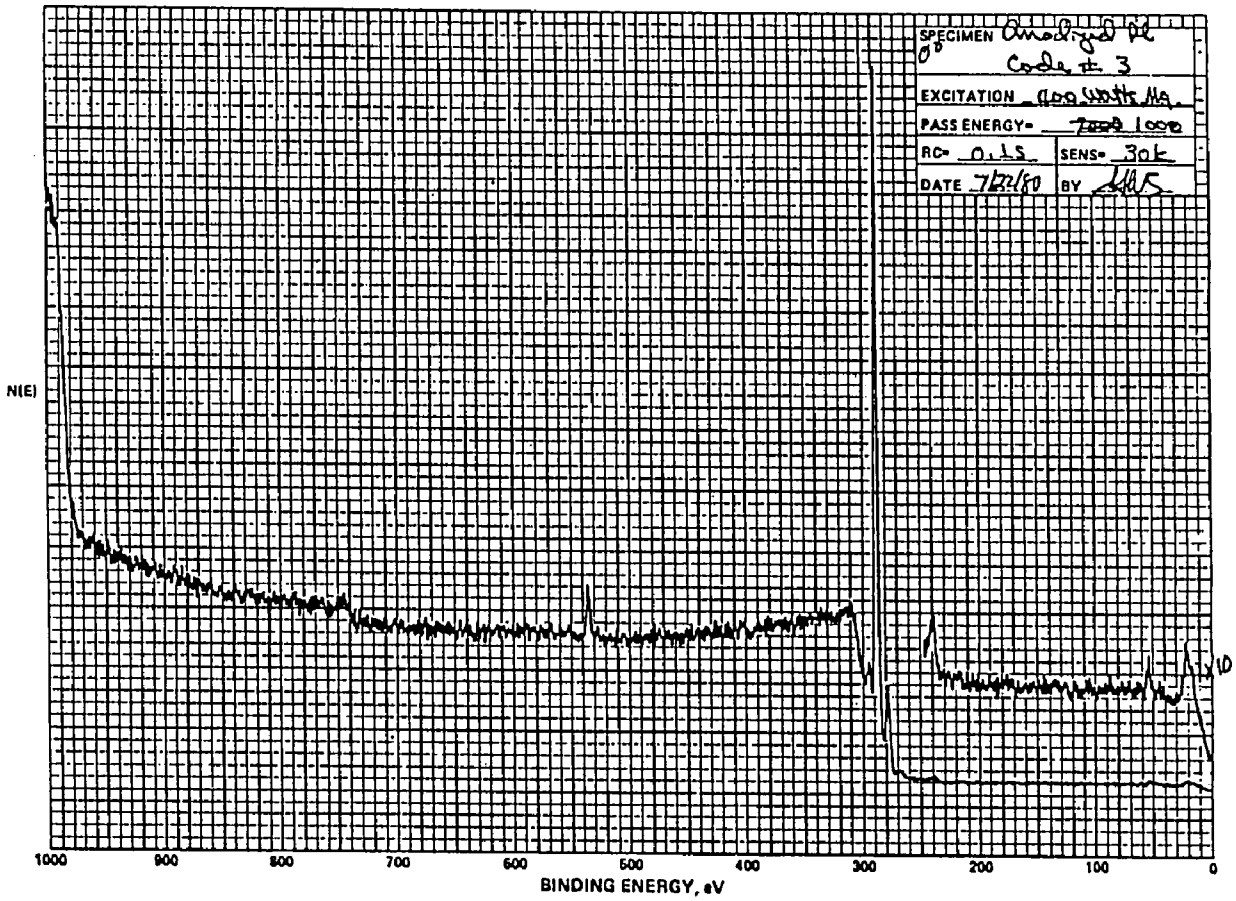

Figure 5-10. X-ray photoelectron spectrum of a polystyrene coating on an anodized aluminum substrate after 2000 cycles in the wear test.

composition of corundum powder in an oil which caused a maximum wear of the rubbing surface. The analysis of friction torque and the condition of the worn surfaces led him to the conclusion that for mixtures richer in abrasive than optimum the rolling of the grains dominates and hence wear is decreased. The optimum concentration of abrasive slurry was not observed in this study (Figure 4-10). This discrepancy can be accounted for when the differences in the experimental conditions are considered. The device used in Valdma's experiment is a closed system in which all the abrasive particles are entrapped between a rotating disk and the specimen. As the abrasive concentration exceeds the optimum composition, multilayer of abrasives is built up. Most abrasive particles make a rolling action and the number of abrasive particles carried by the rotating disk involved in abrading the specimen is decreased, resulting in a decrease in both the friction torque and wear.

The wear apparatus used in this study is different in that it is an open system. A large fraction of abrasive particles is pushed out of the interaction zone (the interfacial region between the moving block and specimen surface) by the moving block, only a small fraction is entrapped. The moving block squeezes the abrasive particles present in the interaction zone into a monolayer and these particles will participate in abrading the material surface. It is very interesting to note that the wear rate of anodic coatings as a function of abrasive concentration fits quite well an equation of the Langmuir adsorption isotherm type (Figure 4-10). In the Langmuir isotherm, the extent of adsorption or the surface coverage increases

with gas pressure, and approaches unit at very high pressures when the adsorbent surface is completely covered by a close-packed monolayer of the adsorbate [233]. The surface coverage, Θ_s, is given by

$$\Theta_s = k\ p\ /\ (1 + k\ p) \qquad (27)$$

where k is an equilibrium constant for the distribution of material between the surface and the gas phase and p the gas pressure. Similarly, the number of abrasive particles present in the interaction zone of the accelerated wear apparatus increases with abrasive concentration until the surface of the interaction zone is covered by a close-packed monolayer of abrasive particles. Further increase in the concentration does not increase the number of abrasive particles in the interaction zone because the redundant particles are pushed out by the moving block. The maximum number of particles per unit area of the interaction zone, therefore, corresponds to a close-packed monolayer. Figure 4-10 shows the experimental results of the wear rate as a function of abrasive concentration and the best fit theoretical curves. The distribution constants obtained from these two curves are 9.0 and 10.8 for anodic coatings formed at 10 and 15 V, respectively. They are essentially the same, indicating that the number of abrasive particles per unit area present in the interaction zone is governed by a law similar to the Langmuir adsorption isotherm.

It is very difficult to determine the surface hardness of an anodic coating on aluminum by conventional methods, because they give the hardness of the base metal. Although it is possible to carry out

microindentation tests on cross sections of coatings which have been mounted in resins and polished by metallographic techniques, this method is tedious and the hardness obtained is not the real hardness of the coatings due to the presence of pores in the coatings. Figure 5-11 shows an example of the microhardness of conventional anodized coatings which varies across the thickness of the coating [234]. The hardness is highest for the layer adjacent to the metal and decreases progressively from the metal to the surface, the effect becoming less as the electrolyte temperature is reduced. This behavior is very similar to that of apparent density (Figures 4-3 and 4-4) and that of wear rate (Figures 4-11 and 4-12). These findings are consistent with the tapered pore structure of anodic films, suggesting a correlation between the wear rate and apparent density. Figure 5-12 shows a linear relation of wear rate to the inverse of apparent density for anodic coatings prepared in different ways. The wear resistance, defined as the ratio of the contact pressure to wear rate, can be determined from the slope of the wear rate vs. contact pressure curve exhibited in Figures 4-8 and 4-9. A linear dependence of the wear resistance upon apparent density is shown in Figure 5-13. These results lead to the conclusion that the apparent density governs the wear property of anodic coatings.

5.6 Wear Theory for Anodized Aluminum under Three-body Abrasion Conditions

Previous discussions have shown that plastic deformation is the rate-controlling process and the surface material is removed primarily

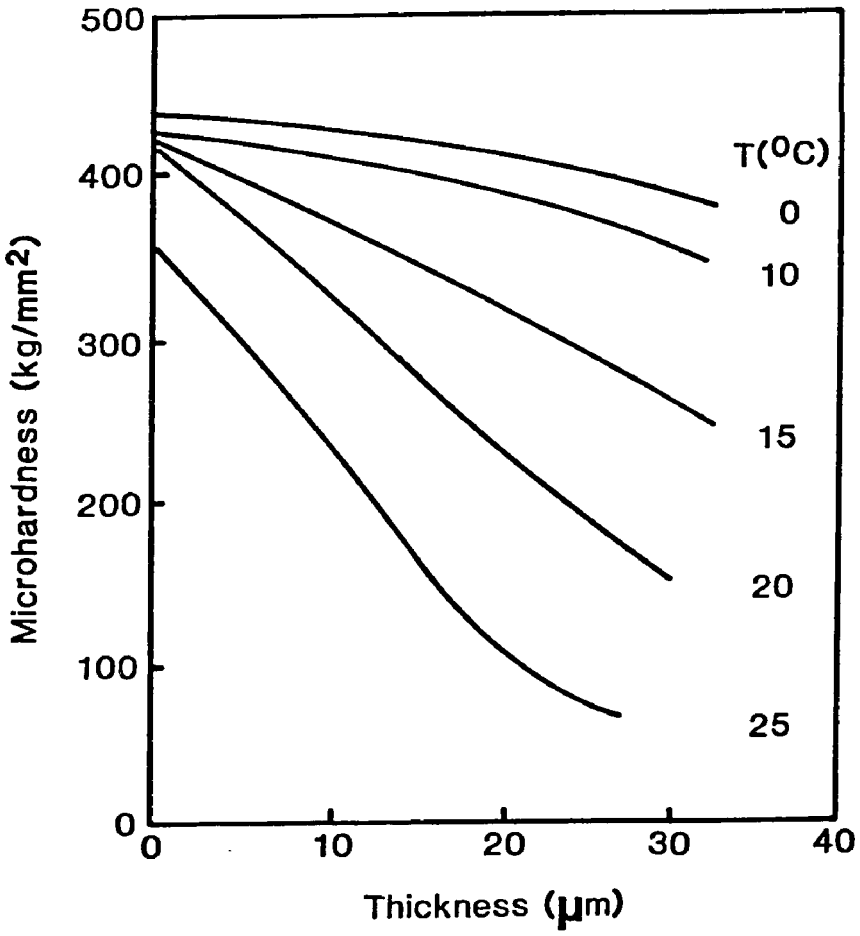

Figure 5-11. Influence of electrolyte temperature on the microhardness of sulfuric acid-anodized coatings on AlMgSi 0.5 alloy at 1.5 amp/dm^2 (taken from [234]).

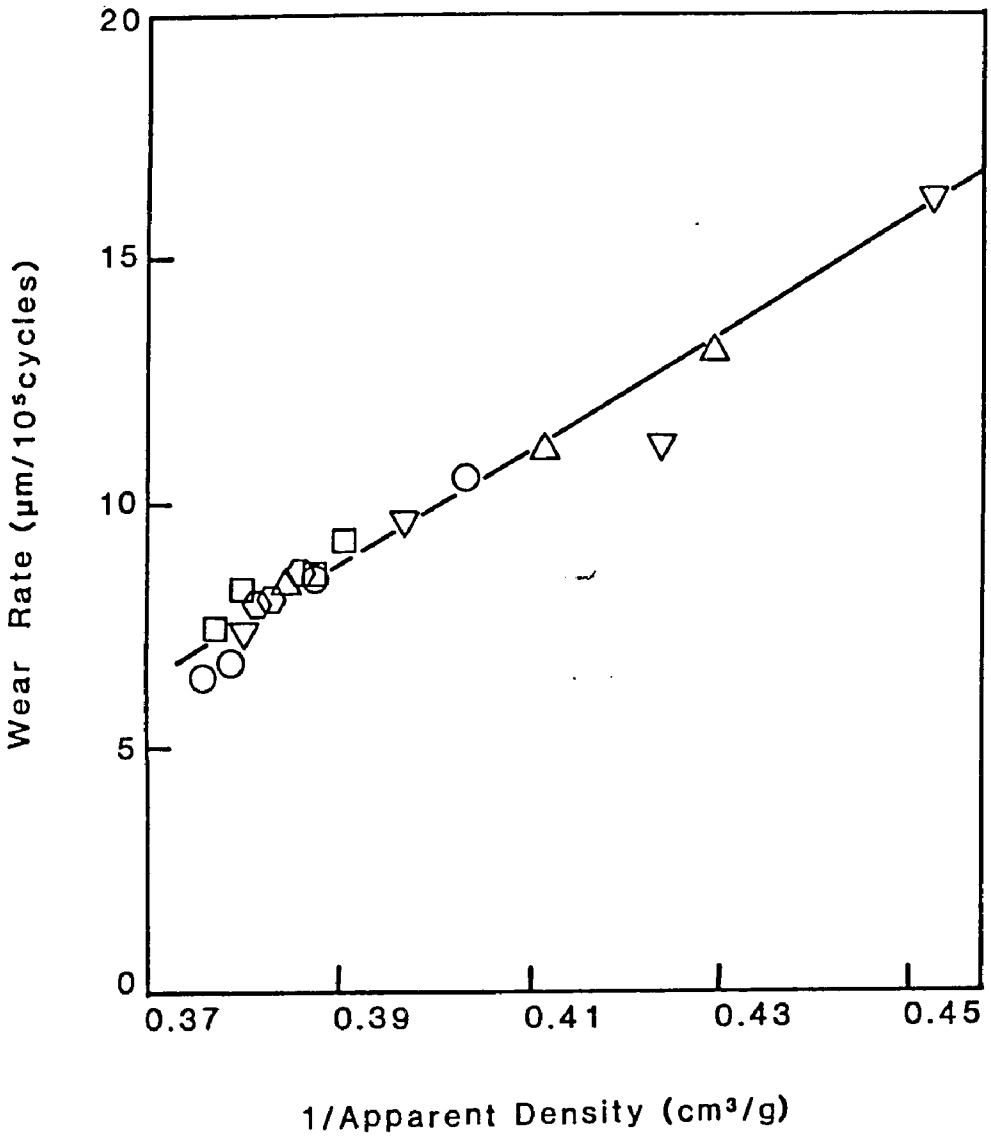

Figure 5-12. Dependence of the wear rate on the apparent density of anodic coatings formed in a wide range of conditions.

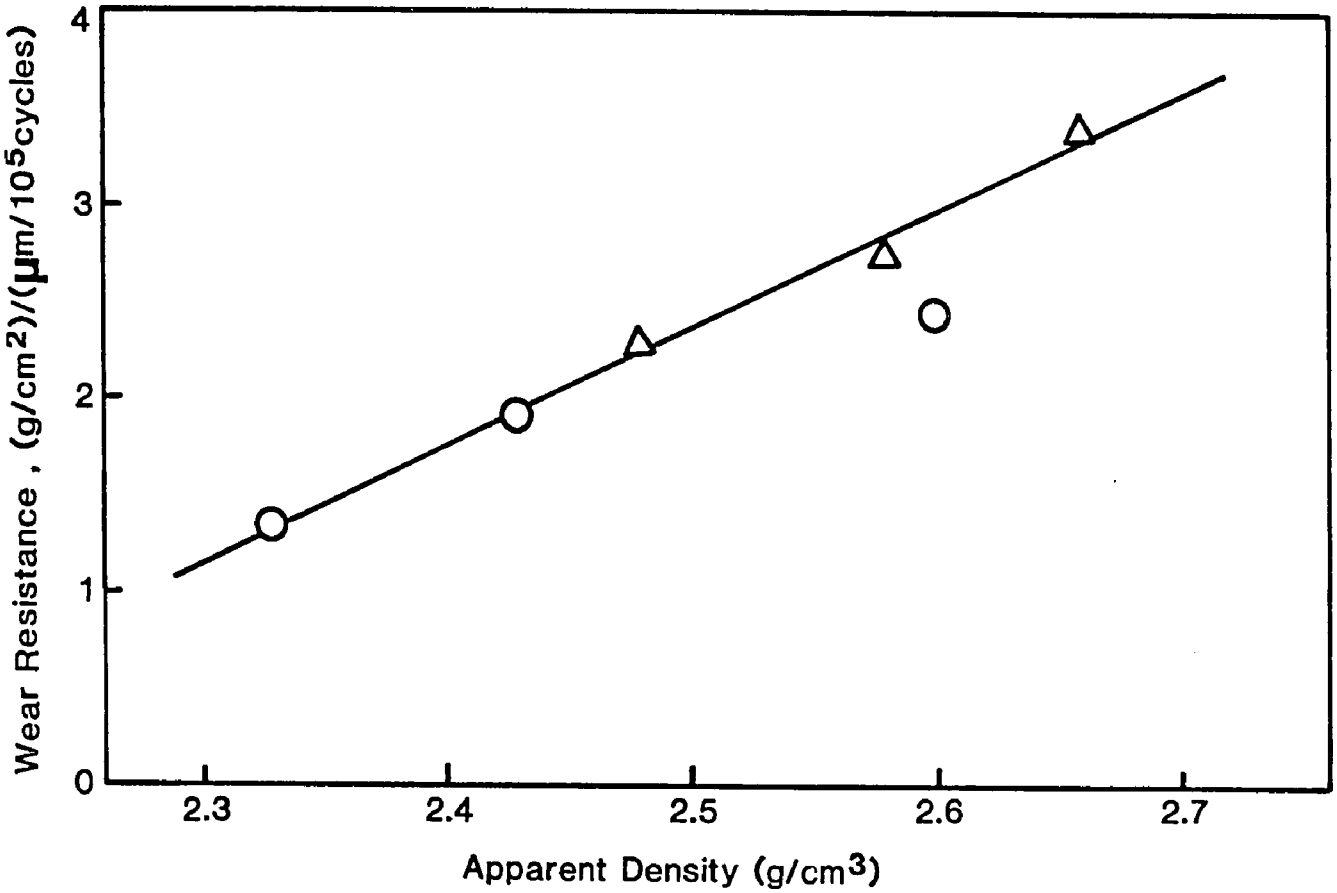

Figure 5-13. A linear relationship between the wear resistance and apparent density of the anodized aluminum formed in 15% H_2SO_4. Triangles and circles represent the data obtained from Figures 4-8 and 4-9, respectively.

by plowing and cutting actions. Because the shape of the abrasive particles is irregular and that rolling as well as abrasion may occur on the material surface under three-body abrasion conditions, it is more realistic to approach this problem from a statistical viewpoint.

Figure 5-14 details the material removal by cutting and plowing mechanisms. When an abrasive particle with its sharp tip contacts the surface and the attack angle of the abrasive particle to the surface is greater than the critical value, it will cut a microchip from the surface and leave ridges on both sides of the groove (Figure 5-14a). If the attack angle is less than the critical value for a sharp tip or if the abrasive particle contacts the surface with its blunt tip, it will plow up material forming ridges around the abrasive particle (Figure 5-14b). The front ridge will be removed as the abrasive particle reaches the edge of the specimen. Moreover, Buttery and Archard [70] have found that in scratch tests repeated transversals of an indentor on the same track causes further material removal from the side ridges. The breakaway of side ridges results from the repeated plastic deformation. The amount of surface material removed by the plow mechanism is much less than that by the cutting mechanism. Most abrasive particles merely roll over the surface, making elastic contact with the surface, and thus do not produce any abrasive wear debris.

The volume dv_i of material removed by the abrasive particle i moving through a distance dS can be expressed as

$$dv_i = f_i A_{gi} dS \tag{28}$$

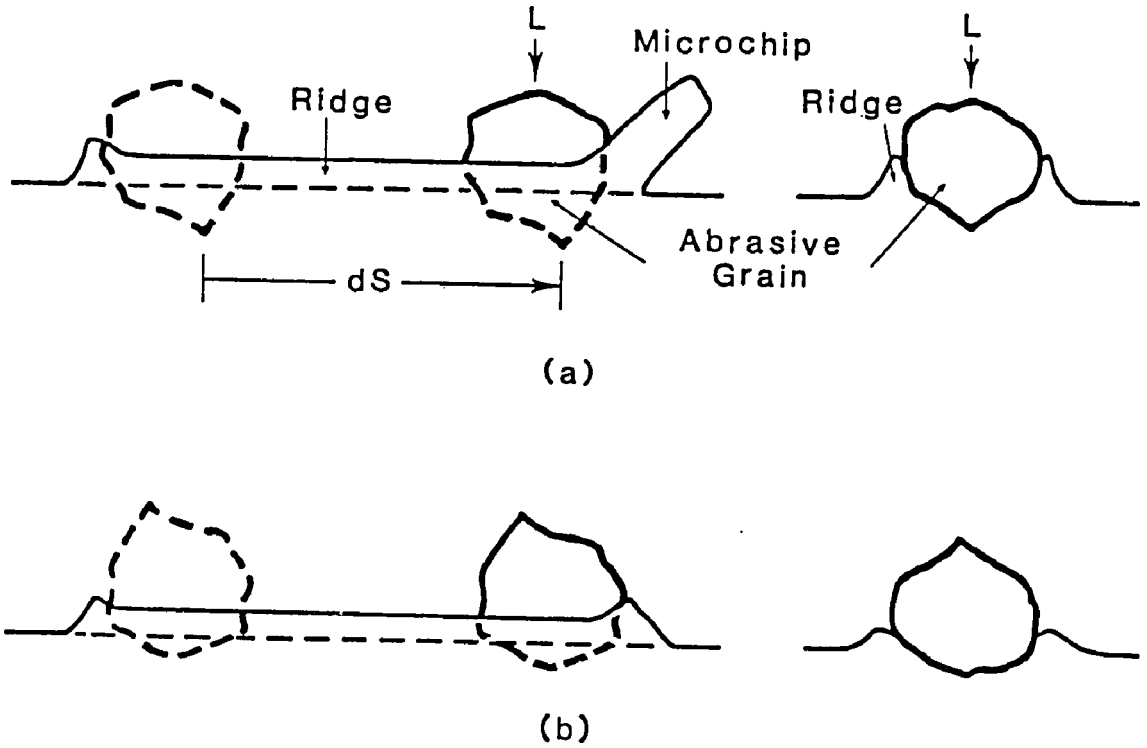

Figure 5-14. Models of material removal by plastic deformation: (a) cutting and (b) plowing mechanisms.

where f_i is the fraction of groove volume removed as wear debris and A_{gi} the groove area swept by the abrasive particle i. f_i may vary from 0 to a maximum value, which depends upon the shape and orientation of the abrasive particle in contact with the wearing surface and the relative hardness of abrasive particle to that of the surface material.

The equilibrium of vertical force requires that

$$L_i = H_s A_{ci} \tag{29}$$

where L_i is the load carried by the abrasive particle i, H_s the surface hardness of anodic coating, and A_{ci} the horizontal projected area of contact. The surface hardness is an apparent property of the anodic coating because of the porous structure. For convenience, the anodic coating is assumed to be homogeneous in the development of the wear equation. Since both A_{gi} and A_{ci} are dependent upon the shape and hardness of abrasive particle i, they can be related by

$$A_{gi} = f_i' A_{ci} \tag{30}$$

where f_i' is a constant. From equations (28), (29), and (30) one can obtain

$$dv_i = f_i f_i' L_1 dS / H_s \tag{31}$$

Assuming that the applied load is equally distributed to all abrasive particles entrapped in the interaction zone, the mean normal

load per particle, L, that contacts the surface is

$$L = g\, d^2\, P \qquad (32)$$

where g is a geometric factor of abrasive particles, d the mean particle diameter, and P the contact pressure. The mean volume removal per particle, dv, is given by

$$dv = g\, f\, d^2\, P\, dS\, /\, H_s \qquad (33)$$

where f is the mean value of the product of f_i and f_i'.

It has been shown in section 5.5 that the number of abrasive particles present in the interaction zone is governed by a law similar to the Langmuir adsorption isotherm and is given by [233]

$$N = N_o\, q\, C\, /\, (1 + q\, C) \qquad (34)$$

where q is a constant characterizing the distribution of abrasive particles inside and outside the interaction zone and C the concentration of abrasive suspension. N_o is the number of abrasive particles per unit area corresponding to a close-packed monolayer and dependent upon the size and shape of abrasive particles

$$N_o = 1\, /\, g'\, d^2 \qquad (35)$$

where g' is also a geometric constant of abrasive particles. The total volume removal per unit area, dV, i.e. the change in the apparent thickness of specimen, dt, can be obtained by combining

equations (33)-(35) to

$$dt = dV = N\,dv = k\,[q\,C / (1 + q\,C)]\,P\,dS / H_s \tag{36}$$

Thus, the linear wear rate is

$$dt/dS = k\,[q\,C / (1 + q\,C)]\,P / H_s \tag{37}$$

where the constant k (= fg/g') is determined by the nature of abrasive, i.e. by the shape and relative hardness of abrasive particles.

Equation (37), which is similar to the generalized wear equation (24), predicts that the wear rate is directly proportional to the contact pressure and is inversely proportional to the surface hardness. It also takes into account the concentration of abrasive suspension. The difficulty of determining the surface hardness of an anodic coating on aluminum limits the applicability of equation (37).

In fact, the anodic oxide coating should be considered as a composite material, containing air cylinders dispersed in alumina matrix. Khrushchov and Babichev [235] have shown that for a composite material the applied pressure is distributed between phases. Since the wear rate is proportional to the applied pressure, the rate of wear of a composite material is given by

$$dt/dS = c_o\,P_o = c_1\,P_1 = c_2\,P_2 \tag{38}$$

where c is a proportionality constant and o, 1, and 2 represent the

anodic oxide film, the aluminum oxide phase, and the air phase, respectively. From equation (38) the following relations can be obtained

$$P_1 = P_o\, c_o / c_1 \quad \text{and} \quad P_2 = P_o\, c_o / c_2 \tag{39}$$

The total load on the specimen, L_t, is divided between the two phases

$$L_t = P_o\, A_o = \gamma\, A_o\, P_1 + (1 - \gamma)\, A_o\, P_2 \tag{40}$$

Hence,

$$\begin{aligned} P_o &= \gamma\, P_1 + (1 - \gamma)\, P_2 \\ &= \gamma\, (c_o/c_1)\, P_o + (1 - \gamma)(c_o/c_2)\, P_o \end{aligned} \tag{41}$$

and

$$c_o = 1 \,/\, [\, \gamma/c_1 + (1 - \gamma)/c_2] \tag{42}$$

where γ is the volume fraction of oxide in the anodic coating and $(1 - \gamma)$ the porosity of the anodic coating. Because the wear rate of the air phase is infinite, c_2 is also infinite. Consequently, the wear rate of anodic film is simplified to

$$dt/dS = c_o\, P_o = (c_1/\gamma)\, P_o \tag{43}$$

The volume fraction of oxide in the anodic coating can be obtained as follows:

$$W = d_r \gamma V = d_a V \tag{44}$$

Hence,

$$\gamma = d_a / d_r \tag{45}$$

where W = weight of anodic coating

V = apparent volume of anodic coating which is equal to the product of coating thickness and specimen size

d_r = real density of aluminum oxide

d_a = apparent density of anodic coating

The combination of equations (37), (43), and (45) gives

$$dt/dS = k\,(d_r/H_r)\,[q\,C / (1 + q\,C)]\,(P/d_a) \tag{46}$$

and

$$H_r = (d_r/d_a)\,H_s \tag{47}$$

where H_r is the real hardness of aluminum oxide.

If the real density and hardness of aluminum oxide formed on a particular aluminum alloy are material properties determined primarily by the nature of anodizing electrolyte, then equation (46) predicts that the wear rate of anodic films produced under various conditions should be proportional to the applied pressure and inversely proportional to the apparent density when the wear tests are carried out under the same conditions. The satisfactory agreement between the

theory and experimental results presented in section 5.5 suggests that the real density and hardness of the anodic films are material properties. They are determined primarily by the nature of the electrolyte employed in producing oxide films, while the anodizing conditions (i.e. anodizing voltage, electrolyte temperature, and anodizing time) have considerable influence on the apparent density and hardness of the oxide coating.

Spencer [207] has mentioned in a review article that the hardness of a "hard anodic coating" is no harder than the conventional anodized coating, because both are essentially an aluminum oxide surface formation. Applying Archimedes' principle to the determination of real density of anodic coatings, Mason [236] has found that the real densities of oxide coatings produced in sulfuric acid solution under various conditions are the same for 1100-H16 aluminum, as summarized in Table 5-1.

5.7 Sealing of Anodized Aluminum

The effect of sealing treatment in hot aqueous solutions on the rate of wear in the early stages is strikingly shown in Figures 4-13 to 4-17. Rapid wear occurs during the first 500-1000 wear cycles after sealing sulfuric acid formed coatings in distilled water, nickel acetate solution, and potassium dichromate solution. Figure 4-13 shows data for a similar coating that was not sealed. In many cases a low wear rate is observed after the outer part of the coating has been worn away. It is apparent that the external part of the sealed coating has a much lower wear resistance under abrasive

Table 5-1. Real Density of Anodic Coatings Produced under Various Conditions (taken from [236]).

Electrolyte	Temperature ^{o}C	Current Density amp/dm^2	Anodizing Time min.	Real Density g/cm^3
15% H_2SO_4	21.1	1.3	15	2.95
	21.1	1.3	30	2.96
	10.0	1.3	30	2.95
	15.6	1.3	30	2.95
	26.7	1.3	30	2.93
	32.2	1.3	30	2.92
7% H_2SO_4	21.1	1.3	30	2.97
	26.7	1.3	30	2.95

conditions, but once this is worn away the wear rate achieves its value for the unsealed coating. Coatings sealed in sodium silicate solution represent a significant exception. These coatings exhibited high wear rates even after sealing for only one minute and the wear rate continued to increase as the sealing time was increased.

The differences in the wear and wettability behavior of anodic coatings sealed in sodium silicate solution and other sealants are ascribed to different mechanisms of sealing. Anodic coating exposed to distilled water, nickel acetate solution or potassium dichromate solution are sealed via a pore-plugging mechanism (figure 2-17). The closure of pore mouths prevents water from penetrating into the pores resulting in an increased water contact angle, while the formation of hydrophilic boehmite increases the wettability of the surface. Figure 5-15 shows the scanning electron micrographs of anodic coatings formed in 15% H_2SO_4 at 20°C and 15 V for 20 min and sealed in boiling distilled water for 1, 2, 5, and 60 min. Close inspection of the photographs reveals that after only one minute of sealing small grains have begun to grow on the coating surface. After only 5 minutes of sealing, the entire surface acquires a velvety appearance which did not change significantly as sealing was continued for 60 minutes. The hydrophilic, textured surface is shown in great detail in Figure 5-16 for the same coating sealed for 60 min. The maximum values of the contact angle exhibited in Figures 4-18 and 4-22 indicate that the pore mouths are closed after one minute of sealing for the 18-min and 20-min coatings. The possibility that it may take much longer to seal the 140-min coating which has greater pore diameter would account for

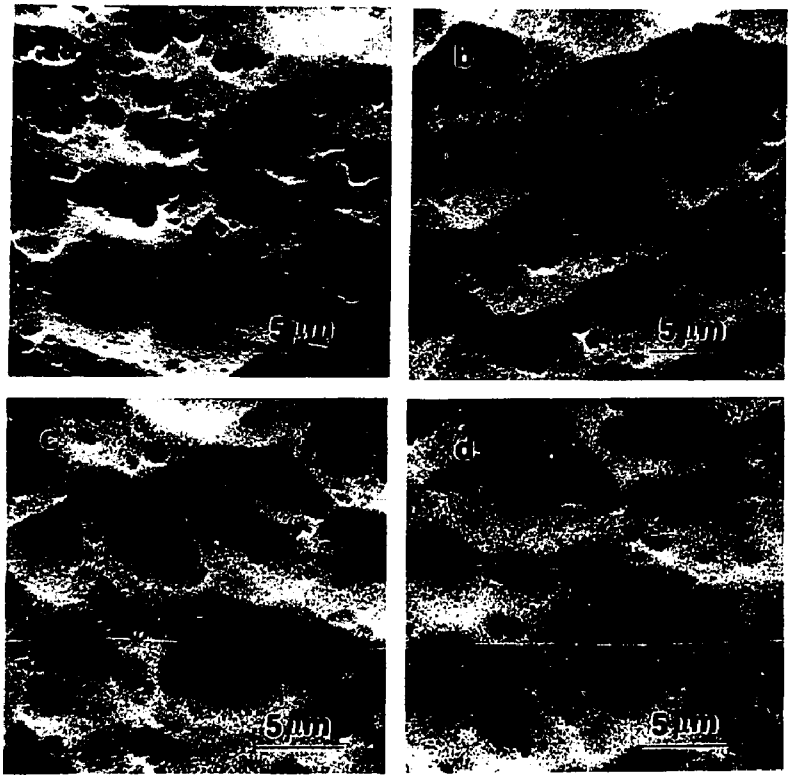

Figure 5-15. Surface topography of anodic coatings formed at 20°C and 15 V for 20 min and sealed in boiling distilled water for (a) 1, (b) 2, (c) 5, and (d) 60 min.

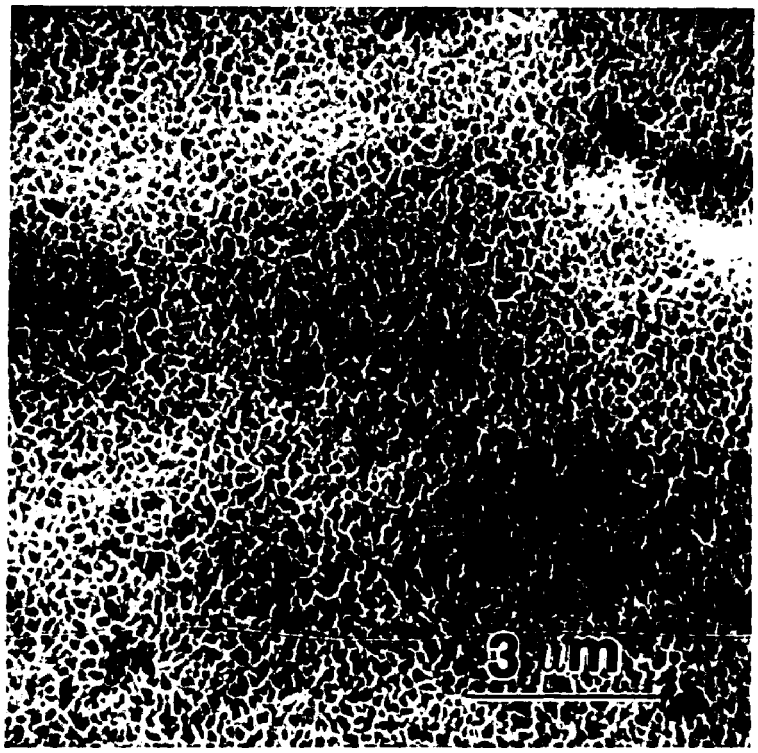

Figure 5-16. Scanning electron micrograph showing the surface texture of the 20-min coating sealed in boiling distilled water for 60 min.

reduced wettability not being observed (Figure 4-23). As soon as the pore mouths are completely plugged, the sealing process and hence the growth of the intermediate layer is controlled by diffusion of water into the anodic coating and acid anions into the sealing solution. This intermediate layer which is soft and less wear resistant accounts for the rapid wear in the early stages. The thickness of this soft outer layer could be estimated from the wear curves shown in Figures 4-13 to 4-17. Figure 5-17 shows schematically the determination of the thickness of the soft outer layer. By extrapolating the rapid and low wear segments to an intercept (B), the difference between A (original film thickness) and B is a measure of the soft layer thickness. The plot of the outer layer thickness against the sealing time in Figure 5-18 indicates that the growth of the intermediate layer is a diffusion-controlled process and the pores in the 18-min coating are plugged in as short as one minute of sealing.

The textured surface was not observed for the same coating sealed for various times in sodium silicate solution (Figure 5-19). It is more likely that sealing proceeds via the mechanism proposed by Murphy (Figure 2-18). The high pH of the sealing solution, which is 11.4, facilitates the replacement of acid anions incorporated in the intercrystallite region by hydroxyl ions and inhibits the precipitation of hydrated aluminum ions. The agglomeration of these modified microcrystallites produces strains in the coating [115], decreasing the wear resistance of the oxide coating. Thus, high wear rates were exhibited by silicate treated coatings throughout the entire wear range in the test. Excellent wettability of these

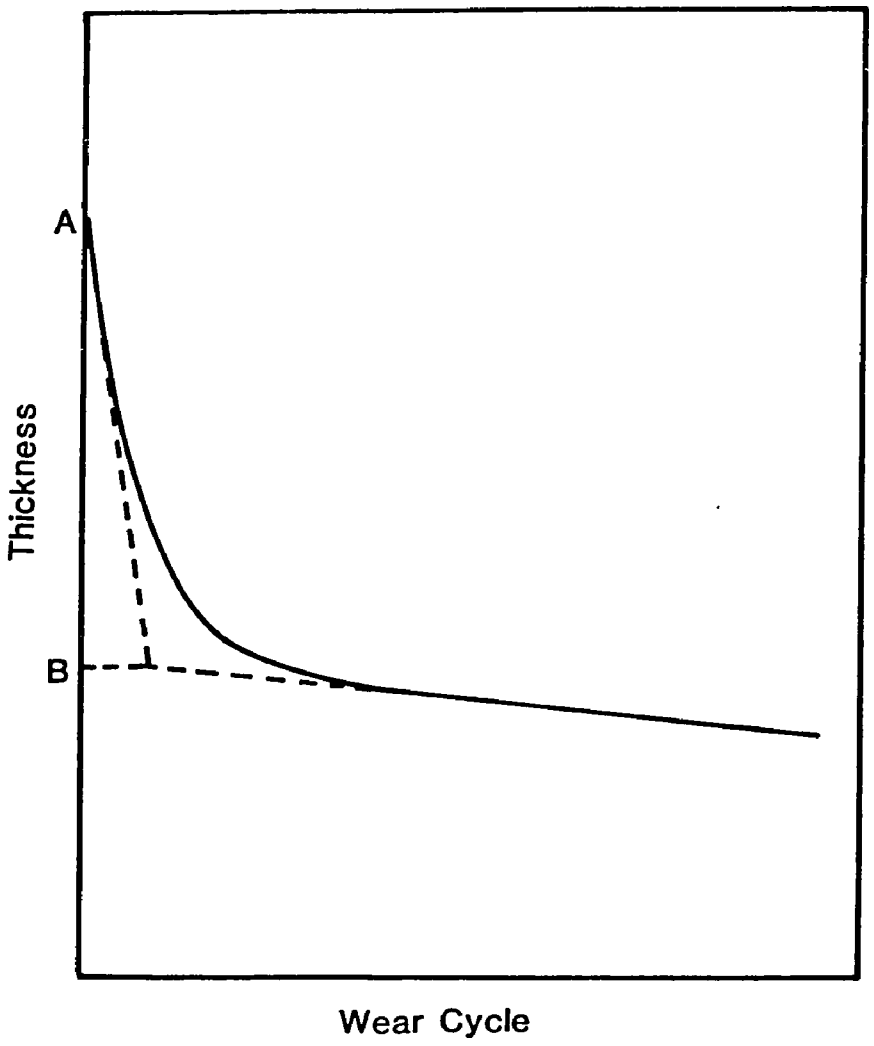

Figure 5-17. Schematic diagram for obtaining the thickness of the soft outer layer in the sealed anodic coating from the wear curve.

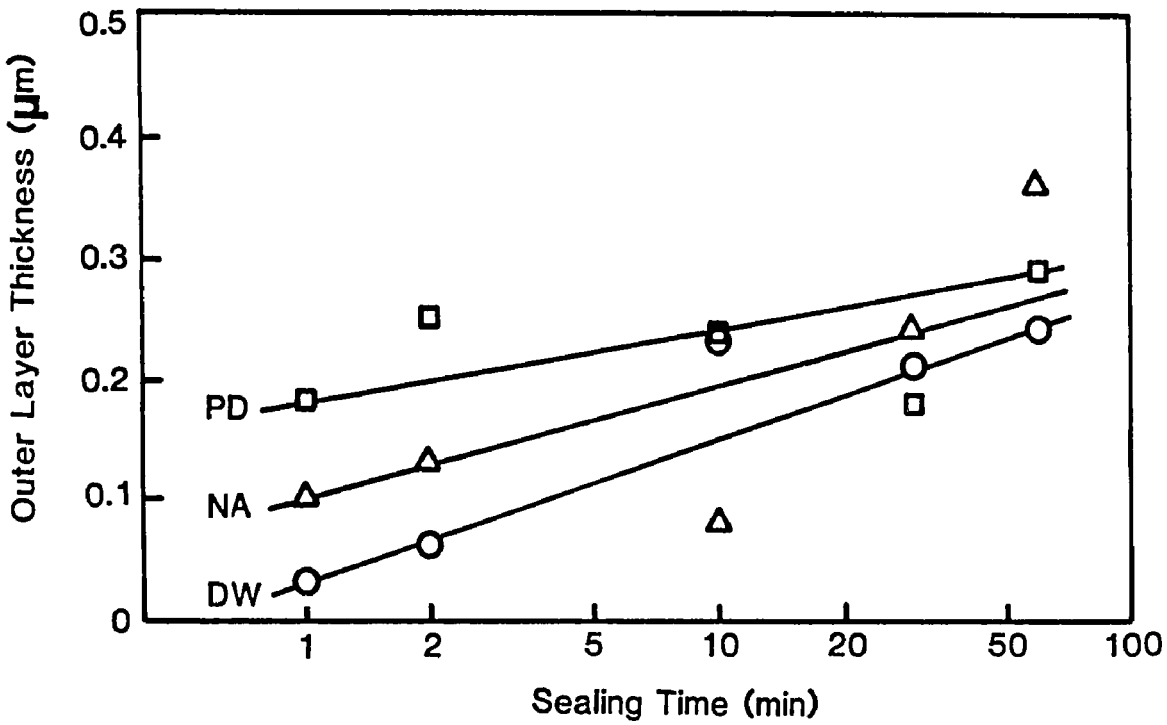

Figure 5-18. Growth of the intermediate layer in the anodic coating sealed in distilled water (DW), nickel acetate solution (NA), and potassium dichromate solution (PD) as a function of sealing time.

coatings probably results from the intact pore mouths and modified cell wall surfaces.

5.8 Wear of Polymer Coatings

Figures 4-26 and 4-27 indicate that the wear resistance of high molecular weight polystyrene is better than that of low molecular weight polystyrene due to an increase in cohesive strength of polymer with increasing molecular weight [237]. The data summarized in Table 4-2 and Figures 4-27 and 4-28 indicate that the wear rates the polymer coatings are influenced by the anodizing and sealing treatment before the application of polymer coatings. Sealing increased the wear rate of polystyrene coatings on anodized substrates formed in sulfuric acid. Both polystyrene and poly-n-butylmethacrylate exhibited lower wear rates on phosphoric acid-anodized aluminum than sulfuric acid-anodized substrate.

The wear behavior of polymer coatings on anodized aluminum substrate is far more complicated than that of polymer or anodized aluminum alone. No attempt has been made here to determine quantitatively the effect of anodized aluminum substrate on the rate of wear of polymer coatings. However, the technique explored in this study has the applicability to the selection of a polymer coating with satisfactory resistance to abrasive wear on an anodized aluminum substrate which has an excellent wear resistance.

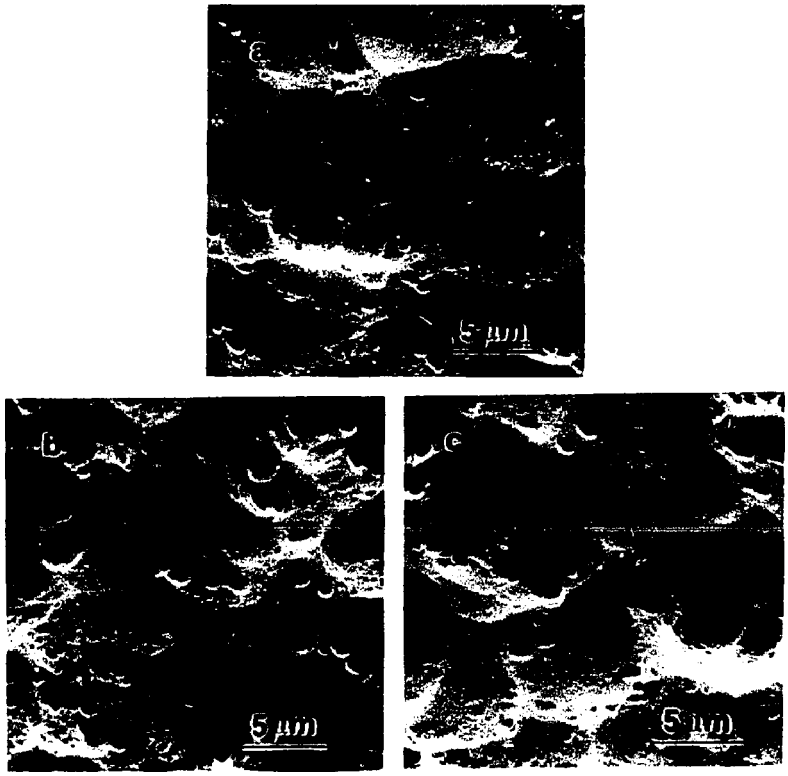

Figure 5-19. Surface topography of anodic coatings formed at 20°C and 15 V for 20 min and sealed in sodium silicate solution for (a) 2, (b) 10, and (c) 60 min.

CHAPTER 6

CONCLUSION

The following conclusions were obtained from the experimental and theoretical work carried out in this study:

1. Optical techniques are useful, non-destructive methods for thickness measurement and the determination of wear rates of anodized aluminum and polymer coatings. The accelerated wear test apparatus in conjunction with the optical techniques explored in this study has the applicability to the selection of optimum surface preparation method for the substrate and the selection of a polymer coating with satisfactory resistance to abrasive wear.
2. The anodic oxide coating has a tapered pore structure and the slant of the cell wall is determined by the anodizing conditions.
3. The apparent density and hardness of the anodic coating are significantly influenced by the anodizing conditions such as the anodizing voltage, electrolyte temperature, and anodizing time, whereas the real density and hardness are determined primarily by the nature of the anodizing electrolyte.
4. The wear rate of anodized aluminum is proportional to the contact pressure and inversely proportional to the apparent density of the oxide film.

5. Plastic deformation is the rate-controlling process of material removal for both anodic and polymer coatings under three-body abrasion conditions employed in this study. Surface material is removed by cutting and plowing mechanisms. Sealing of anodized aluminum surfaces occurs concurrently with the wear process, while superficial oxidation takes place on the surface of polymer coatings.
6. Anodized aluminum exposed to boiling distilled water, nickel acetate solution or potassium dichromate solution is sealed via a pore-plugging mechanism, resulting in a soft outer layer which is worn away more rapidly. Pore closure causes a reduced wettability of the anodized surfaces, while the formation of the textured, crystalline boehmite on the surface increases the wettability. The time of sealing required to close the pore mouths depends on the pore diameter at the surface. Consequently, 18-min and 20-min coatings exhibited a reduced wettability when sealed for short periods in these sealants and good wettability at sealing times in excess of 10 minutes, whereas the reduced wettability was not observed for the 140-coatings. As soon as the pore mouths are plugged, sealing becomes a diffusion-controlled process.
7. Sealing of anodized aluminum in sodium silicate solution proceeds via a surface conversion mechanism proposed by Murphy, in which the entrance to the interior of cell walls is blocked with relatively inert surfaces of gibbsite or

bayerite. Pore mouths are not plugged by this process so that water can easily penetrate into the pores of the oxide coating, resulting in an excellent wettability of the surface at all sealing times. Great strains built up in the coating due to the agglomeration of microcrystallites reduce its resistance to wear.

8. The rate of wear of polymer coatings is determined by the nature of polymers and is also appreciably influenced by the anodizing and sealing treatment before the application of the polymer coating.
9. Anodizing process does not change significantly the surface topography of the underlying metal. Surface graining may be carried out before anodization to optimize the water holding capacity of the non-image areas and to improve the adhesion of photopolymer coating to the anodized substrate.

MANUSCRIPT PUBLISHED DURING THE COURSE OF THIS WORK

"Wear Rates of Anodized Aluminum and Polymer Coatings as Model Systems for Lithographic Printing Plates", Michael C. Hughes, Henry Leidheiser, Jr., Shem-Mong Chou and Wayne Bilder, Ind. Eng. Chem. Prod. Res. Dev., Vol. 22 (1983), pp. 132-38.

REFERENCES

1. Vanden Berg, R. V., Iron Age, 170 (1952), 81.

2. Wernick, S. and Pinner, R., The Surface Treatment and Finishing of Aluminum and Its Alloys, Robert Draper Ltd., Teddington, 1972.

3. Bright, K., Malpass, B. W., and Packham, D. E., Nature, 223 (1969), 1360.

4. Packham, D. E., Bright, K. and Malpass, B. W., J. Appl. Polym. Sci., 18 (1974), 3237.

5. Malpass, B. W., Packham, D. E. and Bright, K., J. Appl. Polym. Sci., 18 (1974), 3249.

6. Blair, R. and Shapiro, C., The Lithographers Manual, The Graphic Arts Technical Foundation, Inc., Pittsburg, 1980.

7. Lerner, M., Plat. Surf. Fin., 66 (1979), 40.

8. Thomas, R. W., Trans. Inst. Met. Fin., 59 (1981), 97.

9. Baier, S. W., Thichness Testing of Electroplated and Related Coatings, Portcullis Press Ltd., Redhill, 1981.

10. Hughes, M. C., Leidheiser, H., Jr., Chou, S., and Bilder, W., Ind. Eng. Chem. Prod. Res. Dev., 22 (1983), 132.

11. Moore, M. A. and King, F. S., Wear, 60 (1980), 123.

12. Wendlandt, W. W. and Hecht, H. G., Reflectance Spectroscopy, Wiley-Interscience, New York, 1966.

13. Spitzer, W. G. and Tanenbaum, M., J. Appl. Phys., 32 (1961), 744.

14. Albert, M. P. and Combs, J. F., J. Electrochem Soc., 109 (1962), 709.

15. Schumann, P. A.,Jr., Phillips, R. P., and Olshefski, P. J., J. Electrochem Soc., 113 (1966), 368.

16. Schumann, P. A., Jr., J. Electrochem. Soc., 116 (1969), 409.

17. Severin, P. J., Appl. Opt., 9 (1970), 2381.

18. Gardner, E. E., J. Test. Eval., 1 (1973), 301.

19. Senitzky, B. and Weeks, S. P., J. Appl. Phys., 52 (1981), 5308.

20. Palik, E. D., Holm, R. T., and Gibson, J. W. , Thin Solid Films, 47 (1977), 167.

21. American Society for Testing and Materials, "Thickness of Epitaxial Layers of Silicon on Substrates of the Same Type by Infrared Reflectance", F95-76 (Reapproved 1981).

22. Saifi, M. A. and Stolen, R. H., J. Appl. Phys., 43 (1972), 1171.

23. Hass, G., J. Opt. Soc. Amer., 39 (1949), 532.

24. Michelson, C. E., Met. Fin., 61 (1963), 78.

25. Charlesby, A. and Polling, J. J., Porc. Roy. Soc., A 227 (1955), 434.

26. Albella, J. M., Martinez-Duart, J. M., and Rueda, F., Opt. Acta, 22 (1975), 973.

27. Wilkins, N. J. M., Corr. Sci., 5 (1965), 3.

28. Wilkins, N. J. M., Corr. Sci., 4 (1964), 17.

29. Fuhrman, F. G. and Collins, F. C., J. Electrochem. Soc., 124 (1977), 1294.

30. Harrick, N. J., Appl. Opt., 10 (1971), 2344.

31. Himics, R. J., Kaplan, M., Desai, N. V., and Poliniak, E. S., Polym. Eng. Sci., 17 (1977), 406.

32. Poling, G. W., J. Electrochem. Soc., 116 (1969), 958.

33. Skoog, D. A. and West, D. M., Principles of Instrumental Analysis, Holt, Rinehart and Winston, Inc., New York, 1971.

34. Hannah, R. W., Appl. Spectroscopy, 17 (1963), 23.

35. Vedder, W. and Vermilyea, D. A., Trans. Faraday Soc., 65 (1969), 561.

36. Dorsey, G. A., Jr., J. Electrochem. Soc., 113 (1966), 172 and 284.

37. Dorsey, G. A., Jr., J. Electrochem. Soc., 115 (1968), 1053 and 1057.

38. Dorsey, G. A., Jr., J. Electrochem. Soc., 116 (1969), 466.

39. Mertens, F. P., Surf. Sci., 71 (1978), 161.

40. Nordal, P. and Kanstad, S. O., Opt. Commun., 24 (1978), 95.

41. Thibault, S., Thin Solid Films, 35 (1976), L33.

42. Cheever, G. D., J. Coat. Technol., 50 (1978), 78.

43. Poling, G. W., J. Electrochem. Soc., 114 (1967), 1209.

44. Burwell, J. T., Jr., Wear, 1 (1957/58), 119.

45. Rabinowicz, E., Friction and Wear of Materials, John Wiley and Sons, Inc., New York, 1965.

46. Eyre, T. S., Treat. Mat. Sci. Tech., 13 (1979), 363.

47. Moore, M. A., Treat. Mat. Sci. Tech., 13 (1979), 217.

48. Misra, A. and Finnie, I., Wear, 60 (1980), 111.

49. Henley, V. F., Anodic Oxidation of Aluminum and Its Alloys, Pergamon Press, New York, 1982.

50. Rabinowicz, E., Dunn, L. A., and Russell, P. G., Wear, 4 (1961), 345.

51. Goddard, J. and Wilman, H., Wear, 5 (1962), 114.

52. Kragelskii, I. V., Friction and Wear, Butterworths and Co., Washington, 1965.

53. Hisakado, T., Bull. JSME, 13 (1970), 129.

54. Shaw, M. C., Mech. Chem. Eng. Trans., 8 (1972), 73.

55. Tsukizoe, T. and Sakamoto, T., Bull. JSME, 17 (1974), 1637.

56. Lal, G. K. and Shaw, M. C., Wear, 29 (1974), 153.

57. Tsukizoe, T. and Sakamoto, T., Bull. JSME, 18 (1975), 65.

58. Sasaki, T. and Okamura, K., Bull. JSME, 3 (1960), 547.

59. Mulhearn, T. O. and Samuels, L. E., Wear, 5 (1962), 478.

60. Sedriks, A. J. and Mulhearn, T. O., Wear, 6 (1963), 457.

61. Maan, N. and Broese Van Groenou, A., Wear , 42 (1977), 365.

62. Gane, N. and Skinner, J., Wear, 24 (1973), 207.

63. Sin, H., Saka, N., and Suh, N. P., Wear, 55 (1979), 163.

64. Suh, N. P., Sin, H-C., and Saka, N., Proc. Int. Conf. Fundamentals of Tribology, MIT Press, Boston, 1980, p. 493.

65. Sedriks, A. J. and Mulhearn, T. O., Wear, 7 (1964), 451.

66. Goddard, J., Harker, H. J., and Wilman, H., Nature, 184 (1959), 333.

67. Avient, B. W. E., Goddard, J., and Wilman, H., Proc. Roy. Soc., A258 (1960), 159.

68. Stroud, M. F. and Wilman, H., Brit. J. Appl. Phys., 13 (1962), 173.

69. Larsen-Badse, J., Wear, 12 (1968), 35.

70. Buttery, T. C. and Archard, J. F., Proc. Inst. Mech. Eng., 185 (1970/71), 537.

71. Shaw, M. C., Wear, 43 (1977), 263.

72. Misra, A. and Finnie, I., Wear, 68 (1981), 33.

73. Misra, A. and Finnie, I., J. Eng. Mat. Tech., 104 (1982), 94.

74. Misra, A. and Finnie, I., Proc. 3rd Int. Conf. Wear of Materials, San Francisco, ASME, NewYork, 1981, p. 426.

75. Aghan, R. L. and Samuels, L. E., Wear, 16 (1970), 293.

76. Archard, J. F., J. Appl. Phys., 24 (1953), 981.

77. Richardson, R. C. D., "Unidirectional Wear Tests on Soft Abrasives and the Wear Resistance of Steel Surfaces of Nearly Uniform Hardness," Tech. report No. 12, National Institute of Agricultural Engineering, 1967.

78. Johnson, R. W., Wear, 16 (1970), 351.

79. Khrushchov, M. M. and Babichev, M. A., Research on the Wear of Metals, National Engineering Laboratory, Glasgow, NEL Translation No. 893 , 1960, ch. 18.

80. Nathan, G. K. and Jones, W. J. D., Wear, 9 (1966), 300.

81. Larsen-Badse, J., Wear, 12 (1968), 357.

82. Wilshaw, T. R. and Hartley, N. E. W., Proc. Eur. Symp. Comminut., Cannes, Verlag Chemie GmbH, Weinheim, 1971.

83. Hirano, H. H. and Levy, A. V., Proc. Int. Conf. Fundamentals of Tribology, MIT Press, Boston, 1980, p. 519.

84. Misra, A. and Finnie, I., Wear, 68 (1981), 41.

85. Khrushchov, M. M., Wear, 28 (1974), 69.

86. Khrushchov, M. M. and Babichev, M. A., Friction and Wear in Machinery, 11 (1956), 1.

87. Khrushchov, M. M. , Proc. Conf. Lubrication and Wear, Institute of Mechanical Engineers, London, 1957, p. 655.

88. Larsen-Badse, J., Trans. AIME, 236 (1966), 1461.

89. Richardson, R. C. D., Wear, 10 (1967), 353.

90. Moore, M. A. and Douthwaite, R. M., Metall. Trans., 7A (1976), 1833.

91. Angus, H. T., Wear, 54 (1979), 33.

92. Khrushchov, M. M. and Babichev, M. A., Friction and Wear in Machinery, 11 (1956), 13.

93. Khrushchov, M. M. and Babichev, M. A., Russian Eng. J., 44 (1964), 43.

94. Richardson, R. C. D., Wear, 10 (1967), 291.

95. Richardson, R. C. D., Wear, 11 (1968), 245.

96. Nathan, G. K. and Jones, D., Proc. Fifth. Conf. Lubrication and Wear, Institue of Mechanical Engineers, London, 1967, Paper 24.

97. Tabor, D., Rev. Phys. Technol., 1 (1970), 145.

98. Cochran, W. C., Aluminum III: Fabrication and Finishing, American Society for Metals, Metals Park, 1967, p. 641.

99. Diggle, J. W., Downie, T. C., and Goulding, C. W., Chem. Rev., 69 (1969), 365.

100. Spencer, L. F., Met. Fin., 67 (1969), 53.

101. Spencer, L. F., Met. Fin., 67 (1969), 70.

102. O'Sullivan, J. P. and Wood, G. C., Proc. Roy. Soc. London, A317 (1970), 511.

103. Tajima, S., Adv. Corr. Sci. Tech., 1 (1970), 229.

104. Wood, G. C., Oxides and Oxide Films, 2 (1973), 167.

105. Cochran, W. C. and Sprowls, D. O., Corrosion Control by Coatings, Science Press, Princeton, 1979, p. 179.

106. Csokan, P., Adv. Corr. Sci. Tech., 7 (1980), 239.

107. Furneaux, R. C., Aluminum Finishing Seminar, the Aluminum Association, Inc., St. Louis, 1982, p. 105.

108. Thompson, G. E. and Wood, G. C., Treat. Mat. Sci. Tech., 23 (1983), 205.

109. Young, L., Anodic Oxide Films, Academic Press, New York, 1961.

110. Kissin, G. H., The Finishing of Aluminum, Reinhold Publishing Co., New York, 1963.

111. Brace, A. W. and Sheasby, P. G., The Technology of Anodizing Aluminum, Technicopy Ltd., Stonehouse, 1979.

112. Keller, F., Hunter, M. S., and Robinson, D. L., J. Electrochem. Soc., 100 (1953), 411.

113. Murphy, J. F. and Michelson, C. E., Conf. Anodizing Aluminum, Nottingham University, Aluminum Development Assoc., London, 1961, p. 83.

114. Hunter, M. S. and Fowle, P., J. Electrochem. Soc., 101 (1954), 481.

115. Murphy, J. F., Plating, 54 (1967), 1241.

116. Michelson, C. E., J. Electrochem. Soc., 115 (1968), 213.

117. Booker, C. J. L. and Wood, J. L., Brit. J. Appl. Phys., 8 (1957), 347.

118. Wood, G. C., O'Sullivan, J. P., and Vaszko, B., J. Electrochem. Soc., 115 (1968), 618.

119. Hollo, M. G., 1st International Congress on Metallic Corrosion, William Clowes & Sons, Ltd., London, 1961, p. 45.

120. Bailey, G. and Wood, G. C., Trans. Inst. Met. Fin., 52 (1974), 187.

121. Manhart, J. H. and Mozelewski, F. A., Plat. Surf. Fin. , 66 (1979), 54.

122. Takahashi, H., Nagayama, M., Akahori, H., and Kitahara, A., J. Electron Microscopy, 22 (1973), 149.

123. Nagayama, M., Tamura, K., and Takahashi, H., Corr. Sci., 12 (1972), 133.

124. Tuck, C. D. S., Corr. Sci., 17 (1977), 777.

125. Takahashi, H. and Nagayama, M., Corr. Sci., 18 (1978), 911.

126. Furneaux, R. C., Thompson, G. E., and Wood, G. C., Corr. Sci., 18 (1978), 853.

127. Cosgrove, L. A., J. Phys. Chem., 60 (1956), 385.

128. Paolini, G., Masoero, M., Sacchi, F., and Paganelli, M., J. Electrochem. Soc., 112 (1965), 32.

129. Wood, G. C. and O'Sullivan, J. P., Electrochim. Acta, 15 (1970), 1865.

130. Diggle, J. W., Downie, T. C., and Goulding, C. W., J. Electroanal. Chem., 18 (1968), 192.

131. Diggle, J. W., Downie, T. C., and Goulding, C. W., J. Electrochem. Soc., 116 (1969), 1347.

132. Diggle, J. W., Downie, T. C., and Goulding, C. W., Electrochim. Acta, 15 (1970), 1079.

133. Diggle, J. W., Electrochim. Acta, 18 (1973), 283.

134. Nagayama, M. and Tamura, K., Electrochim. Acta, 12 (1967), 1097.

135. Nagayama, M. and Tamura, K., Electrochim. Acta, 13 (1968), 1773.

136. Nagayama, M., Tamura, K., and Takahashi, H., Corr. Sci., 10 (1970), 617.

137. Tajima, S., Baba, N., and Shimura, M., Electrochim. Acta, 12 (1967), 955.

138. Mason, R. B., J. Electrochem. Soc., 102 (1955), 671.

139. Applewhite, F. R., Leach, J. S. L., and Neufeld, P., Corr. Sci., 9 (1969), 305.

140. Maeland, A. J., Rittenhouse, R. C., and Bird, K., Plat. Surf. Fin., 63 (1976), 56.

141. Handke, M., Paluszkiewicz, C., and Wyrwa, W., Mat. Chem., 5 (1980), 199.

142. Handke, M., Paluszkiewicz, C., and Wyrwa, W., Mat. Chem., 6 (1981), 197.

143. Dorsey, G. A., Jr., J. Electrochem. Soc., 113 (1966), 169.

144. Dorsey, G. A., Jr., J. Electrochem. Soc., 117 (1970), 1177, 1181, and 1276.

145. Abd Rabbo, M. F., Richardson, J. A., Wood, G. C., and Jackson, C. K., Corr. Sci., 16 (1976), 677.

146. Abd Rabbo, M. F., Richardson, J. A., and Wood, G. C., Corr. Sci., 16 (1976), 689.

147. Shimizu, K., Tajima, S., Thompson, G. E., and Wood, G. C. , Electrochim. Acta, 25 (1980), 1481.

148. Shimizu, K., Thompson, G. E., and Wood, G. C., Thin Solid Films, 77 (1981), 313.

149. Shimizu, K., Thompson, G. E., and Wood, G. C., Thin Solid Films, 81 (1981), 39.

150. Thompson, G. E., Shimizu, K., and Wood, G. C., Nature, 286 (1980), 471.

151. Sharp, D. J., Panitz, J. K. G., Merrill, R. M., and Haaland, D. M., Thin Solid Films, 111 (1984), 227.

152. Randall, J. J. and Bernard, W. J., Electrochim. Acta, 20 (1975), 653.

153. Mason, R. B. and Fowle, P. , J. Electrochem. Soc., 101 (1954), 53.

154. Pullen, N. D., J. Electrodep. Tech. Soc., 15 (1939), 69.

155. Alvey, C. E. and Wood, G. C., Pap. S. Afr. Corr. Conf., 3rd, 1980, Paper 3.

156. Spooner, R. C., Proc. Am. Electropl. Soc., 44 (1957), 132.

157. Wefers, K., Aluminium, 49 (1973), 553 and 622.

158. Plumb, R. C., J. Electrochem. Soc., 105 (1958), 498.

159. Fukuda, Y. and Fukushima, T., Bull. Chem. Soc. Japan, 53 (1980), 3125.

160. Thompson, G. E., Furneaux, R. C., and Wood, G. C., J. Electrochem. Soc., 125 (1978), 1480.

161. Yamamoto, Y. and Baba, N., Thin Solid Films, 101 (1983), 329.

162. Edwards, J. D. and Keller, F., Trans. Electrochem. Soc., 79 (1941), 135.

163. O'Sullivan, J. P., Hockey, J. A., and Wood, G. C., Trans. Faraday Soc., 65 (1969), 535.

164. Baker, B. R. and Pearson, R. M., J. Electrochem. Soc., 118 (1971), 353.

165. Baker, B. R. and Pearson, R. M., J. Electrochem. Soc., 119 (1972), 160.

166. Thompson, G. E., Furneaux, R. C., Goode, J. S., and Wood, G. C., Trans. Inst. Met. Fin., 56 (1978), 159.

167. Thompson, G. E., Furneaux, R. C., Wood, G. C., Richardson, J. A., and Goode, J. S., Nature, 272 (1978), 433.

168. Barber, D. J., J. Electrochem. Soc., 112 (1965), 1143.

169. Thompson, G. E., Furneaux, R. C., and Wood, G. C., Corr. Sci., 18 (1978), 481.

170. Xu, Y., Thompson, G. E., and Wood, G. C., Electrochim. Acta, 27 (1982), 1623.

171. Thompson, G. E. and Wood, G. C., Nature, 290 (1981), 230.

172. Hoar, T. P. and Yahalom, J., J. Electrochem. Soc., 110 (1963), 614.

173. Hunter, M. S. and Fowle, P., J. Electrochem. Soc., 101 (1954), 514.

174. Thompson, G. E., Furneaux, R. C., and Wood, G. C., Trans. Inst. Met. Fin., 55 (1977), 117.

175. Thompson, G. E., Furneaux, R. C., and Wood, G. C., Trans. Inst. Met. Fin., 57 (1979), 123.

176. Cnerki, C. and Siejka, J., J. Electrochem. Soc., 120 (1973), 784.

177. Siejka, J. and Ortega, C., J. Electrochem. Soc., 124 (1977), 883.

178. Dekker, A. and Middelhoek, A., J. Electrochem. Soc., 117 (1970), 440.

179. Hoar, T. P. and Mott, N. F., J. Phys. Chem. Solids, 9 (1959), 97.

180. Diggle, J. W., Downie, T. C., and Goulding, C. W., J. Electrochem. Soc., 116 (1969), 737.

181. Barkman, E. F., Anodized Aluminum, ASTM, Philadelphia, ASTM STP No. 388 , 1965, p. 85.

182. John, S. and Shenoi, B. A., Met. Fin., 74 (1976), 31.

183. Kape, J. M., Fin. Ind., 1 (1977), 13 and 38.

184. Baker, B. R., Aluminum Finishing Seminar, the Aluminum Association, Inc., St. Louis, 1982, p. 177.

185. Wood, G. C. and O'Sullivan, J. P., J. Electrochem. Soc., 116 (1969), 1351.

186. Wood, G. C. and Marron, V. J., Trans. Inst. Met. Fin., 45 (1967), 17 and 107.

187. George, D. J. and Powers, J. H., Plating, 56 (1969), 1240.

188. Campbell, W. J., Conf. Anodizing Aluminum, Nottingham University, Aluminum Development Assoc., London, 1961, p. 137.

189. Gillig, F. G., "Study of Hard Coatings for Aluminum," Tech. report No. 53-151, Wright Air Development Center, 1953.

190. Schuh, A. E. and Kern, E. W., Ind. Eng. Chem., 3 (1931), 72.

191. Arlt, H. G., Proc. ASTM, 40 (1940), 967.

192. Edwards, J., Trans. Inst. Met. Fin., 37 (1960), 121.

193. Roberts, A. G., Crouse, W. A., and Pizer, R. S., ASTM Bull., No. 208, 1955, p. 36.

194. Spooner, R. C., Can. J. Technol., 29 (1951), 479.

195. Laszewska, Z., Met. Fin., 67 (1969), 48.

196. Deal, B. E., Plating, 46 (1959), 823.

197. Brace, A. W. and Pocock, K., Trans. Inst. Met. Fin., 35 (1958), 277.

198. Vanden Berg, R. V., Machine Design, 34 (1962), 155.

199. Hafer, R. F., Plating , 45 (1958), 623.

200. Machlin, I. and Whitney, N. J., Met. Fin., 59 (1961), 55.

201. Koizumi, S., Ninagawa, S., and Ueda, S., J. Met. Fin. Soc. Japan, 19 (1968), 504.

202. Gohausen, H. J., Trans. Inst. Met. Fin., 56 (1978), 57.

203. Witt, C. A. and Gerken, G., Aluminium, 47 (1971), 748.

204. Mauksch, W. and Budiloff, N., Aluminium, 19 (1937), 298.

205. Taylor, F., Met. Ind., 65 (1944), 290.

206. Brace, A. W., Electroplating, 7 (1954), 329 and 376.

207. Spencer, L. F., Met. Fin., 66 (1968), 58.

208. Scott, B. A., Qual. Contr. Met. Fin., Symp., London, 1967, p. 91.

209. Yokoyama, K., Konno, H., Takahashi, H., and Nagayama, M., Plat. Surf. Fin., 69 (1982), 62.

210. Cochran, W. C. and Keller, F., The Finishing of Aluminum, Reinhold Publishing Co., New York, 1963, p. 104, ch. 7.

211. Noble, J. W., III, and Leidheiser, H., Jr., Ind. Eng. Chem. Prod. Res. Dev., 20 (1981), 344.

212. Baier, S. W., Thichness Testing of Electroplated and Related Coatings, Portcullis Press Ltd., Redhill, Volume 2 , 1981, p. 59, ch. 9.

213. Collins, E. A., Bares, J., and Billmeyer, F. W., Jr., Experiments in Polymer Science, John Wiley & Sons, New York, 1973, p. 90.

214. Salgo, V., Adv. Print. Sci. Tech., 2 (1962), 235.

215. Dean, S. W., Jr., Clark, D. G., Friberg, L. S. and Seese, R. G., TAGA, 1972, p. 235.

216. Dean, S. W., Jr. and Ford, J. A., TAGA, 1973, p. 198.

217. Sobotka, W. K., Adv. Print. Sci. Tech., 16 (1982), 352.

218. Zelley, W. G., TAGA, 1972, p. 262.

219. Powers, J. H., TAGA, 1974, p. 23.

220. Manhart, J. H., TAGA, 1977, p. 12.

221. Yumiki, K., Graphic Arts Japan, 22 (1980-81), 77.

222. Pearson, A. W. and Parker, C. A., TAGA, 1981, p. 93.

223. Pearson, A. W., TAGA, 1981, p. 76.

224. Hockey, B. J., J. Amer. Ceram. Soc., 54 (1971), 223.

225. Cutter, I. A. and McPherson, R., J. Amer. Ceram. Soc., 56 (1973), 266.

226. Aghan, R. L. and McPherson, R., J. Amer. Ceram. Soc., 56 (1973), 46.

227. Cutter, I. A. and McPherson, R., J. Amer. Ceram. Soc., 55 (1972), 334.

228. Cutter, I. A. and McPherson, R., Phil. Mag., 20 (1969), 489.

229. Swain, M. V., Wear, 35 (1975), 185.

230. Suh, N. P., Wear, 25 (1973), 111.

231. Weast, R. C. and Astle, M. J., CRC Handbook of Chemistry and Physics, CRC Press, Inc., Boca Raton, 1980-81, p. B-143.

232. Valdma, L. E., Friction and Wear in Machinery, 13 (1959), 17.

233. Atkins, P. W., Physical Chemistry, W. H. Freeman and Company, San Francisco, 1978, p. 944.

234. Sautter, W., Aluminium, 42 (1966), 636.

235. Krushchov, M. M. and Babichev, M. A., Friction and Wear in Machinery, 12 (1958), 5.

236. Mason, R. B., Met. Fin., 55 (1957), 55.

237. Sutherland, J. E., TAGA, 1982, p. 311.

VITA

Shem-Mong Chou, the second child of Yi-Shuey Chou and Chaw-Chih Lin, was born on September 14, 1954 in Taipei, Taiwan. In June 1976, he received his Bachelor of Science degree in Chemistry from National Tsing Hua University in Hsinchu, Taiwan. After graduation he joined the 206th Arsenal of the Combined Service of Forces in Taipei. As an analytical Chemist, he was responsible for developing and improving analytical techniques in determining the chemical composition of engineering materials.

He came to the United States in 1978 to pursue his graduate study at Lehigh University. The graduate training expanded his interests to include many fields such as graphic arts, IC lithographic processes in VLSI technology, and friction and wear of materials as well as enabled him to plan a research project, to carry out the experimental work in a laboratory and to report the results in a clear and understandable manner. He wishes to devote his life to one of these fields.